Title
Manganese Oxide-Coated Sand Geomedia for Treatment of Contaminated Stormwater

Author
Charbonnet, Joseph

Publication Date
2018

Peer reviewed|Thesis/dissertation

Manganese Oxide-Coated Sand Geomedia for Treatment of Contaminated Stormwater

By

Joseph Charbonnet

A dissertation submitted in partial satisfaction of
the requirements for the degree of
Doctor of Philosophy
in
Engineering - Civil and Environmental Engineering
in the
Graduate Division
of the
University of California, Berkeley

Committee in charge:
Professor David L. Sedlak, Chair
Professor Baoxia Mi
Professor Céline Pallud

Fall 2018

Manganese Oxide-Coated Sand Geomedia for Treatment of Contaminated Stormwater

Joseph Charbonnet

Abstract

Manganese Oxide-Coated Sand Geomedia for Treatment of Contaminated Stormwater

by

Joseph Charbonnet

Doctor of Philosophy in Engineering - Civil and Environmental Engineering

University of California, Berkeley

Professor David L. Sedlak, Chair

Managed aquifer recharge is an increasingly popular means of replenishing groundwater supplies by intentionally infiltrating stormwater or tertiary wastewater effluent into the subsurface. Although this practice can recharge depleted aquifers, it poses potential risks to water quality, especially when practiced with stormwater from city streets which may contain contaminants derived from automobiles, asphalt, biocides and consumer products. To provide a means of protecting water quality during managed aquifer recharge, engineered geomedia–materials designed to passively remove contaminants–can be introduced to recharge basins. Manganese oxide-coated sand is a promising engineered geomedia because manganese oxides can oxidize certain organic contaminants and adsorb metal cations. This dissertation describes the use of a manganese oxide-coated sand produced using a novel, room-temperature synthesis for the passive treatment of urban stormwater.

The useful lifetime of manganese oxide-containing geomedia may be limited. After oxidizing organic contaminants and exposure to other solutes typically present in stormwater (e.g., Ca^{2+}, CO_3^{2-}, natural organic matter), the initially high reactivity of the manganese oxide-containing geomedia decreased. The passivation appeared to be related to the reduction of Mn(IV) sites and subsequent accumulation of Mn(II/III). To address the loss of reactivity, methods for regenerating the reactivity of manganese oxide-coated sand were evaluated (Chapter 2). Hypohalites produced the most reactive regenerated phase when dosed in sufficient abundance to fully oxidize all Mn in the failed geomedia to the +4.0 oxidation state. Permanganate also oxidized Mn(III)-rich manganese oxides, but the resultant mineral phase was less reactive with bisphenol A than that produced by HOCl or HOBr. These results imply that mineralogy, in addition to oxidation state, is important to manganese oxide reactivity.

Chlorine was evaluated as a means of *in situ* regeneration by oxidizing reduced Mn without removing the geomedia from columns (Chapter 3). Chemical analyses indicated that the average manganese oxidation state of the geomedia coating increased after exposure to hypochlorous acid (HOCl). The regenerated geomedia demonstrated similar reactivity and longevity to virgin geomedia. X-ray absorption spectroscopy and X-ray diffraction indicated that the virgin and regenerated geomedia coatings had similar manganese oxide structures. These more reactive minerals were nanocrystalline and lacked long-range mineral order, whereas the

failed geomedia coating exhibited greater crystallinity and resembled the manganese oxide cryptomelane. These results suggest that manganese oxide-coated sand may be capable of oxidizing organic contaminants urban stormwater for many years and that it is possible to regenerate the oxidative capacity of manganese oxide-coated sands without excavating stormwater recharge systems.

Manganese oxide-coated sand was also assessed for its ability to remove metal contaminants from stormwater. The presence of Cu, Zn, Cd and Pb in urban runoff pose potential risks to humans and aquatic organisms. Batch and column experiments were conducted to evaluate the capacity of manganese oxide-coated sand to adsorb metals in a stormwater matrix containing background ions and natural organic matter (Chapter 4). In batch tests the geomedia adsorbed over 95% of Cu, Cd and Pb in conditions typical of natural organic matter-free stormwater. In the presence of natural organic matter, however, the geomedia had a lower capacity for metal removal. Results from column tests indicate that, even in the presence of natural organic matter, a typical stormwater infiltration system containing manganese oxide-coated sand would have a lifetime of over 20 years before the complete breakthrough of Cu and Zn and of over 800 years before the complete breakthrough of Cd or Pb. In field applications, the geomedia could become saturated or release adsorbed metals because of changes in chemical conditions. Therefore, chemical treatments were evaluated for their ability to recover adsorbed metals from the geomedia and restore the adsorption capacity of the manganese oxide-coated sand. A mild acid wash (i.e., pH 3 HCl) restored the adsorptive capacity of the geomedia with minimal degradation of the Mn coating. The regenerated geomedia demonstrated similar performance to the virgin geomedia.

The research described in this dissertation indicates that manganese oxide-coated sand may be effective for treating urban stormwater during managed aquifer recharge. High levels of removal of organic contaminants and toxic metals could be sustained for decades with regenerative treatments. In managed aquifer recharge systems, other geomedia will likely be used in conjunction with manganese oxides, and their contributions to pollutant remediation may be complementary or inhibitory. For instance, biochar could protect manganese oxides from fouling by natural organic matter, but anoxic conditions induced by upstream carbonaceous geomedia could reduce manganese oxides. Further research is needed to determine the optimal configurations of geomedia in unit process treatment trains in order to target contaminants across a range of stormwater qualities.

TABLE OF CONTENTS

LIST OF FIGURES

LIST OF TABLES

ACKNOWLEDGEMENTS

I wish to convey heartfelt gratitude to those who have helped during my journey through graduate school. My doctorate is the culmination of the tremendous efforts of a host of people.

My sincere thanks to my adviser, David Sedlak, who has been incredibly generous with me. His persistent insistence on quality over quantity is more valuable to environmental chemistry than any reaction mechanism. By allowing me the freedom to explore new fields and ideas he has taught me the value of initiative and self-reliance.

I am thankful to the members of my peer support group: Jen Lawrence, Rachel Allen and Karina Chavarria. Their professional support facilitated many of my achievements and their personal support sustained me through the end of my PhD. My confreres in ReNUWIt helped to give my work meaning and I value their companionship. Key among these are my fellow SUWIR leaders and podcasters, Skuyler Herzog, Zach Stoll and Scott Miller. I'm proud to number all of these people among my dear friends.

I offer my gratitude to Case van Genuchten, who was incredibly helpful in my work with X-ray spectroscopy. I am likewise grateful to the undergraduates I had the privilege of supervising: Julianne Rolf, Francis Ledesma and Yanghua Duan. Their hard work is an indispensable but often unsung component of my research. I was not always the mentor that these talented young scientists deserved, but they taught me a great deal and are already growing into superlative researchers in their own right. My thanks also to all of the members of the Sedlak Group and O'brien Lab during my tenure as a researcher for helping make my work high-quality yet human.

My tremendous upbringing by my family is the greatest gift I have received in my life. I wish to thank my father, Jeff, who has been a model of leadership and devotion to education that I strive to emulate every day. My sister, Veronica, was my first scientific collaborator. By letting me tag along on trips to the neighborhood creek and mosquito-trapping expeditions she sparked in me a love of water and of inquiry that has never abated. Most of all my mother, Sara, has done more than anyone to shape me as a scientist. My first PI, she inculcated in me a love of learning, curiosity and zeal for experimentation, and still did the dirty work of staying up late with me to complete science fair projects. She is a master of the craft of pedagogy and scientific instruction.

Finally, I would like to thank my best friend and wife, Elizabeth. Her insight and advice throughout this process have been indispensable. The last six years have been her struggle as much as mine, but her support through it all is a shining example of the perfect life partner. She is a better environmental engineer than I will ever be and a better spouse too. Marrying her was the best decision I ever made during my time at Berkeley.

CHAPTER 1. Introduction

Some material reproduced with permission from Grebel; J. E.; Charbonnet, J. A.; Sedlak, D. L. Oxidation of Organic Contaminants by Manganese Oxide Geomedia for Passive Urban Stormwater Treatment Systems. *Water Research* **2016,** *88,* 481-491.

1.1 Urban Water Scarcity and Managed Aquifer Recharge

Cities around the world face increasing stress on their water systems. In developing countries, these challenges are often a consequence of growing populations and a shortage of the capital necessary for investment in large-scale, centralized infrastructure (Larsen et al., 2013). Higher standards of living, urbanization and technological advances will cause fundamental shifts in global water utilization, with water demand for industrial and agricultural uses projected to increase by nearly 50% over the next two decades (Gleeson et al., 2012). Strains on water systems in developing regions are often exacerbated by arid or semiarid climates that naturally provide more limited water resources (Mekonnen and Hoekstra, 2016).

In developed nations, challenges include aging infrastructure, shifts in population density, and climate change-driven drought conditions (Hering et al., 2013). Much of Europe and the United States are industrially advanced and have largely escaped severe water shortages, and yet experience political and social pressures to develop and implement more sustainable water resources (van der Steen and Howe, 2009). These innovations are centered around the principles of integrated urban water management with the goal of achieving fully resilient, sustainable, and integrated "One Water" cities (Owen, 2015). Developed regions in Israel, Singapore, Australia and the western United States face serious water shortages as a consequence of drought and political uncertainty (Page et al., 2010; Siegel, 2015). These challenges have motivated infrastructure enhancements and institutional reforms to improve water security (National Research Council, 2012).

The southwestern United States, with an arid climate, growing population and complex physical and legal systems of water management, presents a particularly salient case study of the need for urban water innovation (Kallis et al., 2009). In this region, many cities import water across long distances to augment their local supplies (Loraine and Pettigrove, 2006). For example, the Colorado River alone supplies water across seven US States and Mexico, contributing to the water supply of 30 million people (Ficklin et al., 2013).

Imported water is especially crucial to cities in southern California: Between 60 and 70% of southern California's water supply is imported (Figure 1.1) (Pagán et al., 2016). Imported water frequently requires expensive and energy-intensive infrastructure (Liu et al., 2016; Stokes and Horvath, 2006). For example, California's State Water Project is the largest single consumer of electricity in the state (California Department of Water Resources, 2018). Fiscal constraints, the need for water security and the environmental impact of imported water have motivated interest in alternative local water supplies in the region. For instance, the City of Los Angeles, CA set the goal of procuring 50% of its water locally by the year 2035 (Mayor's Office of Sustainability, 2018). The City of Santa Monica, CA intends to completely eliminate its use of imported water by 2020 (Weiser, 2017).

Figure 1.1 Major water reservoirs and aqueducts in the state of California. Detail from (Belock, 2009).

Groundwater can serve as an important local water source in some of southern California's municipalities, though many cities now consume groundwater in an unsustainable manner (Gorelick and Zheng, 2015). Managed aquifer recharge is an increasingly popular tool in water-stressed urban areas for replenishing groundwater supplies and augmenting locally available water (Alidina et al., 2014a; Bichai et al., 2015). Managed aquifer recharge secures inexpensive water from sources such as stormwater and tertiary treated wastewater and infiltrates it into the subsurface, typically through porous media (Alidina et al., 2014b).

Where the ground is covered by impermeable surfaces, precipitation that would otherwise infiltrate into groundwater instead runs off as stormwater (Grebel et al., 2013). These sizable wet weather flows make the capture of stormwater for managed aquifer recharge attractive to many cities, because such systems could passively convert much of this runoff into a local water supply for both potable and non-potable use (Daigger, 2009; Page et al., 2014). For instance, roughly half of all precipitation in the Los Angeles Basin—more than 74×10^6 m^3 of stormwater annually—runs off of impermeable surfaces and through urban watersheds that lead to the ocean. If just the first 2 cm of each rain event were captured and infiltrated, 71×10^6 m^3 of recharge would be added to the local groundwater, enough to supply the water of 1.5 million people (Los Angeles and San Gabriel Rivers Watershed Council, 2010). This would account for 11% of the

water consumed in the City of Los Angeles (Los Angeles Department of Water and Power, 2013). For comparison, the Los Angeles Aqueduct, which conveys water from the Owens Valley, typically supplies approximately 180×10^6 m^3 of water to the region (Los Angeles Department of Water and Power, 2013).

Managed aquifer recharge infrastructure can be centralized or distributed, ranging from vegetated curbside swales to large-scale infiltration basins and drywells (Edwards et al., 2016; Los Angeles County Flood Control District and City of Los Angeles Department of Public Works Bureau of Sanitation, 2014). Engineers have long used small-scale infiltration systems such as rain gardens and bioswales to increase the permeable surface area in urban environments, but these designs were intended to minimize peak flows and prevent combined sewer overflows (Andres et al., 2018; Ellis, 2000). Communities in water-stressed regions are now investing in large-scale, centralized infiltration systems capable of providing substantial volumes of aquifer recharge. For example, the Rory M. Shaw Wetlands Park in Los Angeles is a $52 million project to convert an abandoned 46-acre gravel quarry and landfill site into a wetland and groundwater infiltration system. This system will collect urban stormwater from a 929-acre watershed for 590 acre-feet of projected annual recharge (Figure 1.2) (Los Angeles County Flood Control District and City of Los Angeles Department of Public Works Bureau of Sanitation, 2014).

Figure 1.2 The Rory Shaw Wetlands Park in Los Angeles, CA in plan view (left) and artist's rendering (right). Adapted from (Los Angeles County Flood Control District and City of Los Angeles Department of Public Works Bureau of Sanitation, 2014).

1.2 Stormwater Contamination

Infiltrating urban stormwater into subsurface storage could adversely impact water quality. Stormwater can contain metals, nutrients, pathogens and organic compounds of concern (Makepeace et al., 1995; Soller et al., 2005). Perceived risk related to the introduction of anthropogenic contaminants into water supplies during managed aquifer recharge has limited its adoption in some locations (Page et al., 2010; Zhang et al., 2014).

Many organic contaminants are commonly found in stormwater (Table 1.1) (Grebel et al., 2013). Polycyclic aromatic hydrocarbons, including fluoranthene and pyrene, are among the most frequently studied contaminants (Takada et al., 1990). These compounds routinely occur in high concentrations due to their release from asphalt and deposition from automobile exhaust (Pitt et al., 1995). They are often monitored in stormwater because they are toxic to humans and wildlife (National Research Council, 1972).

Table 1.1 Selected organic stormwater contaminants and their structures, concentrations and limits.

Compound	Structure	Stormwater Conc. (µg/L)		Water Quality Criteria (µg/L)	
		Mean	Max.	Surface Water	Drinking Water
Fluoranthene	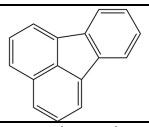	—	130[a]	—	180*
Pyrene	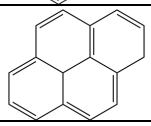	—	120[a]	—	830*
Bisphenol A	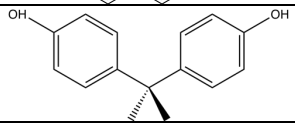	0.14[b]	4.0[d]	—	20[$]
Nonylphenol	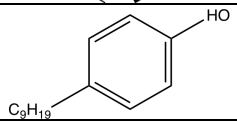	0.21[b]	3.6[a]	1.7*	0.3[+]
Benzophenone	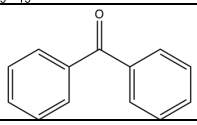	0.016[b]	0.068[b]	—	—
Benzophenone-3	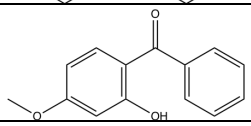	0.007[b]	0.012[b]	—	—
Benzotriazole	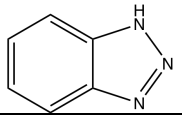	0.211[b]	0.917[b]	—	—
Mercaptobenzothiazole	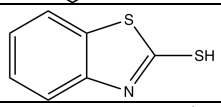	—	5.4[a]	—	—
Diuron	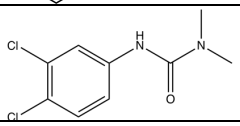	—	190[a]	0.2[+]	1.8[#]
2,4-D	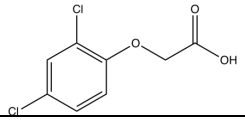	—	67[a]	—	70[†]
Fipronil	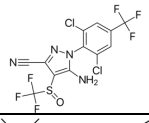	0.067[c]	10[c]	0.011*	—
Bifenthrin	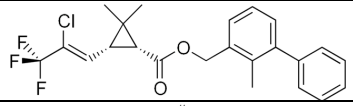	—	0.07[a]	—	—

*U.S. EPA recommended water quality criteria; [#]U.S. EPA Integrated Risk Information System 10^{-6} lifetime cancer risk; [+]European Union Water Framework Directive; [†]U.S. EPA drinking water maximum contaminant level; [$]Minnesota Department of Health Guidance

References: a) Grebel et al., 2013; b) Careghini et al., 2015; c) Gan et al., 2012; d) Minnesota Department of Health, 2014

Organic plasticizers are likewise present in stormwater. Phenols, benzophenones and benzotriazoles are used to harden, bind, cure, and enhance the color of plastics and tire rubber, and as additives in automotive fluids, biocides, and personal care products (Careghini et al., 2015). These chemicals are often endocrine disruptors, possible carcinogens and harmful to the reproductive and hormonal functions of fish (International Agency for Research on Cancer et al., 2013). Particular interest has been focused recently on how plasticizing compounds used in tire rubber vulcanization may be particularly toxic to economically valuable coho salmon (Du et al., 2017).

Biocides are another class of concern because they frequently occur in urban runoff at sufficient concentrations to be toxic to aquatic arthropods (i.e., >1 µg/L) (Blanchoud et al., 2004; Gan et al., 2012). Herbicides, including diuron and 2,4-dichlorophenoxyacetic acid (2,4-D), are applied in urban landscaping and for weed control along transportation corridors, and are easily transported into runoff (California Department of Transportation, 2003). Insecticides, including phenylpyrazoles (e.g., fipronil; brand name Frontline) and pyrethroids (e.g., bifenthrin), are used in urban pest control or applied to household pets. They are subsequently transported into stormwater by rain events or irrigation (Gilliom, 2006).

Metals comprise another important class of stormwater contaminants and are often found at concentrations an order of magnitude higher than water quality standards (Table 1.2). Cu is found in stormwater due to the wear and corrosion of roofing materials, automobile tires, brake pads and electrical components (Davis et al., 2001; Liu et al., 2005). Zn is prevalent in high concentrations in stormwater and is released from automobile components and galvanized steel guardrails (Liu et al., 2005; Pagotto et al., 2001). Sources of Cd in stormwater include highway guardrails, tires and brakes, and automotive fluids (Sansalone and Buchberger, 1997). Pb primarily derives from the products of leaded gasoline and coal combustion (Sansalone and Buchberger, 1997; Sherman et al., 2015).

Table 1.2 Selected metallic contaminants in stormwater and their dissolved concentrations and limits (Pitt et al., 2015).

Metal	Concentration (µg/L)		Water Quality Criteria (µg/L)	
	Mean	Maximum	Surface Water*	Drinking Water†
Cu	16	1800	3	1300
Zn	117	13000	81	5000
Cd	1.5	62	0.72	5
Pb	8	525	2.5	15

*U.S. EPA recommended water quality criteria, normalized to 100 mg/L - $CaCO_3$ hardness; †U.S. EPA drinking water maximum contaminant level

The metals that are of concern for managed aquifer recharge may be different from those that are problematic when stormwater runoff is discharged to surface waters. Cu and Zn are primarily concerns in stormwater due to their toxicity to aquatic organisms (Sansalone and Buchberger, 1997). Other metals, such as Cd and Pb, are primarily concerns in stormwater due to their human health risks (Genç-Fuhrman et al., 2007). In particular, Cd and Pb are frequently

associated with dust, which can be resuspended in urban transportation corridors and contaminate stormwater (Grebel et al., 2013).

1.3 Stormwater Composition

The chemical composition of stormwater varies dramatically with geography, geology, climate and urban land use. Stormwater collected from less disturbed parts of a watershed can closely resemble rainwater, while stormwater lower in a watershed can more resemble stream water. As stormwater passes over urban hardscapes and soils, its alkalinity increases due to the dissolution of carbonate minerals (Pitt et al., 1995). The pH of urban highway runoff ranges from 4.5 to 9.0 (California Department of Transportation, 2003). Similarly, dissolved organic carbon content can vary–typically from 1 to 75 mg-C/L–depending on location in the watershed and interval since the previous rain event (California Department of Transportation, 2003).

The chemical composition of stormwater is important to pollutant removal because many solutes can have an inhibitory effect on contaminant removal processes. Ionic strengths exceeding 10 mM (Amrhein et al., 1992), concentrations of dissolved organic matter greater than 10 mg-C/L (Liu et al., 2015), and pH values below 5.0 (Gadde and Laitinen, 1974) can inhibit the adsorption of dissolved metals. A water pH above 5.5 or concentrations of divalent cations or carbonate above 10 mM can slow the oxidation of organic contaminants (Jiang et al., 2017; Lin et al., 2009; Remucal and Ginder-Vogel, 2014). Dissolved organic matter concentrations as low as 1 mg-C/L can diminish the rate of oxidation of organic contaminants (Zhang et al., 2011). These impacts are a concern for protecting water quality across different spatial and temporal settings. Different treatment technologies may be necessary to treat stormwater of different compositions depending on season and location.

The variable nature of stormwater can complicate efforts to assess and compare treatment technologies. For this reason, simulated stormwater solutions can be used in experiments to address the effects of dissolved constituents on treatment in a controlled manner. The simulated stormwater formulation used in this research contains the major ions and natural organic matter (NOM) found in stormwater at concentrations near the average of stormwater composition across the US (Table 1.3) (Grebel et al., 2016; Pitt et al., 2015; Ulrich et al., 2015).

Table 1.3 Composition of simulated stormwater. Ionic strength = 4.6 mM.

Constituent	Concentration
Ca^{2+}	0.75 mM
Mg^{2+}	0.075 mM
Na^{+}	1.8 mM
NH_4^{+}	0.072 mM
SO_4^{2-}	0.33 mM
HCO_3^{-}	1.0 mM
Cl^{-}	1.7 mM
NO_3^{-}	0.072 mM
$H_2PO_4^{-}$	0.016 mM
NOM	0–10 mg-C/L*
pH	5–8.5

*NOM added in the form of Suwannee River NOM reverse osmosis isolate or Sigma Humic Acid

1.4 Engineered Geomedia for Stormwater Infiltration

During stormwater infiltration, captured water is often percolated through porous media (e.g., gravel or sand). Although porous media can improve water quality through complex biological, chemical and transport processes, these mechanisms are poorly understood (Edwards et al., 2016; Ellis, 2000). Until recently, the primary focus of most stormwater infiltration systems was flood mitigation, and thus the hydraulic properties of the media were the principal design criteria (Zhang et al., 2014). Managed aquifer recharge requires greater consideration of water quality than flood-control measures and therefore justifies more careful selection of infiltration media.

Engineered geomedia could provide a means of improving water quality during the recharge process, provided that they do not significantly reduce infiltration rates (Hatt et al., 2008). Engineered geomedia are materials that can be deployed in infiltration systems to diminish contaminant loads by removing or transforming contaminants. These geomedia can be integrated into infiltration systems in a similar manner to conventional media; however, engineered geomedia could remove contaminants via passive mechanisms, such as sorption, precipitation or oxidation, with lower costs for installation, operation and maintenance than water or wastewater treatment plants (Moglen, 2009).

Mn(III/IV)-oxides are a promising class of minerals for use as engineered geomedia because they can oxidize organic contaminants and adsorb metal cations often found in stormwater (Laha and Luthy, 1990; Stone and Morgan, 1984; Zhang and Huang, 2005). By oxidizing organic compounds, manganese oxides mitigate the risk of organic contaminant release posed by sorptive, carbonaceous materials. Further, the possibility of removing both metals and organic pollution makes manganese oxides well-suited to treat stormwater. To employ these useful properties during managed aquifer recharge, manganese oxides, which typically occur as fine-grained materials, could be coated on sand to increase their hydraulic conductivity and avoid their release from the surficial layer of the infiltration basin.

1.5 Manganese Oxide Geomedia

Mn(III/IV)-oxides naturally occur in a wide assortment of crystal polymorphs (Robinson et al., 2013). MnO_6 octahedra form the fundamental unit of manganese oxide minerals (Figure 1.3). These octahedra are arranged into distinct structures including layers (phyllomanganates) and tunnels (tectomanganates) (Feng et al., 2010). For instance, birnessite (sometimes identified as acid birnessite or δ-MnO_2) is a commonly-studied form of manganese oxide consisting of layered sheets (McKenzie, 1971; Morgan and Stumm, 1964; Stone, 1987). Hausmannite ($Mn(III)_2Mn(II)O_4$) has a spinel lattice, while pyrolusite (β-MnO_2) has a 1 × 1 tunnel structure. Hollandite (α-MnO_2)-type minerals, such as cryptomelane, have a 2 × 2 tunnel motif (Remucal and Ginder-Vogel, 2014).

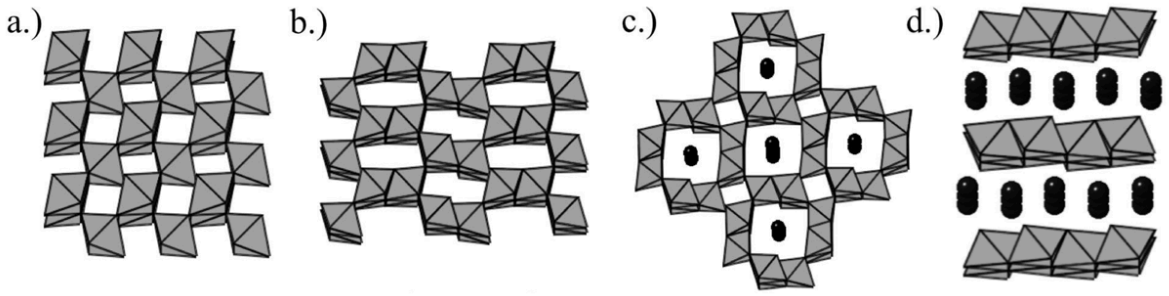

Figure 1.3 The structures of various manganese oxide minerals. MnO_6 octahedra are shown in gray while cations are shown in black. Among other orientations, MnO_6 octahedra may be arranged in a) 1 × 1 tunnels, as in pyrolusite, b) 2 × 1 tunnels, as in ramsdellite, c) 2 × 2 tunnels, as in cryptomelane and d) sheets, as in birnessite. Individual structures adapted from (Robinson et al., 2013).

1.5.1 Reactivity with Organic Compounds

Manganese oxides can oxidize organic compounds that contain Lewis base moieties (e.g., phenols, anilines and thiols). These functional groups are often present in contaminants of concern for managed aquifer recharge (Figure 1.4) (Laha and Luthy, 1990; Remucal and Ginder-Vogel, 2014; Stone, 1987; Zhang and Huang, 2005). In the initial, often rate-limiting step of the oxidation process, the organic compound forms an inner-sphere complex with a Mn(IV)-OH group. This complex undergoes a one-electron transfer, consequently reducing Mn(IV) sites to Mn(III) and Mn(III) sites to Mn(II), which may be released from the surface (Ukrainczyk and McBride, 1992).

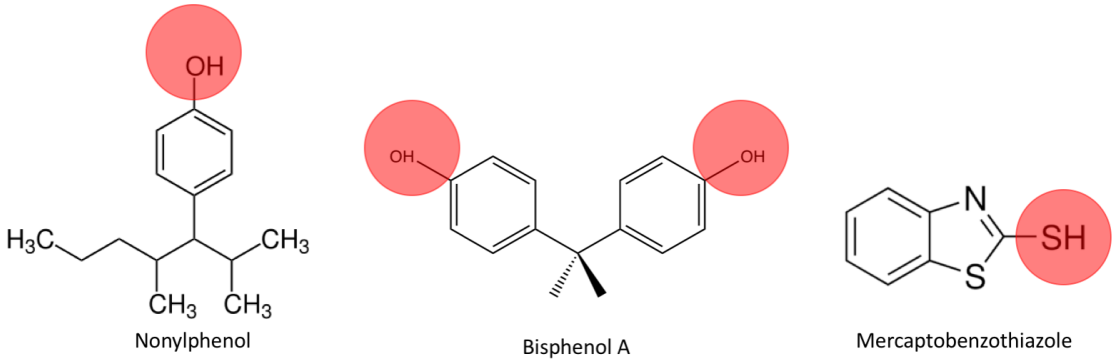

Figure 1.4 Stormwater contaminants used in the manufacture of commercial plastics and tire rubber. Electron-donating moieties (highlighted) facilitate their rapid oxidation by manganese oxides.

To determine the feasibility of using manganese oxides in geomedia, the oxidation of ten common organic stormwater contaminants was evaluated in triplicate batch experiments with powdered birnessite (Grebel et al., 2016). Each organic compound was added at a 150 nM concentration to vials containing 6.0 mg/L birnessite at pH 7 in a simulated stormwater matrix at room temperature (21 ± 2 °C). The initial reaction rate constant, $k_{initial}$, for the reaction with the birnessite was measured for each organic compound (Table 1.4).

Table 1.4 Rate constants for the oxidation of various organic contaminants with powdered birnessite in pH 7 simulated stormwater. Compounds with reaction rate constants below the limit of quantification are listed as $<<10^{-9}$ L g^{-1} s^{-1}. Adapted from (Grebel et al., 2016).

Compound	**$k_{initial}$ (L g^{-1} s^{-1})**
N-octylphenol	$57.7 \pm 0.53 \times 10^{-3}$
Bisphenol A	$1.84 \pm 0.34 \times 10^{-3}$
2-Mercaptobenzothiazole	$0.917 \pm 0.75 \times 10^{-3}$
Diuron	$66.7 \pm 0.48 \times 10^{-6}$
Prometon	$2.69 \pm 0.16 \times 10^{-6}$
Fluoranthene	$1.29 \pm 0.18 \times 10^{-6}$
Fipronil	$<<10^{-9}$
Benzotriazole	$<<10^{-9}$
TCPP	$<<10^{-9}$
Pendimethalin	$<<10^{-9}$

Aromatic compounds with electron-donating moieties (Shorter, 1994) (i.e., n-octylphenol, 2-mercaptobenzothiazole and bisphenol A) reacted most quickly. Though prometon and diuron contain ring-activating functionalities, they reacted more slowly because they also exhibited steric hindrance at the most likely reaction site (prometon) or had electron-withdrawing groups that reduced the reactivity of the compound (diuron). The sole polycyclic aromatic hydrocarbon tested, fluoranthene, possessed only moderate reactivity because it contains no

easily substituted protons due to a homogeneous distribution of its pi electrons. Compounds with many electron-withdrawing moieties or no clear oxidation site, including TCPP, benzotriazole, fipronil and pendimethalin did not react with the birnessite at discernible rates.

Because of its widespread environmental occurrence, toxicity and rapid, well-characterized reaction mechanism with manganese oxides, bisphenol A is frequently used as a representative organic contaminant in studies on organic contaminant oxidation by manganese oxides (Gao et al., 2011; Im et al., 2015; Lin et al., 2013). Although bisphenol A and other electron-rich contaminants are relevant to stormwater infiltration systems (Im and Löffler, 2016), it should be noted that the oxidation rates of bisphenol A by manganese oxide geomedia are likely among the most rapid for organic compounds. Many organic contaminants do not react with manganese oxides and would require other types of geomedia for their removal in managed aquifer recharge systems.

1.5.2 Loss of Reactivity

After prolonged oxidation of organic compounds, manganese oxides lose reactivity (Balgooyen et al., 2017). Some of this passivation is due to the reduction of Mn(IV) and increase in the abundance of Mn(III) and Mn(II). Adsorbed Mn(II) can have a pronounced impact on the structure and reactivity of these minerals (Lin et al., 2009). For instance, comproportionation between Mn(II) and Mn(IV) sites can produce structural Mn(III), which may exhibit different properties from the parent mineral (Elzinga and Kustka, 2015).

Divalent cations, particularly Mn^{2+}, can adsorb to the manganese oxide surface and decrease the number of sites available to react with organic contaminants (Barrett and McBride, 2005; Lin et al., 2013). The mechanisms of this passivation, however, may be specific to the local coordination environment of the surface site, nearby vacancies and the long-range crystal structure of the mineral (van Genuchten and Peña, 2017).

To determine the degree to which stormwater matrix composition and the reduction of manganese oxides impacted the reactivity of manganese oxide-coated sand, preliminary experiments were conducted with 20 g of cryptomelane-coated sand packed in glass columns with polyethylene fittings (16-mm inner diameter) to a height of 72 mm. The porosity of the packed columns was 0.33. Columns were fed simulated stormwater solutions buffered at pH 5.0, 7.0 and 8.5 by 1 mM $NaHCO_3$, or at pH 8.5 by 1 mM $NaB(OH)_4$ in a N_2-sparged, carbonate-free solution. The columns were operated under saturated upwards flow conditions at 0.4 mL/min (equivalent to an infiltration rate of 9.5 cm/h, which is a typical infiltration rate for stormwater infiltration systems) (Hatt et al., 2008). A continuous flow of simulated stormwater containing 5 μM bisphenol A as a model organic contaminant was pumped through the columns for over 1000 pore volumes at room temperature (21 ± 2 °C).

Initially, all bisphenol A was oxidized by the geomedia regardless of simulated stormwater composition (Figure 1.5). However, geomedia exposed to solutions containing carbonate at pH 7.0 and pH 8.5 exhibited a rapid decline in performance, while high bisphenol A removal was sustained in carbonate-buffered simulated stormwater at pH 5. In the carbonate-free, borate-buffered stormwater at pH 8.5, a high degree of bisphenol A oxidation was also

observed throughout the duration of the experiment, with the removal of approximately 80% of the influent bisphenol A sustained for over 1000 pore volumes.

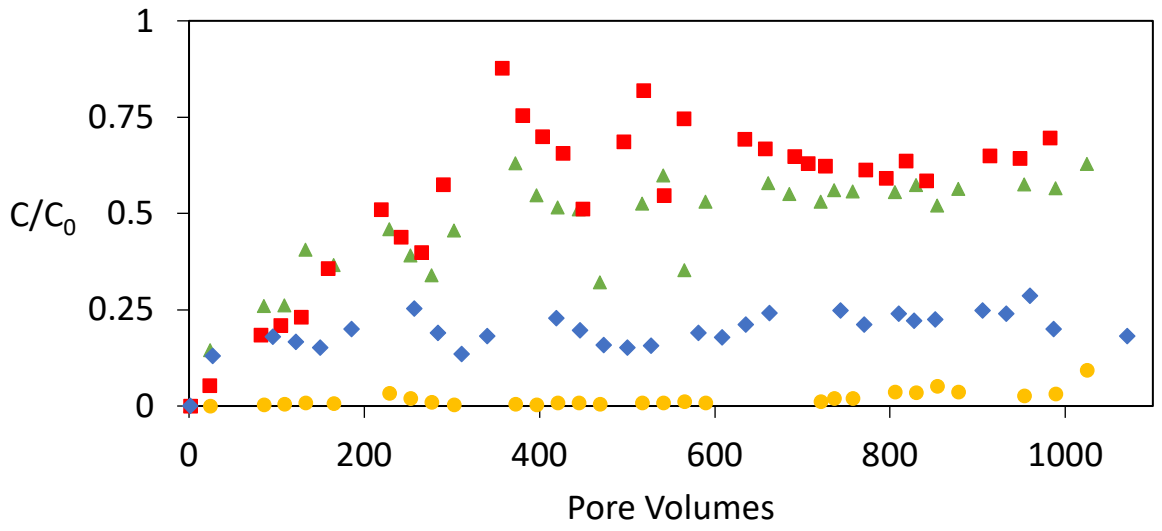

Figure 1.5 C/C_0 of bisphenol A from columns in various simulated stormwater conditions over time. Simulated stormwater was buffered by 1 mM carbonate at pH 5 (circles), 7 (triangles) and 8.5 (squares) and by 1 mM borate at pH 8.5 (diamonds) and had 5 µM influent bisphenol A. Columns contained 20 g cryptomelane-coated sand.

These data are consistent with the explanation that acidic pH values enhance the reactivity of manganese oxide (Lin et al., 2013):

$$MnO_{2(S)} + 4H^+ + 2e^- \rightarrow Mn^{2+} + 2H_2O \quad (1.1)$$

These results also suggest that the passivation of the manganese oxide was not solely dependent on the amount of organic compound oxidized and that constituents in the stormwater also play a role in geomedia weathering. Specifically, CO_3^{2-} ($pK_{a2} = 10.33$) was more abundant in the carbonate-buffered stormwater at pH 7.0 and pH 8.5 than in either the carbonate-buffered stormwater at pH 5.0 or the carbonate-free stormwater. This implies that the carbonate ion may have played a role in the passivation of the manganese oxide, possibly through the precipitation of carbonate minerals, such as $CaCO_3$ or $MnCO_3$.

Experiments conducted with birnessite-coated sand indicate that NOM has a modest impact on the reactive longevity of manganese oxide-coated sand (Grebel et al., 2016). Columns of manganese oxide exposed to 10 mg-C/L NOM in a simulated stormwater matrix passivated slightly faster than columns treating bisphenol A in NOM-free simulated stormwater (Figure 1.6). This may have been due to surface fouling by NOM or reduction of manganese oxides by phenolic groups in the NOM (Sunda et al., 1983; Tipping and Heaton, 1983; Yao and Millero,

1996). The effect is likely moderated, however, by electrostatic repulsion between the negatively-charged NOM and manganese oxide surface.

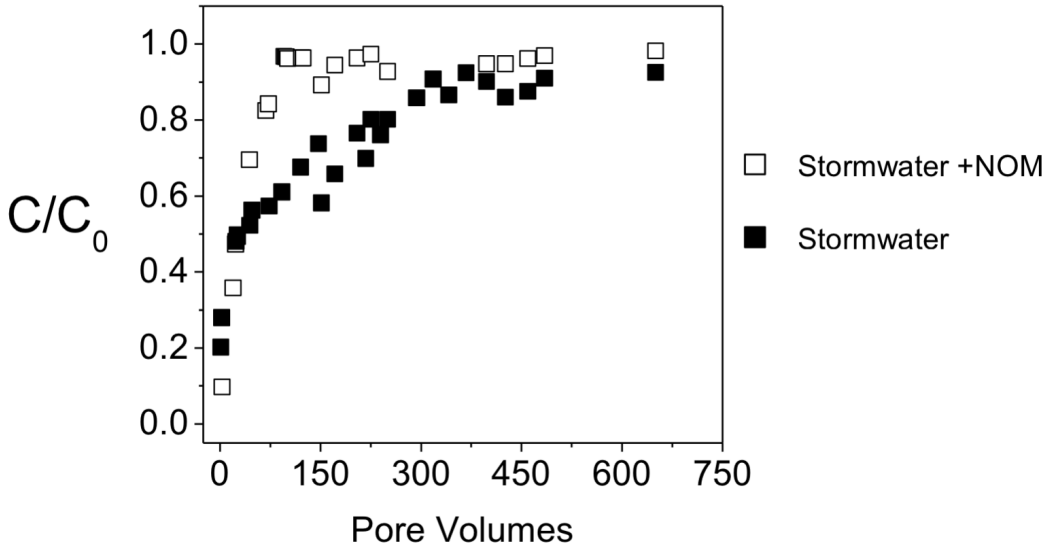

Figure 1.6 C/C_0 of bisphenol A in simulated stormwater with (white symbols) and without (black symbols) NOM. pH 7 simulated stormwater contained no NOM or 10 mg-C/L Suwannee River NOM and 5 μM influent bisphenol A. Columns contained 20 g birnessite-coated sand. Adapted from (Grebel et al., 2016).

1.5.3 Reactivity Regeneration

It may be possible to restore the reactivity of passivated manganese oxide-coated sand by re-oxidizing the reduced manganese associated with the surface. If the reactivity of the manganese oxide-coated sand could be restored *in situ*, the regeneration would lengthen the lifetime of the infiltration system without costly, labor-intensive excavation, making the use of this engineered geomedia less expensive and more practical for communities.

Abiotic oxidation of Mn(II) by O_2 is thermodynamically favored, but in homogeneous systems it is slow (Morgan, 1964). However, this oxidation mechanism is autocatalytic, meaning the initially precipitated manganese oxide solids (generally, $MnO_{x(s)}$) catalyze subsequent oxidation of aqueous Mn(II) and of $MnOOH_{(s)}$ and $Mn_2O_{3(s)}$ (Kessick and Morgan, 1975; Morgan, 1967). The homogeneous reaction is first-order with respect to [Mn(II)] and P_{O2}, while the heterogeneous reaction is first-order with respect to [Mn(II)], P_{O2} and $[MnO_{x(s)}]$, yielding the rate law for the oxidation of Mn(II):

$$-\frac{d[Mn(II)]}{dt} = k_0[Mn(II)]P_{O2} + k_1[Mn(II)]P_{O2}[MnO_x] \qquad \text{(Eq. 1.1)}$$

where k_0 and k_1 are the homogeneous and heterogeneous rate constants for Mn(II) oxidation, respectively (Morgan, 2005, 1964).

This reaction has been observed for oxidants including $KMnO_4$, ClO_2, HOCl, HOBr and O_3 (Allard et al., 2013; Kessick and Morgan, 1975; Melichová et al., 2001; Reisz et al., 2008; Van Benschoten et al., 1992). Therefore, under conditions of excess oxidant, the rate law for the oxidation of Mn(II) may be generalized to:

$$-\frac{d[Mn(II)]}{dt} = k'_0[Mn(II)] + k'_1[Mn(II)][MnO_x] \qquad \text{(Eq. 1.2)}$$

where k'_0 and k'_1 are the pseudo-first order homogeneous and pseudo-second order heterogeneous rate constants for Mn(II) oxidation, respectively.

Chlorine oxidizes Mn(II) at much faster rates than oxygen (Hao et al., 1991; Kessick and Morgan, 1975). The autocatalytic nature of the oxidation by chlorine is demonstrated by the dominance of the heterogeneous (second) term in Eq. 1.2; the half-life of Mn(II) is 4×10^5 times longer in the homogeneous reaction than the heterogeneous reaction (i.e., ($k'_1 \times$ [Mn(II)]) is 4×10^5 times larger than k'_0) in the presence of 5 mg/L $MnO_{2(s)}$ (Hao et al., 1991). Consequently, the mechanism for this reaction may be expressed by:

$$Mn(II) + HOCl + H_2O \xrightarrow{\text{slow}} MnO_{2(s)} + Cl^- + 3H^+ \qquad (1.2)$$

$$Mn(II) + MnO_{2(s)} \xrightarrow{\text{fast}} MnO_{2(s)}\text{-->}Mn(II)_{(s)} \qquad (1.3)$$

$$>Mn(II)_{(s)} + HOCl + H_2O \xrightarrow{\text{moderate}} MnO_{2(S)} + Cl^- + 3H^+ \qquad (1.4)$$

where $>Mn(II)_{(s)}$ is the adsorbed Mn(II) species (Hao et al., 1991). $>Mn(OH)_2$ is the most nucleophilic Mn(II) species, and hence most rapidly oxidized, followed by $>Mn(OH)^+$ and $>Mn^{2+}$, respectively (Allard et al., 2013; Morgan, 2005).

Hypobromous acid oxidizes Mn(II) at significantly faster rates than hypochlorous acid (Melichová et al., 2001). At ratios of bromine to chlorine as low as 1%, bromine dominates the oxidation of Mn(II) due to the capacity of transient and highly reactive bromine species including BrCl and Br_2O to act as electron shuttles between HOCl and Mn(II) (Allard et al., 2013). There is a pH dependence to this reaction mechanism, because HOBr ($pK_a = 8.8$) is more electrophilic and hence a more rapid oxidant than OBr^- (Schwarzenbach et al., 2016). Therefore, at pH values between 9 and 11, $>Mn(OH)_2$ ($p^*K_{1,>Mn(II)} = 8.2$, $p^*K_{2,>Mn(II)} = 9.2$) and HOBr coexist in abundances which are small but sufficient for the reaction between HOBr and $>Mn(OH)_2$ to contribute significantly to the overall oxidation of Mn(II) (Allard et al., 2013).

Potassium permanganate is an even more effective oxidant; transforming Mn(II) rapidly even under heterogeneous conditions (Van Benschoten et al., 1992). At pH 7 and 1 mg/L $KMnO_4$, the half-life of Mn(II) oxidation is 6 seconds, as compared to 3.5 days for HOCl under the same conditions (Allard et al., 2013). This oxidation is sufficiently fast such that Mn(II) adsorption (Reaction 1.3) becomes the rate limiting step in the oxidation of Mn(II) by $KMnO_4$ (Van Benschoten et al., 1992), resulting in the oxidation mechanism described above being completed by:

$$>Mn(II)_{(s)} + 2KMnO_4 \xrightarrow{\text{very fast}} 3MnO_{2(S)} + O_2 + 2K^+ \qquad (1.5)$$

The fast oxidation of reduced Mn by these chemical oxidants could facilitate the *in situ* regeneration of passivated manganese oxide geomedia.

1.5.4 Adsorption of Metal Cations

Due to isomorphic substitutions and vacancies, manganese oxides typically exhibit low pH_{pzc} values (i.e., 1.5-6), where the pH_{pzc} is defined as the pH at which the total net particle charge, σ_p, is equal to zero as expressed by:

$$0 = \sigma_p = \sigma_{in} + \sigma_s = \sigma_{in} + \sigma_{is} + \sigma_{os} \quad \text{at } pH_{pzc} \qquad \text{(Eq. 1.3)}$$

where σ_{in} is the net structural charge, and σ_s is the net immobilized complex charge (i.e., the sum of the ion charge in the Stern layer from inner sphere (σ_{is}) and outer sphere (σ_{os}) complexes) (Sposito, 2008). This property results in a negative surface charge at environmentally relevant pH conditions (McKenzie, 1981).

Consequently, manganese oxides typically have a high affinity for metal cations. Manganese oxides strongly adsorb metal cations via both specific and non-specific interactions (Cao et al., 2015; McCann et al., 2015; Peña et al., 2010; Wan et al., 2015). The strength of metal cation adsorption generally increases as the pH at which the metal hydrolyzes (i.e., p^*K_1) decreases (Sposito, 2008).

Pb and Cd adsorb to manganese oxide via surface complexation (Wang and Stumm, 1987). The large ionic radii of Pb^{2+} and Cd^{2+} cause them to be poorly solvated and also gives them relatively labile, polarizable electron configurations, making them more likely to form covalent bonds with surface functional groups (Sposito, 2008). In particular, Pb forms dative pi bonds with the manganese oxide surface (Misono et al., 1967; Wan et al., 2015) and enters into the interlayer and tunnels of common manganese oxides, resulting in very strong adsorption (O'Reilly and Hochella, 2003). Pb can also be incorporated into the manganese oxide lattice (Villalobos et al., 2005).

Following the selectivity series of Group IIB metals, Zn is adsorbed less strongly than Cd. Despite its smaller ionic radius, Zn can form mononuclear inner-sphere complexes with the manganese oxide surface, but it is not incorporated into the manganese oxide structure, even under conditions resulting in coprecipitation of Zn and Mn minerals (Boonfueng et al., 2009).

Cu adsorbs to manganese oxides more strongly than Zn, following the trend of adsorptive affinity increasing with the Irving-Williams order (Irving and Williams, 1953; van Lienden et al., 2010). Cu also adsorbs more strongly than Cd, due to its transition metal electron configuration, which facilitates surface complexation (Liu et al., 2005; Sposito, 2008).

These adsorptive properties could make manganese oxide-coated sand an effective tool for removing metallic contamination from stormwater. However, the manganese oxide geomedia will eventually become saturated with inorganic adsorbates and lose its ability to remove toxic metal cations. It may be possible to regenerate the adsorption capacity of the geomedia *in situ* and collect the metals. This process would also mitigate the risk that metal contaminants could be desorbed due to intermittent flow, or due to a decrease in pH or increase in ionic strength

(e.g., as caused by deicing salts) (Adams et al., 2009; Mullane et al., 2015). There are many possible candidates for stripping metals from manganese-oxide geomedia. For example, a dilute solution of EDTA can form dissolved complexes with metals bound to the manganese oxide surface (Sun et al., 2001), though this chelating agent could also dissolve the Mn(IV) coating (Bromfield and David, 1978).

A dilute, inorganic acid might also displace adsorbed metals if the solution pH could be lowered to a value below the adsorption edge. The adsorption edge for adsorbates is often quantified by the pH_{50}, the pH value at which half of the maximum cation adsorption is achieved (Sposito, 2008). For adsorption on iron oxides, the pH_{50} values of Pb^{2+}, Cu^{2+} and Cd^{2+} follow the order $pH_{50,Pb} < pH_{50,Cu} < pH_{50,Cd}$, consistent with the general trend that pH_{50} decreases as the affinity of the adsorbate increases (Wang and Stumm, 1987). Therefore, it is likely that regeneration with acid will first cause the desorption of Zn and Cd, followed by Cu, and finally Pb. Because of the insolubility of manganese oxide (Gustafsson, 2014), this acidic regeneration could possibly be accomplished without substantial dissolution of the mineral.

1.6 Motivation and Research Objectives

1.6.1 Motivation and Intended Outcome

The widespread adoption of managed aquifer recharge systems capable of safely recharging urban stormwater will require inexpensive, reliable technologies for removing chemical contaminants. The research described in this dissertation focuses on the development, use and regeneration of manganese oxide-coated sand as an engineered geomedia for the removal of organic and metallic stormwater contaminants. While many properties of manganese oxides have been evaluated from the perspective of their role in biogeochemistry, their use for stormwater remediation and drinking water treatment are relatively poorly understood. Though this research focused on stormwater, manganese oxide geomedia could also be used to treat other source waters, including municipal wastewater effluent and agricultural runoff.

While structure-reactivity relationships for organic compounds in reaction with manganese oxides have been extensively studied, little is understood about the mineralogy-reactivity relationships of different phases of manganese oxides. This lack of understanding is relevant to natural and engineered systems. Changes to the structures and coordination environments of manganese oxide minerals as they undergo reduction or oxidation could affect their reactivity in nuanced ways. Engineers and chemists would benefit from insight into the dynamics of such changes.

This research is intended to improve knowledge of both applied and mechanistic aspects of manganese oxide-coated sand as communities adopt managed aquifer recharge. The results of this research advance the engineering and scientific understanding underpinning technology for managed aquifer recharge applications. My specific objectives are as follows:

1.6.2 Objective 1: Develop a simple approach to produce and regenerate manganese oxide-coated sand that can be used as reactive geomedia for organic contaminant oxidation

Although manganese oxides and manganese oxide-coated sands may be useful as reactive geomedia for treating organic contaminants, their synthesis often involves harsh conditions, such as high temperature or very low pH. Less extreme conditions for generating manganese oxide-coated sand would facilitate its production at the scale required for its use in water treatment applications. Additionally, manganese oxide-coated sand loses its reactivity with organic contaminants over time. The necessity of excavating failed geomedia would be costly to municipal utilities and could make the application of manganese oxide-coated sand infeasible. A method of *in situ* regeneration would obviate the need for expensive maintenance or replacement of geomedia.

To address this objective, methods of synthesizing highly reactive cryptomelane-coated sand and of regenerating its reactive capacity using HOCl were developed (Chapters 2 and 3). Approaches to synthesis and regeneration were conducted under conditions designed to simulate the application of manganese oxide-coated sand in stormwater infiltration systems and evaluated with spectroscopic and chemical analyses. Research indicated the reactivity and duration over which manganese oxides could provide stormwater treatment benefits in managed aquifer recharge systems. The insights obtained also contribute to a better understanding of manganese oxide mineralogy-reactivity relationships and the role of Mn(III)-rich oxides in the treatment and passivation process.

1.6.3 Objective 2: Evaluate the removal of metallic contaminants by manganese oxide-coated sand and develop a method of regenerating its metal sorption capacity

Stormwater contamination by metals poses threats to human and ecosystem health. Cu, Zn, Cd and Pb are of particular concern in stormwater due to their abundance and toxicity. Manganese oxides can adsorb metal cations, but their efficacy in the presence of solutes and significant NOM concentrations, such as in stormwater, is largely unknown. Furthermore, as an adsorptive treatment mechanism, the potential for geomedia failure due to saturation or desorption is a risk which, if unaddressed, could make manganese oxide-coated sand less desirable as a geomedia for metals-impacted stormwater.

In this research, the capacity of manganese oxide-coated sand to adsorb metals in stormwater was evaluated (Chapter 4). The treatment efficacy of the geomedia was evaluated in batch and column experiments conducted under conditions similar to those of stormwater infiltration systems. An acidic wash was used to remove adsorbed metals from the geomedia. After the metals were desorbed, the potential for reuse of the geomedia was evaluated. This study provides insights into the versatility of manganese oxide-coated sand as a geomedia for treatment of both metallic and organic contaminants in stormwater and in other impacted urban waters that could be used for managed aquifer recharge.

CHAPTER 2. Regeneration of Manganese Oxide-Coated Sand Reactivity by Oxidative Treatment

Some data herein collected by Duan, Y. and van Genuchten, C. M.

2.1 Introduction

Manganese oxides are capable of oxidizing organic contaminants, such as phenols and anilines (Laha and Luthy, 1990; Stone and Morgan, 1984), until they lose their reactivity due to changes in their surface properties (Balgooyen et al., 2017; Grebel et al., 2016). Although the ability of manganese oxides and manganese oxide-coated sand geomedia to oxidize organic contaminants makes them promising for engineered applications, their eventual loss of reactivity may limit their use in managed aquifer recharge or tertiary wastewater treatment (Forrez et al., 2010; Lin et al., 2013). The decline of reactivity may be due to the loss of reactive sites or the accumulation of reaction products on the mineral surface (Remucal and Ginder-Vogel, 2014). Therefore, a chemical treatment that oxidizes Mn(II/III) or that removes reaction products could restore the reactivity of passivated manganese oxide-coated sand. Chemical regenerants would facilitate the continued use in engineered systems of manganese oxide geomedia after its initial passivation without costly and labor-intensive media replacement (Dillon et al., 2009).

Although Mn(II) oxidation by dissolved oxygen is thermodynamically favored, the slow kinetics of the homogeneous reaction make it impractical for geomedia regeneration (Morgan, 2005). The abiotic Mn(II) oxidation process is typically autocatalytic, meaning that the initially-precipitated manganese oxide provides nucleation sites for the subsequent, more rapid oxidation of Mn(II) (Kessick and Morgan, 1975; Liu et al., 2012; Morgan, 1967). Although the catalyzed Mn(II) oxidation is faster than the homogeneous reaction, O_2 is a slow oxidant relative to other chemicals (Knocke et al., 1991a).

Several chemical oxidants could serve as potential *in situ* regenerants of the passivated geomedia. Permanganate has been shown to oxidize Mn(II) at pH values relevant to water treatment (Knocke et al., 1991b; Van Benschoten et al., 1992). H_2O_2 oxidizes Mn(II) to $MnOOH_{(S)}$ at high pH values, though it can reduce Mn(III) minerals at acidic pH values (Jacobsen et al., 1998; McKenzie, 1971; Reisz et al., 2008). Chlorine oxidizes Mn(II) to manganese oxide at a faster rate than O_2 (Hao et al., 1991; Van Benschoten et al., 1992), and hypobromous acid oxidizes Mn(II) to manganese oxide at faster rates than chlorine (Melichová et al., 2001). Small amounts of bromide, which is converted to HOBr by HOCl, significantly accelerate the rate of Mn(II) oxidation by HOCl (Allard et al., 2013). Mn(II) oxidation is also facilitated by the presence of carbonate and pH values above 8.5, because dissolved Mn(II) carbonate and hydrolysis species are stronger nucleophiles (Morgan, 2005). These effect may be important for engineered systems where geomedia regeneration could occur in the presence of low bromide concentrations or elevated pH values (Grebel et al., 2010).

While their ability to oxidize Mn(II) suggests that chemical oxidants that could regenerate failed manganese oxide geomedia, comparatively little research has been conducted on the oxidation of Mn(III)-rich manganese oxides. The oxidation mechanism for Mn(III) is distinct from Mn(II) oxidation and may be important to the regeneration of this geomedia (Murray et al., 1984; Webb et al., 2005).

If passivation were caused by the accumulation of adsorbed Mn^{2+} or organic reaction products, chemicals that do not oxidize Mn(II/III) might regenerate the oxidation capacity of the failed manganese oxide (Lin et al., 2009). For example, fouling by organic compounds could be ameliorated by treatment with a water miscible solvent. Exposure to acid could result in the release of adsorbed Mn^{2+} or the dissolution of precipitated carbonate minerals (e.g., $MgCO_{3(S)}$) (Duckworth and Martin, 2003).

The objective of this research was to determine the effectiveness of chemical treatments for regenerating the capacity of passivated manganese oxide-coated sand to oxidize organic contaminants. H_2O_2, $KMnO_4$, HOCl, HOBr, HCl and methanol were tested for their ability to restore reactivity to the geomedia. The use of a chemical treatment to restore activity to manganese oxide-containing geomedia *in situ* would facilitate the reuse of this material in engineered applications such as managed aquifer recharge systems, without the need for expensive removal and replacement of the geomedia.

2.2 Materials and Methods

All chemicals used in the synthesis and regeneration of manganese oxide-coated sand or for producing simulated stormwater were used as received from Fisher Chemical without further purification. Ultrapure water from a Milli-Q system (R = 18.2 MΩ) was used for all dilutions and syntheses. All experiments were performed at room temperature (21 ± 2 °C).

Manganese oxide-coated sand was synthesized with a modified version of the cryptomelane synthesis method developed by McKenzie, as described in Chapter 3 (McKenzie, 1971). Manganese oxide-coated sand (20 g) was packed in glass columns with polyethylene fittings (16-mm inner diameter) to a height of 72 mm. The porosity of a packed column was 0.33 and the pore volume was 4.78 mL. The columns were operated under saturated upwards flow conditions at 0.4 mL/min (equivalent to an infiltration rate of 9.5 cm/h, which is a typical infiltration rate for stormwater infiltration systems) (Hatt et al., 2008). A NaBr tracer test (Figure 2.1) demonstrated an average hydraulic residence time within the column of 17.0 min and a variance of 11.5 min^2, with little, if any, short circuiting due to edge effects.

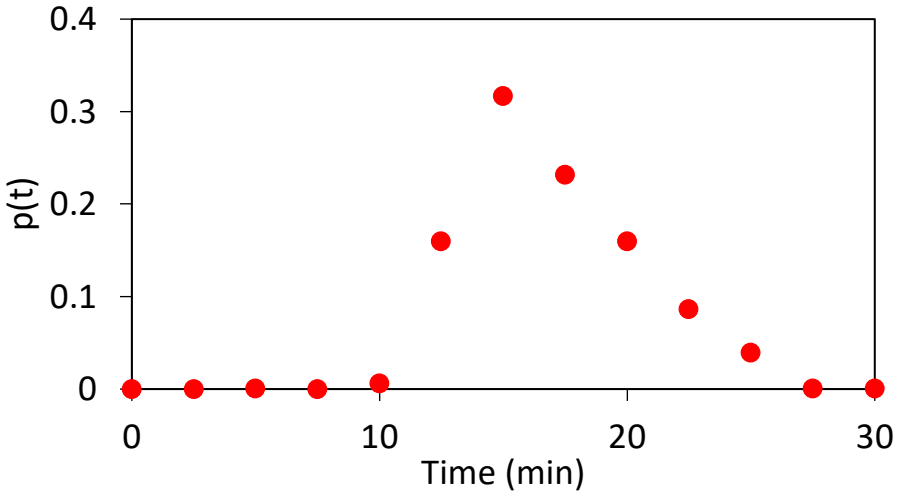

Figure 2.1 Probability density function of Br^- effluent from column during tracer test.

The Péclet number (Pe) can be derived from the first moment of the axial dispersion model, where the average hydraulic residence time is the first moment of tracer residence time and θ is the ideal plug flow reactor residence time (i.e., V/Q) (Hunt, 2013, p. 106):

$$\int_0^\infty t\, p(t)dt = \theta\left(1 + \frac{2}{Pe}\right) \qquad \text{(Eq. 2.1)}$$

The Péclet number was derived in this system:

$$17.00\ min = \frac{4.78\ mL}{0.40\ mL/min}\left(1 + \frac{2}{Pe}\right) \xrightarrow{yields}\ Pe = 4.73 \qquad \text{(Eq. 2.2)}$$

This result (i.e., Pe > 1) demonstrated that advection dominated dispersion in the hydraulics of this system, and that a plug flow model is not unreasonable (Hunt, 2013, p. 87).

The geomedia was reacted with 5 µM bisphenol A in pH 7, NOM-free simulated stormwater (Table 1.3) for approximately 1300 pore volumes (262 hours), until C/C_0 for bisphenol A exceeded 0.80, and then flushed with Milli-Q water for 10 pore volumes (2 hours), as detailed in Chapter 3.

Within 24 hours the failed geomedia was removed from columns, homogenized and air dried at 30 °C. The dried geomedia was stored under N_2 in an amber glass container for no more than 2 weeks before use in batch regeneration experiments. The failed manganese oxide-coated sand was regenerated in batches at pH 6, 8 and 10 (± 0.2) with various concentrations of either H_2O_2, $KMnO_4$, HOCl, HOBr or a mixture of HOCl and HOBr ("HOX") such that $\frac{[Br]}{[Cl]} = 0.1$. Methanol and trace metals-grade HCl (pH 2 and 3) were also evaluated for regeneration capacity.

For each regenerant tested, 3.25 g of failed geomedia was treated with 10 mL of regenerant solution in amber glass borosilicate bottles which were constantly stirred on a tube

rotator for 24 h. Oxidative regenerant solutions were buffered at pH 6 with 10 mM sodium acetate and at pH 8 and pH 10 with 10 mM sodium borate. Batch regeneration with the oxidants was conducted at 10% stoichiometric excess. Stoichiometric oxidant demand was calculated as the e^- equivalents required to return the Mn on the failed geomedia to an average oxidation state of +4.0. The Mn coating density of the geomedia was quantified by dissolving the manganese-oxide coating of a 0.5 g geomedia sample in 10 mL of 30 mM ascorbic acid and quantifying dissolved Mn by ICP-MS. The iodometric titration method was used for chemical determination of the average Mn oxidation state (Murray et al., 1984). Geomedia samples were rinsed with Milli-Q water three times to remove residual regenerant and dried at 30 °C prior to analysis. Using the same procedure, geomedia was regenerated with at pH 10 HOCl, HOBr or HOX at 11%, 55%, 550% or 1100% of the stoichiometric oxidant demand, and with HCl and methanol. HOCl, HOBr and $KMnO_4$ were quantified by the DPD method using a Shimadzu UV-2600 UV-Vis Spectrophotometer (Moberg and Karlberg, 2000). H_2O_2 was quantified by the Ti(IV) oxalate method (Sellers, 1980). Samples of the regenerant solution were filtered through a nylon 0.22-μm syringe filter and immediately analyzed for oxidant concentration.

To control for the effects of pH on reactivity, the failed geomedia was treated with the applicable buffers but no chemical oxidants. To control for the effects of oxidants, uncoated acid-washed sand was treated with the chemical oxidants. Neither treatment produced reactive geomedia.

Geomedia reactivity was evaluated in triplicate batch experiments in which an excess of manganese oxide was present. Under these conditions, bisphenol A exhibited first-order decay ($r^2 \geq 0.98$) over 3 to 5 half-lives (depending on geomedia reactivity). In these experiments, 1 g of manganese oxide-coated sand was stirred on a tube rotator for 90 minutes in a sealed 25 mL amber glass vial with 20 mL of pH 7 simulated stormwater containing 5 μM bisphenol A. The observed pseudo-first order rate constant, k', is equal to the product of the second-order rate constant, k_{BPA}, and the concentration of the Mn-oxide, $C_{MnOxide}$:

$$-\frac{dC_{BPA}}{dt} = k' * C_{BPA} = k_{BPA} * C_{MnOxide} * C_{BPA} \quad \text{(Eq. 2.3)}$$

Samples were analyzed for bisphenol A concentration with an Agilent 6460 high performance liquid chromatography tandem-mass spectrometry system in the electrospray ionization mode using a previously described method (Grebel et al., 2016).

Mn K-edge X-ray absorption spectroscopy (XAS) data were collected at beam line 4-1 of the Stanford Synchrotron Radiation Lightsource. Spectra were recorded at liquid nitrogen temperature (i.e., 77 K) in fluorescence mode out to k of 12.5 $Å^{-1}$ as described in Chapter 3. The fractions of Mn(II), Mn(III) and Mn(IV) in the samples were quantified with the SixPack software using linear combination fits of the spectra of reference standards of aqueous Mn(II), α-Mn_2O_3 and δ-MnO_2 obtained from a previous study (van Genuchten and Peña, 2017; Webb, 2005). Negative components were not allowed and the sum of the components was not constrained to 1.0. The abundances of each oxidation state summed to slightly less than 100%, likely due to small differences between the coordination environment of the Mn(II), Mn(III) and Mn(IV) in the geomedia and in the reference standards.

2.3 Results and Discussion

The virgin geomedia had a reaction rate constant with bisphenol A of $k_{BPA,virgin}$ = 12.1 ± 2.0 L/(g MnOxide•h) (Figure 2.2). This rate constant is approximately an order of magnitude faster than the reaction rate constants of bisphenol A with manganese oxide-coated sands synthesized by other methods (Grebel et al., 2016; Lin et al., 2013). The failed gomedia was almost completely unreactive with bisphenol A in batch experiments, with $k_{BPA,failed}$ = 0.03 ± 0.01 L/(g MnOxide•h).

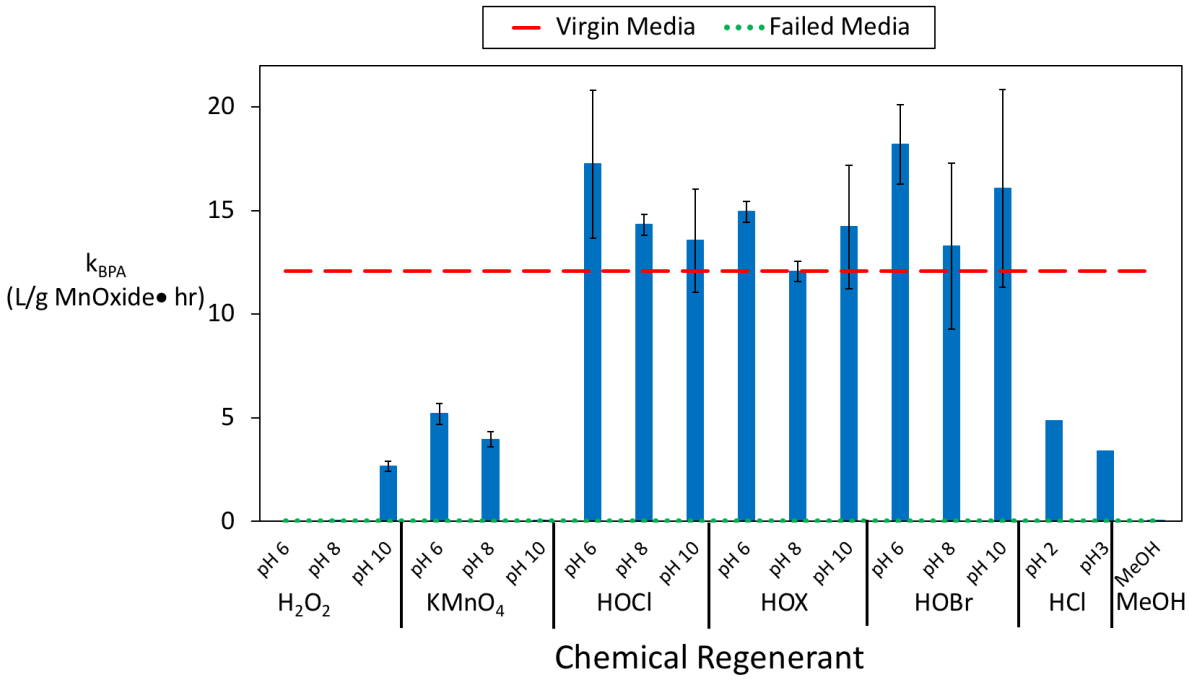

Figure 2.2 Second-order reaction rate constants of bisphenol A with manganese oxide-coated sands regenerated under various chemical conditions. The rate constants of virgin manganese oxide-coated sand (red dashed line) and failed manganese oxide-coated sand (green dotted line) are provided for comparison.

Iodometric titration determined that the virgin geomedia had an average oxidation state of +3.94 ± 0.07 which decreased to +3.76 ± 0.05 in the failed geomedia. This decrease of 0.18 in average Mn oxidation state measured by titration was slightly less than that measured by XANES. Linear combination fits (Table 2.2) of the Mn K-edge XANES spectra (Figure 2.3) indicated that Mn(IV) made up 89.0% of the Mn in the virgin geomedia coating and decreased to 80.2% in the failed geomedia. Mn(III) made up 6.4% of the Mn in the virgin geomedia coating and increased to 10.3% in the failed geomedia. Mn(II) did not comprise a significant portion of the Mn in any sample. These XANES results suggest a decrease of between 0.24 and 0.38 in average Mn oxidation state.

Table 2.1 XANES Linear Combination Fits to estimate the distribution of Mn oxidation states following batch regeneration.

	XANES Linear Combination Fit			
Sample	Mn(II)	Mn(III)	Mn(IV)	R-Factor
Virgin Geomedia	< 0.01	0.064	0.890	0.0011
Failed Geomedia	< 0.01	0.103	0.802	0.0008
H_2O_2 pH 10 Regen	< 0.01	0.081	0.830	0.0013
$KMnO_4$ pH 6 Regen	< 0.01	0.045	0.891	0.0017
HOCl pH 6 Regen	< 0.01	0.059	0.881	0.0014
HOBr pH 6 Regen	< 0.01	0.053	0.858	0.0014
HCl pH 2 Regen	< 0.01	0.064	0.888	0.0011
Methanol Regen	< 0.01	0.088	0.806	0.0009

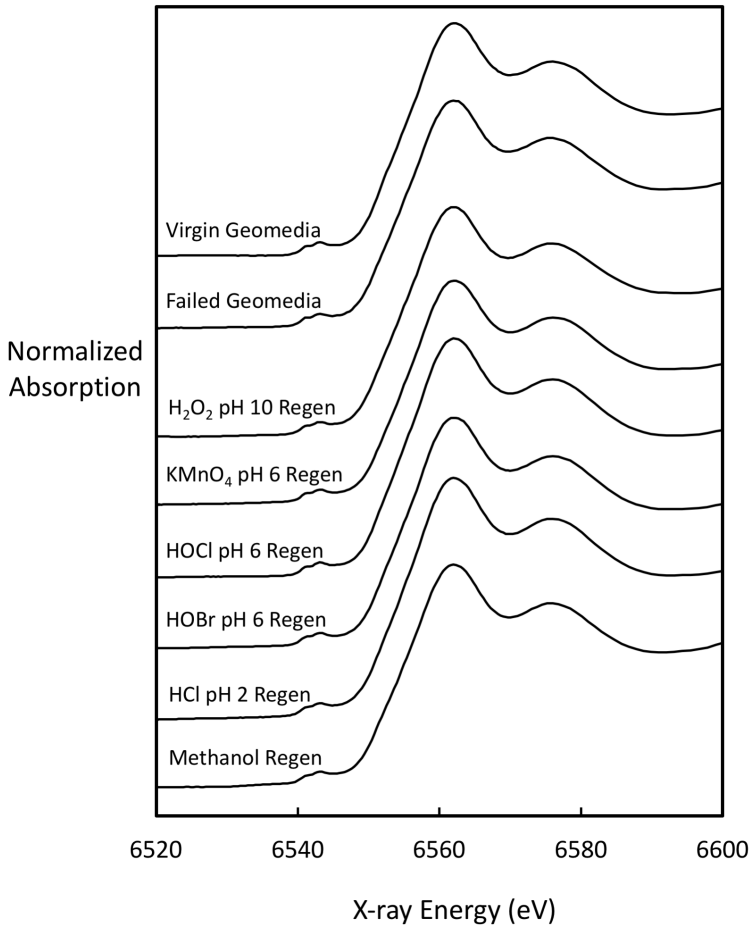

Figure 2.3 Mn K-edge XANES spectra of virgin and failed geomedia and of geomedia regenerated in batch.

The chemical regenerants produced manganese oxide-coated sand of greatly varying reactivity. H_2O_2 did not restore any reactivity when applied to the failed geomedia at pH 6 or pH 8; however, at pH 10 about 20% of the reactivity with bisphenol A was restored. All of the H_2O_2 was consumed during the 24 h regeneration period under all pH conditions. H_2O_2 may have been a more effective oxidant at high pH due to the prevalence of Mn(II) hydrolysis species (i.e., $MnOH^+$ and $Mn(OH)_2^0$) and small amounts of carbonate-complexed Mn(II) (e.g., $Mn(CO_3)_2^{2-}$), which undergo oxidation 1 to 2 orders of magnitude faster than Mn^{2+} (Allard et al., 2013; Morgan, 2005).

The negligible differences in the reactivities of failed and H_2O_2-treated geomedia are reflected in their similar average Mn oxidation states. Iodometric titration measurements indicated that treatment with H_2O_2 at pH 10 did not significantly increase the average Mn oxidation state of the failed geomedia. Linear combination fits of the XANES spectra indicated that Mn(IV) comprised 83.0% of Mn in the regenerated geomedia compared to 80.2% in the failed geomedia. Mn(III) comprised 10.3% of Mn in the failed geomedia compared to 8.2% in the geomedia treated with H_2O_2. Together these results imply that H_2O_2 treatment did not significantly change the coordination environment of the failed manganese oxide.

Despite the fact that $KMnO_4$ was used in the synthesis of the virgin geomedia, it did not restore reactivity when applied at pH 10, but did restore about 40% of reactivity at pH 6 and 8. This result is likely due to electrostatic repulsion between the negatively charged geomedia surface and the MnO_4^- anion at high pH, inhibiting electron transfer between the two. All of the $KMnO_4$ was consumed during the 24 h regeneration under all pH conditions.

The average oxidation state of the regenerated geomedia corresponded to its reactivity. Iodometric titrations indicated that regeneration by $KMnO_4$ at pH 6 and pH 8 both increased average Mn oxidation states to +3.87± 0.05. The linear combination fit of the geomedia regenerated with $KMnO_4$ at pH 6 indicated that the amount of Mn(III) dropped by more than half, from 10.3% to 4.5%, while the share of Mn(IV) increased from 80.2% to 89.1%–levels comparable to that of the virgin geomedia. The EXAFS spectrum of the geomedia regenerated with $KMnO_4$ indicates that significant changes in Mn coordination environment occurred during regeneration (Figure 2.4). Manganese oxide EXAFS spectra have a large characteristic peak centered around k = 6.5 $Å^{-1}$ (arrow in Figure 2.4) (Manceau and Combes, 1988). This feature has a similar shape in the virgin geomedia and geomedia regenerated with $KMnO_4$. The EXAFS spectrum also exhibits a double beat feature from k = 7-8 $Å^{-1}$ (* symbol in Figure 2.4), which is indicative of a local coordination environment similar to that of cryptomelane (Kim et al., 2011).

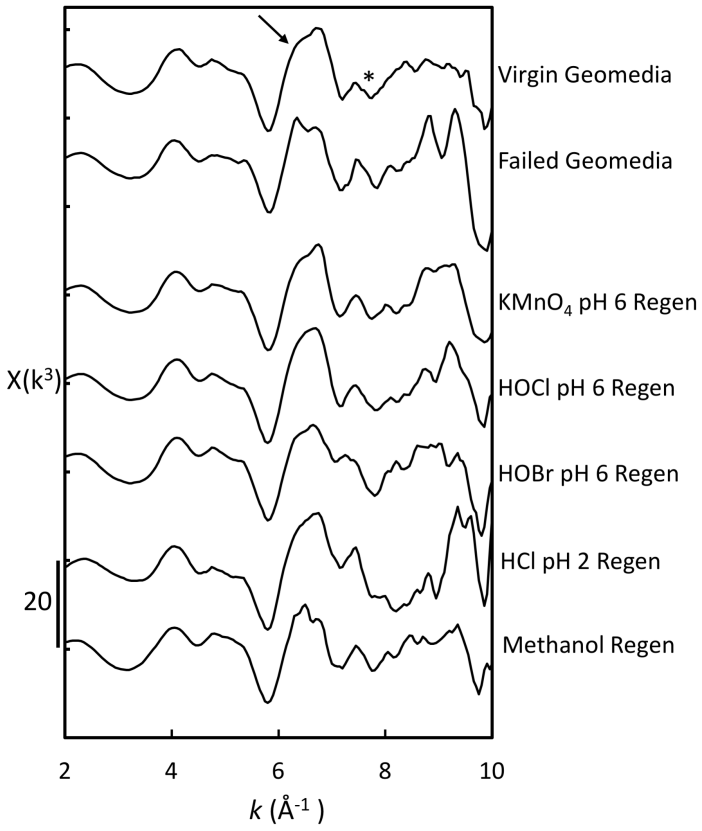

Figure 2.4 The Mn K-edge EXAFS spectra of virgin, failed and regenerated manganese oxide-coated sand geomedia.

The hypohalites were the most effective regenerants tested; all of the hypohalites restored geomedia reactivity with bisphenol A to approximately that of the virgin geomedia (Figure 2.2). Iodometric titration found that geomedia regenerated with HOCl had an average oxidation state of +3.92 ± 0.1. This result was corroborated by XANES linear fits, which found that regeneration with HOCl and HOBr raised the portion of Mn(IV) present in the geomedia coating from 80.2% to 88.1% and 85.8%, respectively. Mn(III) prevalence decreased from 10.5% to 5.9% and 5.3%, respectively.

Treatment with HOCl and HOBr produced geomedia coatings with similar EXAFS spectra. Each exhibited the "staircase" pattern from k = 4-5 $Å^{-1}$ that is characteristic of manganese oxides and humpbacked asymmetry in the large feature at k = 6.5 $Å^{-1}$, similar to that seen in cryptomelane. The feature at k = 6.5 $Å^{-1}$was rounded, as seen in the virgin geomedia, rather than displaying the prominent shouldering seen in the failed geomedia. The geomedia regenerated with hypohalites also had a second feature at k = 7.5 $Å^{-1}$, which is similar to the peak observed in the virgin geomedia but distinct from the double beat feature seen in cryptomelane. All of the hypohalite regenerant was consumed during the 24 h regeneration regardless of pH or relative bromine abundance. There were no clear trends in the reactivity of the regenerated phases produced at different pH values or bromide abundances. These results support the hypothesis that the hypohalites generated similar phases of manganese oxide, despite differences in the rate of manganese oxidation due to differences in pH and bromide concentration (Allard et al., 2013).

Treatment with both permanganate and the hypohalites significantly raised the average oxidation state of the geomedia coating. Nonetheless, the geomedia regenerated with the hypohalites had comparable reactivity to the virgin geomedia, while the geomedia regenerated with $KMnO_4$ was less reactive. This result suggests that while the average oxidation state is a useful indicator of the reactivity of manganese oxides with organic compounds, it does not capture all of the factors affecting the reactivity of the manganese oxide phase. Differences in mineral structure, in addition to oxidation state, are likely important to manganese oxide reactivity. The density of vacancy sites and Mn(III) groups on the manganese oxide surface can explain some of the variations in reactivity with organic compounds observed between different manganese oxide minerals (Hou et al., 2014; Villalobos et al., 2014). Many studies have investigated the degradation of different organic compounds by a single type of manganese oxide, yet little research has investigated the relative oxidation rates of a single organic compound by multiple, well-characterized polymorphs of manganese oxide (Remucal and Ginder-Vogel, 2014). Such research could provide valuable insight into how manganese oxide structural characteristics, including vacancy site density, long-range order and local coordination environment of reactive sites, influence the reactivity of the mineral.

Varying oxidant concentrations resulted in similar reactivities of the geomedia regenerated with HOCl or HOBr (Figure 2.5). No reactivity with bisphenol A was regenerated after dosing failed geomedia with 11% of the stoichiometric oxidant demand, and only a modest amount of reactivity was regenerated after treatment with regenerants that met 55% of the oxidant demand. However, when there was enough HOCl or HOBr to fully oxidize the Mn on the failed geomedia, the regenerated geomedia showed similar reactivity to that of the virgin geomedia. Though there was a trend of slightly increased reactivity when the oxidant dose exceeded the stoichiometric demand, this effect was small relative to the effect of fully oxidizing the Mn in the failed geomedia. These data again suggest that higher average oxidation states of manganese oxides can result in greater reactivity with organic compounds, but so long as the Mn is fully oxidized, the rate at which passivated Mn is oxidized has little impact on the reactivity of the resultant mineral.

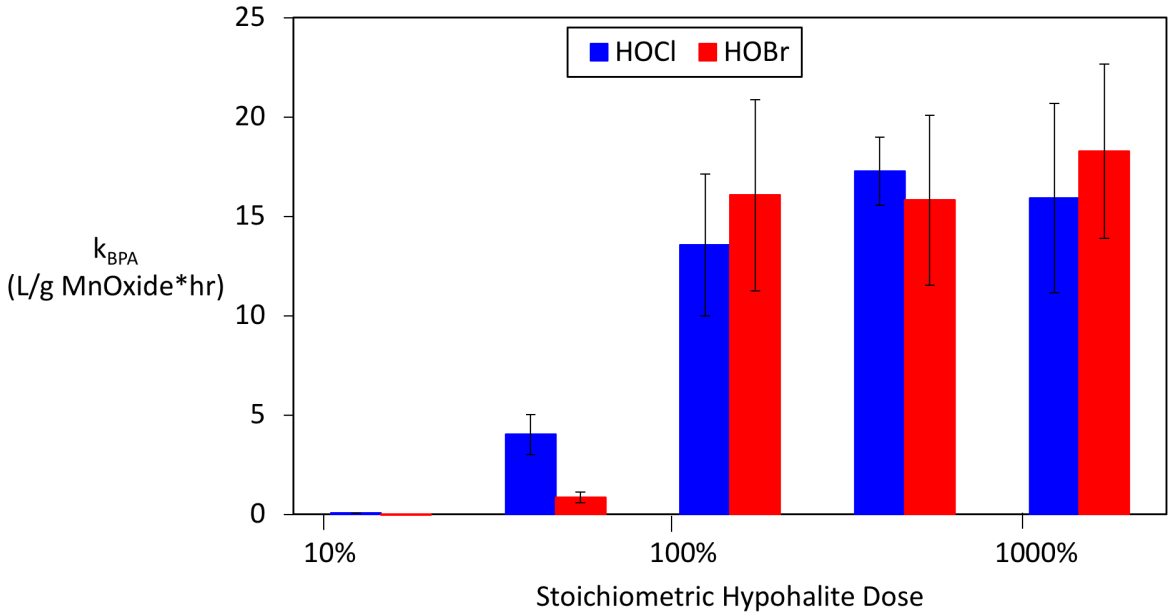

Figure 2.5 Second-order reaction rate constants for the oxidation of bisphenol A by manganese oxide-coated sands regenerated with various doses of hypohalites (log scale). Stoichiometric oxidant demand was calculated as the e- equivalents required to raise the mass of Mn on the failed geomedia to an average oxidation state of +4.0.

Treatments with regenerants that did not oxidize Mn(II/III) were less effective in restoring reactivity than treatments with oxidants. Regeneration with HCl at pH 2 and pH 3 restored about 25% of the reactivity of the failed geomedia. This may have been due to the dissolution of Mn(III) groups, which are more soluble than Mn(IV) (Kozawa and Yeager, 1965; Trouwborst, 2006). The XANES spectrum of the geomedia regenerated by HCl at pH 2 shows an increase in average Mn oxidation state, with the proportion of Mn(IV) increasing from 80.2% to 88.8%, and Mn(III) decreasing from 10.3% to 6.4%. Because reduced forms of Mn diminish manganese oxide reactivity (Balgooyen et al., 2017), the increase in average Mn oxidation state and changes in crystal structure may have generated a more reactive manganese oxide phase.

Another possible explanation for the increase in reactivity after treatment with acid is ion exchange of protons with Mn^{2+} on the surface of the failed geomedia. Less than 2% of the Mn present in the failed geomedia was ion-exchangeable, yet this species may have contributed to passivation due to its large inhibitory effect on the oxidation of organics (Barrett and McBride, 2005). To test the impact of adsorbed Mn^{2+}, failed geomedia was washed with 100 mM $MgCl_2$ solution, which removed 72% of the adsorbed Mn^{2+} (as compared to a wash with 100 mM $CaCl_2$), yet no reactivity was restored to the geomedia. Given the minimal inhibitory effect of Mg^{2+} on manganese oxide reactivity relative to that of Mn^{2+}, most of the reactivity would be restored to the geomedia if ion-exchangeable Mn^{2+} was a major contributor to passivation (Lin et al., 2009).

Treatment with methanol did not restore any reactivity to the failed geomedia, further confirming the hypothesis that sorbed bisphenol A or transformation products did not

meaningfully contribute to the failure mechanism observed. XANES linear combination fits suggest that the oxidation state of the failed geomedia was little changed by regeneration with methanol. After methanol treatment, the Mn(IV) remained just 80.6% of the total Mn, while Mn(III) was 8.8%. The EXAFS data likewise suggest that there was little change in the Mn coordination environment due to treatment with methanol. The spectra for the failed geomedia and the geomedia treated with methanol are similar, with large peaks at k = 6.5 $Å^{-1}$ that demonstrate distinctive shouldering on the right side of the peak.

Several conclusions can be drawn from this research, which screened the efficacy of chemical regenerants of manganese oxide-coated sand. First, the most effective regenerants restored nearly all Mn to the Mn(IV) oxidation state. Both the virgin geomedia and geomedia regenerated with HOCl had an average Mn oxidation state greater than +3.90, while the failed geomedia had an average Mn oxidation state of +3.76 ± 0.05. Secondly, the reactivity of the manganese oxide was not solely dependent on its average oxidation state. Though the geomedia regenerated by $KMnO_4$ and HCl had significantly higher average Mn oxidation states than the failed geomedia, they did not have the same reactivity as the virgin geomedia or geomedia regenerated with hypohalites. This result implies that mineral structure is also important to reactivity. Finally, the results of reactivity tests and the X-ray absorption spectroscopy data suggest that all treatments with hypohalites produced a similar, highly oxidized phase, so long as they were applied in sufficient abundance. Because stoichiometric excess of the oxidant, pH, and Br/Cl ratio did not significantly alter the regenerated phase, these data suggest that this highly reactive phase was produced in reaction with hypohalites at various rates of Mn oxidation.

As previously discussed, the oxidation of Mn(III)-rich oxides may be more relevant to this system than the oxidation of Mn(II) because Mn(II) did not accumulate on the surface of the failed geomedia in large amounts. Unfortunately, such reactions have not been extensively studied (Webb et al., 2005). Determination of the mechanisms of Mn(III)-oxide oxidation, independent of the oxidation of Mn(II), could provide insight into the reasons for increased reactivity in manganese oxide-coated sand treated with hypohalites and the relatively lower reactivity of geomedia treated with other oxidants.

Practically, the results of these screening tests suggest that subsequent research should pursue the use of HOCl and other hypohalites as chemical regenerants of manganese oxide-coated sand geomedia. Such treatments could restore the reactivity of passivated geomedia in a simple, cost-effective manner.

CHAPTER 3. Chemical Regeneration of Manganese Oxide-Coated Sand for Oxidation of Organic Stormwater Contaminants

Reproduced with permission from Charbonnet, J.A.; Duan, Y.; van Genuchten, C. M.; Sedlak, D. L. Chemical Regeneration of Manganese Oxide-Coated Sand for Oxidation of Organic Stormwater Contaminants. *Environmental Science & Technology* **2018** DOI: 10.1021/acs.est.8b03304

3.1 Introduction

Many water-stressed cities are considering investments in aquifer recharge projects in which urban stormwater, municipal wastewater effluent or water from other potentially contaminated sources is intentionally percolated into a drinking water aquifer (Bradshaw and Luthy, 2017; Daigger, 2009; Page et al., 2014). However, urban stormwater contains low concentrations (i.e., typically less than 10 μg/L) of trace organic contaminants derived from asphalt, automobile wear and exhaust, biocides and consumer products that could be deleterious to human and ecosystem health (Grebel et al., 2013; Jasper et al., 2013; Makepeace et al., 1995) and municipal wastewater effluent contains low concentrations of organic compounds (e.g., pharmaceuticals, personal care products and urban use pesticides) (Bolong et al., 2009; Clara et al., 2005). Consequently, aquifer recharge has the potential to contaminate groundwater with trace organic compounds (Andres et al., 2018; Page et al., 2010).

During managed aquifer recharge, captured water is often percolated through gravel or sand (Dillon et al., 2009; Pitt et al., 2012). Manganese oxides are naturally occurring minerals that are capable of oxidizing many organic contaminants that contain electron-rich moieties, including substituted phenols, anilines, and thiols (Laha and Luthy, 1990; Lin et al., 2009; Stone, 1987). Therefore, the introduction of manganese oxides as geomedia in an infiltration system could provide an inexpensive means of treating organic contamination during the recharge process (Hatt et al., 2008; Lin et al., 2013).

Bisphenol A ($C_{15}H_{16}O_2$) is a contaminant of concern in stormwater and municipal wastewater effluent due to its potential impacts on the endocrine system (Vandenberg et al., 2007). The reactions of bisphenol A with manganese oxides have been well-characterized (Im and Löffler, 2016). In the initial step of the oxidation process, bisphenol A forms a surface complex with a Mn(IV)-OH group which then undergoes a one-electron transfer, reducing Mn(IV) sites to Mn(III) and Mn(III) sites to Mn(II) (Stone, 1987; Zhang et al., 2008). The phenolate radical produced in the initial reaction can either diffuse away from the surface and react with other radicals to produce polymeric compounds, or react again with the manganese oxide surface (Im et al., 2015; Remucal and Ginder-Vogel, 2014).

To exploit these reactions during managed aquifer recharge, manganese oxide-coated sand is preferable to pure manganese oxide minerals because of its higher hydraulic conductivity and lower propensity for transport away from the surficial layer of the infiltration basin (Liu et al., 2005). After exposure to organic contaminants and other natural constituents (e.g., Ca^{2+}, NOM) the reactivity of manganese oxide-containing geomedia decreases (Grebel et al., 2016). This passivation process appears to be related in part to the reduction of Mn(IV) sites and subsequent accumulation of Mn(II/III) (Balgooyen et al., 2017; Lin et al., 2013). Re-oxidation of Mn(II) by atmospheric O_2 is unlikely to restore the reactivity of the geomedia due to its slow kinetics under environmentally relevant conditions (Von Langen et al., 1997). Biogenic production of a reactive manganese oxide phase (i.e., enzymatic catalysis of Mn(II) oxidation by O_2) is possible, but it would be difficult to implement and control in field applications (Learman et al., 2011). It may be possible, however, to restore the reactivity of passivated geomedia with a chemical oxidant. Such a process could facilitate the *in situ* regeneration of the reactivity of the manganese oxide-coated sand, obviating the need for costly excavation, and making the use of this engineered geomedia less expensive and more practical.

The objective of this research was to develop a simple approach to produce and regenerate manganese oxide-coated sand that can be used as reactive geomedia for oxidizing organic contaminants. By understanding the mechanisms and rates of the geomedia passivation through spectroscopic and chemical analysis, it was possible to gain insight into approaches that could be used to prolong the useful lifetime of the geomedia and regenerate its activity after failure.

3.2 Materials and Methods

3.2.1 Reagents and Simulated Stormwater

All chemicals used in the synthesis and regeneration of manganese oxide-coated sand or for producing simulated stormwater were used as received from Fisher Chemical without further purification. A d-14 bisphenol A internal standard was obtained from Polymer Source, Inc. Ultrapure water was produced with a Milli-Q system (R = 18.2 MΩ) and was used for all dilutions and for geomedia synthesis. All experiments were performed at room temperature (21 ± 2 °C).

Simulated stormwater was made as described by Grebel et al., 2016 (Table 1.3) which exhibited similar performance to that observed in authentic stormwater. The simulated stormwater had pH 7.0 ± 0.1, contained 1 mM total inorganic carbon and had an ionic strength of 4.5 mM. NOM was not added to the simulated stormwater. Previous research indicated that NOM concentrations typical of stormwater (i.e., 10 mg-C/L) result in only a modest decline in bisphenol A removal in both simulated and authentic stormwater (Grebel et al., 2016).

3.2.2 Manganese Oxide-Coated Sand

Manganese oxide-coated sand was synthesized by modification of the cryptomelane synthesis method described by McKenzie (1971), which is similar to that reported by Lin et al. (2013). Fisher Ottawa sand sieved to 20-30 mesh (595-841 μm) (100g) was washed in 1 N nitric acid for 24 hours. The sand was subsequently rinsed with Milli-Q water until the pH of the rinse effluent was above 6.0. After air drying, the sand was added to 250 mL of 2 N acetic acid containing 0.5 M $MnSO_4$ in a 1L beaker. The sand was stirred vigorously with a magnetic stir bar as 200 mL of 0.43 M potassium permanganate solution was added drop-wise over 30 minutes. The mixture was continuously stirred for an additional 90 minutes and allowed to settle overnight. After settling, the supernatant was decanted and the coated sand was air dried at 30 °C. The dry sand was sieved with 40 mesh and rinsed with Milli-Q water five times to remove loose manganese oxide and then re-dried prior to use in experiments. When not in use, all geomedia was stored in sealed amber glass bottles under N_2 at room temperature.

3.2.3 Geomedia Longevity Tests

Four replicate glass columns with polyethylene fittings (16-mm inner diameter) were packed with 20 g of manganese oxide-coated sand to a height of 72 mm. Prior to packing, columns and tubing were washed by flushing with a 1% HCl solution followed by Milli-Q water. Columns were operated with saturated upwards flow using a peristaltic pump and Tygon and PTFE tubing to deliver the simulated stormwater. Simulated stormwater containing 5 μM bisphenol A was pumped through the columns at 0.4 mL/min, equivalent to an infiltration rate of 9.5 cm/h. Geomedia from one sacrificial replicate column was analyzed 98 hours (approximately 500 pore volumes) into the longevity test. Column performance was monitored until the effluent bisphenol A exceeded 80% of influent concentration, at which point a plateau in performance occurred, and the geomedia was deemed failed (Grebel et al., 2016). Failed geomedia was rinsed with Milli-Q water for 2 hours (10 pore volumes) to remove any residual organic compounds, then left in columns with ends capped for no more than three days.

Bisphenol A was quantified by an Agilent 6460 high performance liquid chromatography tandem-mass spectrometry (HPLC/MS-MS) system with electrospray ionization. Liquid chromatography was performed using an Agilent Zorbax SB-C18 column with 2.1 mm × 50 mm dimensions and 3.5 μm pore size. A mobile phase flow rate of 0.3 mL/min was used with 100 μL sample injection volumes.

Total and dissolved manganese in the effluent were measured with unfiltered and 0.22-μm syringe-filtered samples, respectively. Samples were collected in plastic centrifuge tubes (1 mL) and immediately acidified by the addition of a solution of 1% HCl and 0.5% HNO_3 (4 mL) before quantification by an Agilent 7700 Series Inductively Coupled Plasma-Mass Spectrometer (ICP-MS).

3.2.4 Geomedia Regeneration

To determine the viability of *in situ* regeneration, failed geomedia was left undisturbed following longevity tests and regenerated in columns. A solution of 0.31 mM HOCl buffered with 10 mM sodium acetate at pH 6 was applied at 0.4 mL/min over 50 hours (i.e., five times the stoichiometric demand of e^- equivalents required to oxidize the Mn(II/III) on the failed geomedia to Mn(IV)). Geomedia from one sacrificial replicate column was analyzed 10 hours (50 pore volumes) into the longevity test, when stoichiometric demand was met. Regenerated geomedia was rinsed with Milli-Q water for 2 hours (10 pore volumes) after treatment to remove any residual regenerant, then left in the columns with ends capped for no more than two days. HOCl was quantified by the DPD method using a Shimadzu UV-2600 UV-Vis Spectrophotometer (Moberg and Karlberg, 2000).

3.2.5 Geomedia Characterization

The Mn coating density of the geomedia was quantified by dissolving the manganese-oxide coating of a 0.5 g sample with 10 mL of 30 mM ascorbic acid and quantifying dissolved Mn by ICP-MS. Average Mn oxidation state was determined by the iodometric titration method

(Murray et al., 1984). Ion-exchangeable Mn was quantified by stirring 0.25 g of manganese oxide-coated sand in a 25 mL solution of 100 mM $CaCl_2$ overnight, then sampling through a 0.22 μm filter and quantifying Mn by ICP-MS.

The pH_{pzc} of the manganese oxide-coated sand was determined by sonicating 1 g of the geomedia in 5 mL Milli-Q water for 3 minutes to remove the coating. A 10 μL aliquot of the coating material suspension was mixed with up to 990 μL of dilute HCl to produce various pH conditions. The zeta potential was immediately measured using a Malvern Zetasizer Nano. A linear fit of zeta potential vs. pH was used to determine the pH_{pzc}.

X-ray diffraction (XRD) analysis was performed with a D8 Discover GADDS Powder XRD with a Fine-Focus Sealed Source (Cu-Kα radiation). To remove interference by the sand substrate, 3 g of sand was sonicated in 10 mL acetone for 5 min to remove the coating. The suspended manganese oxide in the supernatant was evaporatively deposited dropwise onto a zero-background SiO_2 sample holder.

Scanning electron microscopy was performed with a Zeiss EVO MA10 scanning electron microscope at 20 kV and a 1 nA current. Energy dispersive X-ray spectroscopy (EDS) was performed with a EDAX Genesis Imaging/Mapping analyzer.

Mn K-edge X-ray absorption spectroscopy (XAS) data were collected at beam line 4-1 of the Stanford Synchrotron Radiation Lightsource. Data were collected at liquid nitrogen temperature (i.e., 77 K) in transmission and fluorescence modes out to a k value of 12.5 $Å^{-1}$. Transmission data were collected using ion chambers for measurements of I_0 and I_t, while fluorescence data were collected using a PIPS detector. Due to the relatively low Mn concentration and the heterogeneous nature of the samples (Mn-rich coating, SiO_2 core), the fluorescence data were of superior quality and were thus used in data analysis. The monochromator was detuned 50% to prevent second-order harmonics and the fluorescence data were collected using a PIPS detector. The vertical dimension of the X-ray beam during data collection was 2 mm and the horizontal dimension was 10 mm. The XANES region was measured with 0.35 eV steps, whereas 0.05 $Å^{-1}$ steps were used for the EXAFS region. 5 to 10 scans were collected for fluorescence measurements. A Mn(0) foil was used to calibrate the beam, with the maximum in the first derivative set to 6539 eV. Spectra were aligned, averaged and background-subtracted using SixPack software (Webb, 2005) following standard methods described previously (van Genuchten and Peña, 2017). The EXAFS spectra were extracted using k^3-weighting and were Fourier-transformed over the *k*-range 2 – 10 $Å^{-1}$ using a Kaiser-Bessel window with dk of 3 $Å^{-1}$. Samples were compared to the spectra of aqueous Mn(II), α-Mn_2O_3 and δ-MnO_2, obtained from a previous study (van Genuchten and Peña, 2017). The XANES spectra of the samples were used to derive changes in Mn(II), Mn(III), and Mn(IV) content (ΔMn(II), ΔMn(III), and ΔMn(IV)) from the virgin to the failed geomedia and from the failed to the regenerated geomedia. Because the fraction of Mn(II), Mn(III), and Mn(IV) derived from linear combination fits of the XANES spectra can vary depending on the selection of reference materials (Manceau et al., 2012), we performed four sets of linear combination fits using five reference materials with data from previously published papers (Manceau et al., 2012; Marafatto et al., 2015; van Genuchten and Peña, 2017) on aqueous Mn(II), manganite, bixbyite, ramsdellite and δ-MnO_2. The linear combination fits were performed with the SixPack software. For the linear combination fits, negative components were not allowed and the sum of the components

was not constrained to 1.0. We report the average and standard deviation of ΔMn(II), ΔMn(III), and ΔMn(IV) values across the four linear combination fits, with the full linear combination fit output given. This approach decreases errors in interpreting linear combination fit output due to the selection of particular reference materials.

3.3 Results and Discussion

3.3.1 Geomedia Performance: Oxidation

After approximately 1300 pore volumes (i.e., 262 hours) of exposure to a 5 μM BPA solution of synthetic stormwater, the manganese oxide-coated sand failed (i.e., C/C_0 exceeded 0.80) (Figure 3.1). Relative to the birnessite-coated sand with a similar Mn coating density tested by Grebel et al., (2016) which failed after approximately 250 pore volumes under identical conditions, this material exhibited exceptional performance. In addition, this manganese oxide-coated sand was produced at ambient temperatures, facilitating easier large-scale production than syntheses requiring high reaction temperatures (McKenzie, 1971, 1970). Relatively few previous studies have demonstrated differences in the rate of oxidation of organic compounds by different manganese oxide minerals under well-controlled conditions.

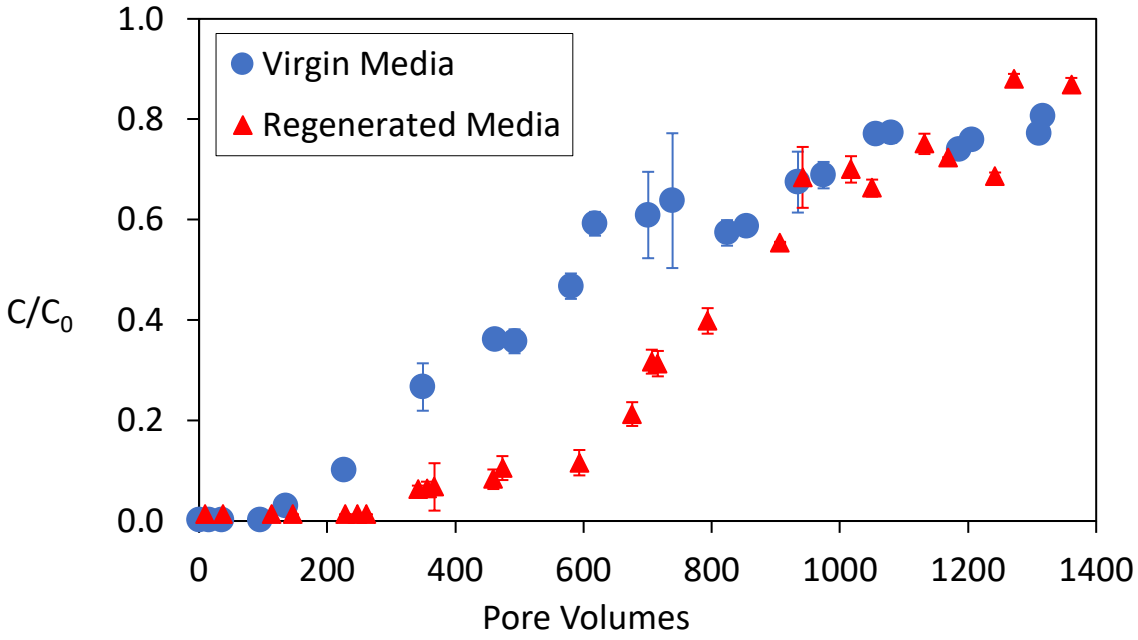

Figure 3.1 Concentration of bisphenol A leaving columns packed with 20 g of manganese oxide-coated sand. Longevity tests were conducted at a 0.4 mL/min flow rate with simulated stormwater containing 5 μM bisphenol A. Geomedia was regenerated *in situ* at pH 6 with [HOCl] = 0.31 mM for 50 hours. Error bars from quadruple (virgin media) and triplicate (regenerated media) column samples are smaller than symbols in some cases.

An average of 10.6 ± 0.5 of the 13.9 µmoles of influent bisphenol A (76%) were oxidized during the first 580 pore volumes of experimentation. An average of 16.1 ± 1.4 of the 31.4 µmoles of bisphenol A that entered the column during the entire 1300 pore volume experiment were oxidized. The reduction of manganese oxide implies that each transformed molecule of bisphenol A transferred an average of 21 electrons to manganese oxides in the column (see calculations; Section 3.3.2), which is consistent with previous reports that the initial products of bisphenol A oxidation also react with manganese oxides (Im et al., 2015).

The mass of Mn eluted from the columns due to reductive dissolution corresponded with the observed trends in bisphenol A oxidation. During the initial 40 minutes (3 pore volumes) of operation, Mn levels in the column effluent were above 80 µM (inset in Figure 3.2), virtually all of which was dissolved. These data suggest there was an initial period of rapid Mn reduction to Mn^{2+}, possibly due to a small proportion of highly reactive groups on the manganese oxide surface. From 3 to 580 pore volumes, the geomedia removed more than half of influent bisphenol A yet effluent Mn concentrations remained below 0.5 µM (Figure 3.2). This result was consistent with the reduction of Mn(IV) to Mn(III), which would not produce high levels of soluble Mn. Between 580 and 975 pore volumes, effluent Mn concentrations increased, possibly due to the reduction of Mn(III) that was generated in the earlier stages of operation. After 975 pore volumes, effluent manganese decreased as the geomedia became less reactive. Approximately 6.4 mg of a total of 40.2 mg Mn (16%) was lost throughout the column operation period.

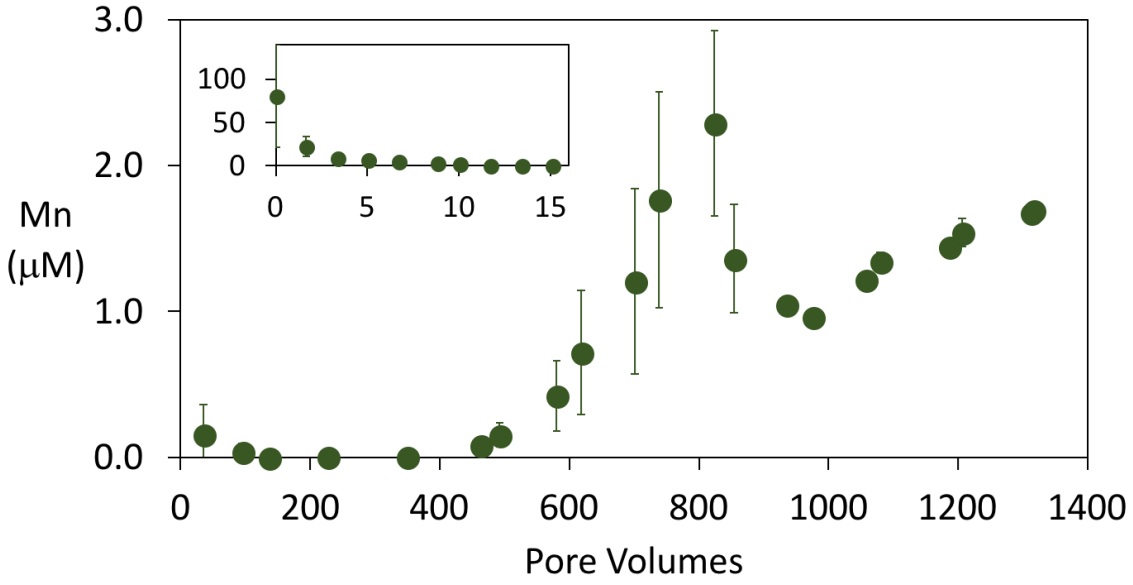

Figure 3.2 Total Mn leaving columns packed with 20 g of manganese oxide-coated sand. Inset shows the initial period of Mn release. Dissolved Mn concentrations were within 6% of total Mn for all time points. Error bars from quadruple column samples are smaller than symbols in some cases.

The release of Mn from geomedia is a water quality concern for aesthetic reasons (Sain and Dietrich, 2015). Although effluent Mn concentrations exceeded the US EPA secondary standard for maximum total dissolved Mn of 0.91 μM (US Environmental Protection Agency, 2004) near the start of the experiment, Mn release from this geomedia is not a major concern due to the relatively high concentration of the reactive compound giving rise to Mn(II) release (i.e., bisphenol A) and the likelihood of Mn(II) dilution, adsorption and re-oxidation as the water infiltrates the aquifer.

3.3.2 Electron equivalents transferred to manganese oxide

The reductive dissolution of the manganese oxide and decrease in average Mn oxidation state observed by iodometric titration indicates that 337 μequivalents of electrons were transferred to the manganese oxide. This result implies that each transformed molecule of bisphenol A transferred an average of 21 electrons to manganese oxides in the column.

The electron equivalents transferred from reductive dissolution can be calculated by:

$$\left(2.01 - 1.69\ \frac{\text{mg Mn}}{\text{g geomedia}}\right) * 20\text{g geomedia} * \frac{1\ \text{mol Mn}}{54.9\ \text{g Mn}} * (3.94 - 2.0)\ \frac{\text{equivalents}}{\text{mol Mn}} = 226\ \mu\text{equivalents} \qquad \text{(Eq. 3.1)}$$

The electron equivalents transferred from reduction of geomedia-associated Mn can be calculated by:

$$\left(1.69\ \frac{\text{mg Mn}}{\text{g geomedia}}\right) * 20\text{g geomedia} * \frac{1\ \text{mol Mn}}{54.9\ \text{g Mn}} * (3.94 - 3.76)\ \frac{\text{equivalents}}{\text{mol Mn}} = 111\ \mu\text{equivalents} \qquad \text{(Eq. 3.2)}$$

This yields a total electron transfer of:

$$226 + 111 = 337\ \mu\text{equivalents of electrons} \qquad \text{(Eq. 3.3)}$$

The equivalents of electrons transferred per mole oxidized bisphenol A are calculated by:

$$\frac{337\ \mu\text{equivalents e}^-}{16.1\ \mu\text{moles BPA oxidized}} = 20.9\ \text{electrons/mole oxidized BPA} \qquad \text{(Eq. 3.4)}$$

3.3.3 Geomedia Performance: Regeneration

The concentration of HOCl leaving the column during the regeneration process (Figure 3.3) increased from below 4 μM to over 0.21 mM after the theoretical chlorine demand was met (i.e., 1380 pore volumes into the experiment), suggesting the HOCl quickly oxidized the reduced Mn. During the initial 1.67 hours (8 pore volumes) of regeneration up to 140 μM of dissolved

Mn were detected in the water exiting the column. After this initial wash-out period, the effluent Mn concentration markedly decreased. However, during the 2-hour rinse with Milli-Q water following regeneration, the Mn in the effluent increased to over 21 µM, most of which was in the particulate phase.

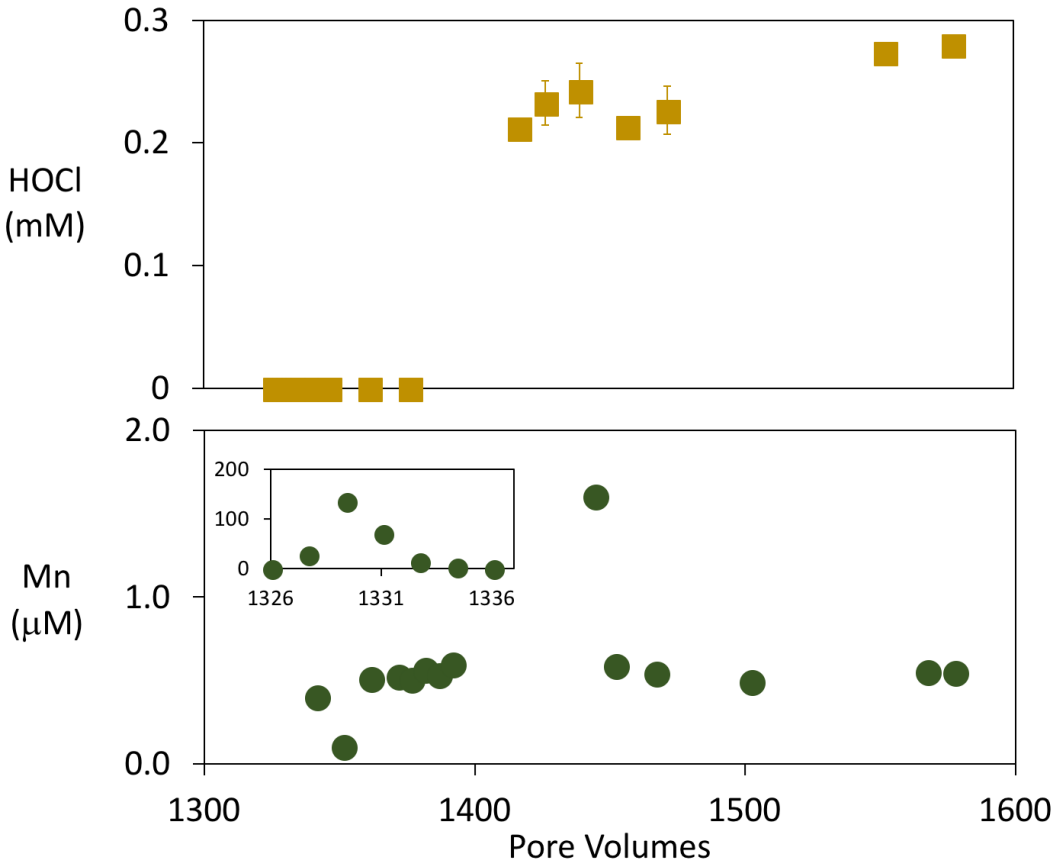

Figure 3.3 HOCl (top) and Mn (bottom) in effluent from column regeneration. 50-hour regeneration with [HOCl] = 0.31 mM (5 times stoichiometric dose). HOCl concentrations below the 4 µM limit of detection are reported as 0. Mn in effluent during initial phase of regeneration is presented in the inset. Regeneration experiments began 1326 pore volumes into column experiments.

Effluent manganese concentrations likely remained low for most of the regeneration period due to the oxidation of reduced Mn(II) and Mn(III) to Mn(IV)-oxides by HOCl. The large release of manganese observed at the beginning of the regeneration period and during the rinse with Milli-Q water imply that manganese can be released following changes in influent composition between stormwater and oxidant solution. In particular, manganese oxide solids may slough off of the geomedia immediately following regeneration.

After regeneration, the manganese oxide-coated sand performed in a manner similar to that observed in the virgin geomedia (Figure 3.1). The regenerated geomedia initially removed

all influent bisphenol A before failing after 1270 pore volumes (253 hours). The regenerated geomedia sustained high reactivity with bisphenol A considerably longer than the virgin geomedia. Practically, these results suggest that regenerating manganese oxide-coated sand with HOCl could at least double its usable lifetime before failure due to the mechanism observed in this study.

3.3.4 Geomedia Characterization

The virgin manganese oxide-coated sand had a manganese coating density of 2.01 ± 0.25 mg Mn/g geomedia and an average Mn oxidation state of +3.94 ± 0.07 (Figure 3.4) as measured by iodometric titration. Likely due to initially rapid reduction of Mn, the coating density and oxidation state of manganese on the geomedia decreased over the first 500 pore volumes: the Mn coating density dropped to 1.53 ± 0.18 mg Mn/g geomedia, while the average Mn oxidation state decreased to +3.77 ± 0.04. The manganese coating density and the average oxidation state did not significantly change after these initial decreases. After approximately 1300 pore volumes, the failed manganese oxide-coated sand had a coating density of 1.69 ± 0.26 mg Mn/g geomedia and an average oxidation state of +3.76 ± 0.05.

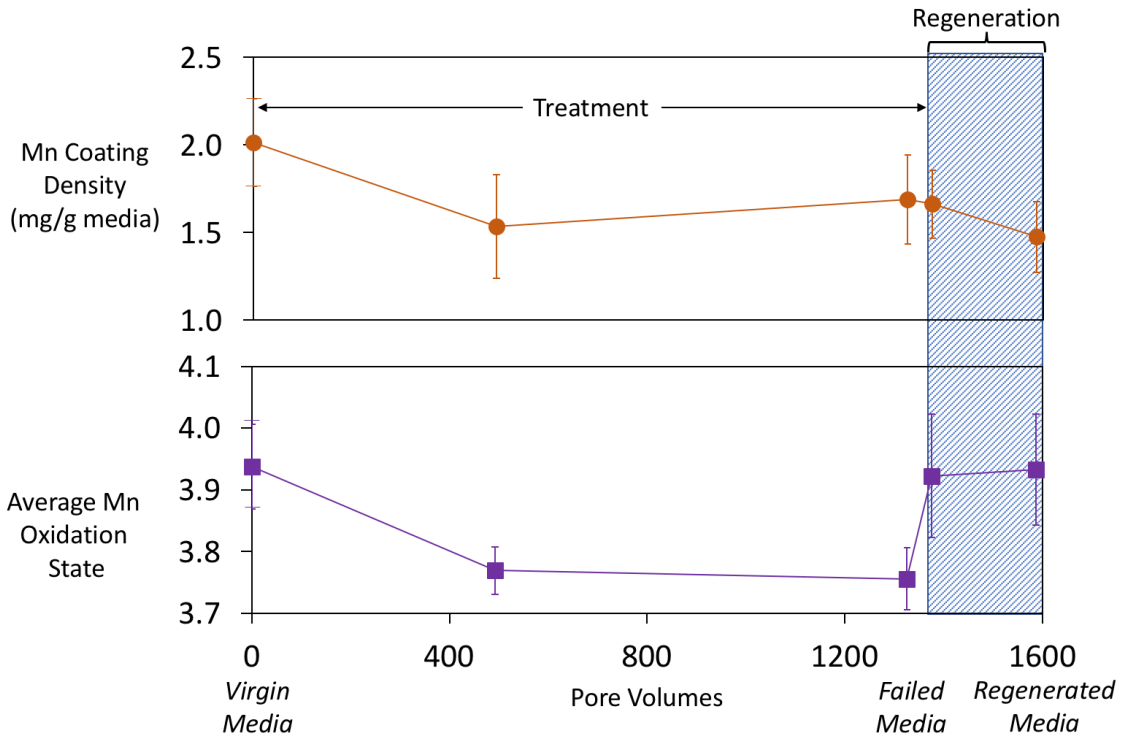

Figure 3.4 Evolution of Mn coating density of geomedia (top) and average Mn oxidation state (bottom) of geomedia in columns during longevity test (0-1326 pore volumes) and *in situ* regeneration (1326-1587 pore volumes) with HOCl. Virgin, failed and regenerated geomedia are indicated below the x-axis.

After regeneration at 5 times stoichiometric demand for 50 hours, the Mn coating density was 1.47 ± 0.20 mg Mn/g sand. Thus, over one test-regeneration cycle, 27% of the manganese in the geomedia was lost. Once stoichiometric oxidant demand was met (50 pore volumes into column regeneration), the average Mn oxidation state increased to +3.92 ± 0.1. This value was not significantly changed by additional exposure to HOCl, suggesting the reduced manganese oxide was quickly oxidized to its final state by the HOCl and that a stoichiometric excess of oxidant was not necessary to restore the reactivity of the geomedia.

The pH_{pzc} of the coating of the geomedia remained constant, with values of approximately 3.3 for the virgin, failed, and regenerated geomedia. This value is typical of manganese oxides and suggests that the geomedia will remain negatively charged at typical stormwater pH values irrespective of its degree of passivation or whether or not it has been regenerated (McKenzie, 1981).

The geomedia was also characterized at different locations within the column, with each quartile (from most upstream to most downstream) analyzed separately after approximately 500 and 1300 pore volumes of longevity testing (Figure 3.5). After failure, the geomedia in the most upstream quartile had a coating density of 1.55 ± 0.03 mg Mn/g sand, whereas the most downstream quartile of the column had a coating density of 1.95 ± 0.24 mg Mn/g sand. The reductive dissolution of Mn(IV/III) to Mn(II) was demonstrated by a decrease in Mn coating density in the upstream portions of the column, and by the higher average oxidation state of the coating in the upstream portions of the column relative to the downstream portions.

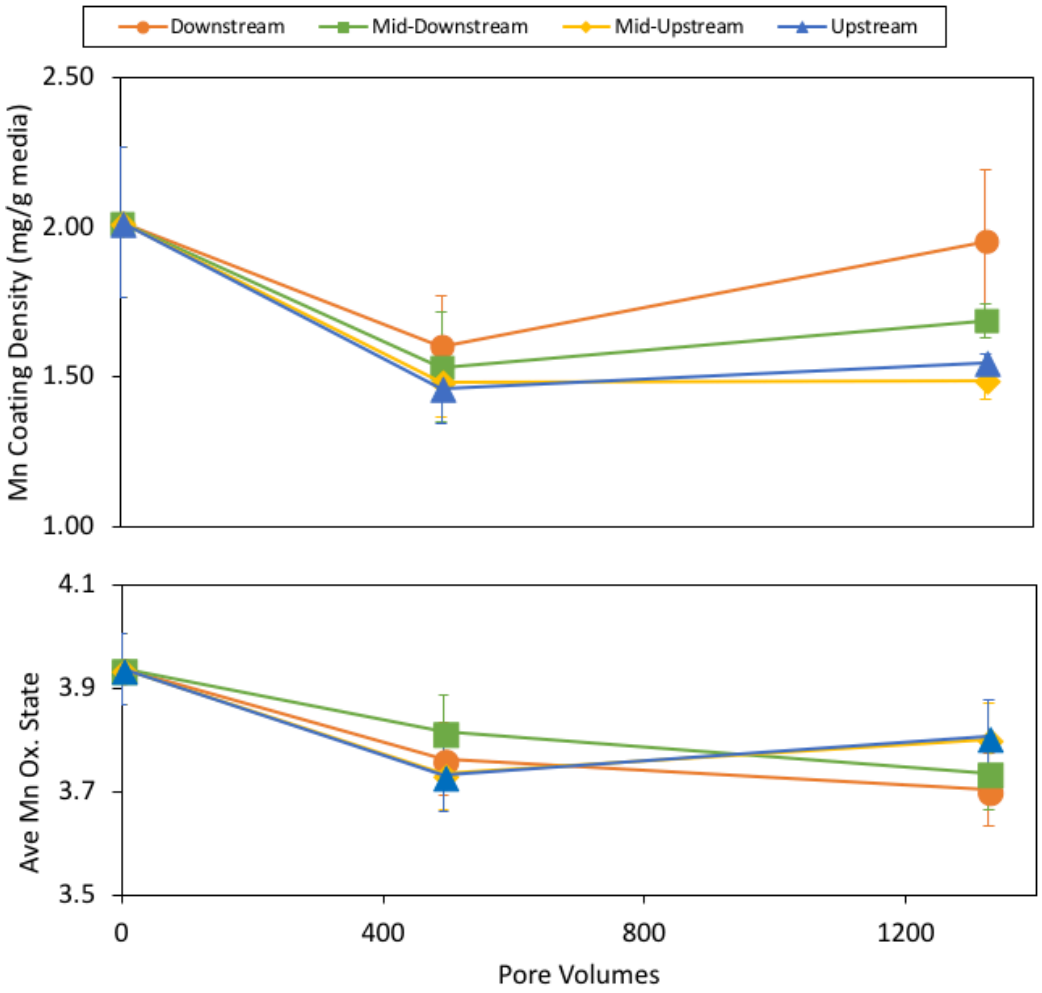

Figure 3.5 Changes in manganese coating on sand during longevity testing showing change in Mn coating density (top) and average Mn oxidation state (bottom) by quartile of column. Error bars represent the standard error in triplicate samples from the same quartile of the sacrificial column.

Scanning electron microscopy images indicated no significant change in manganese oxide-coated sand morphology during the failure-regeneration cycle (Figure 3.6). Energy dispersive X-ray spectroscopy element mapping also showed similar extents of Mn coverage in all samples (Table 3.1).

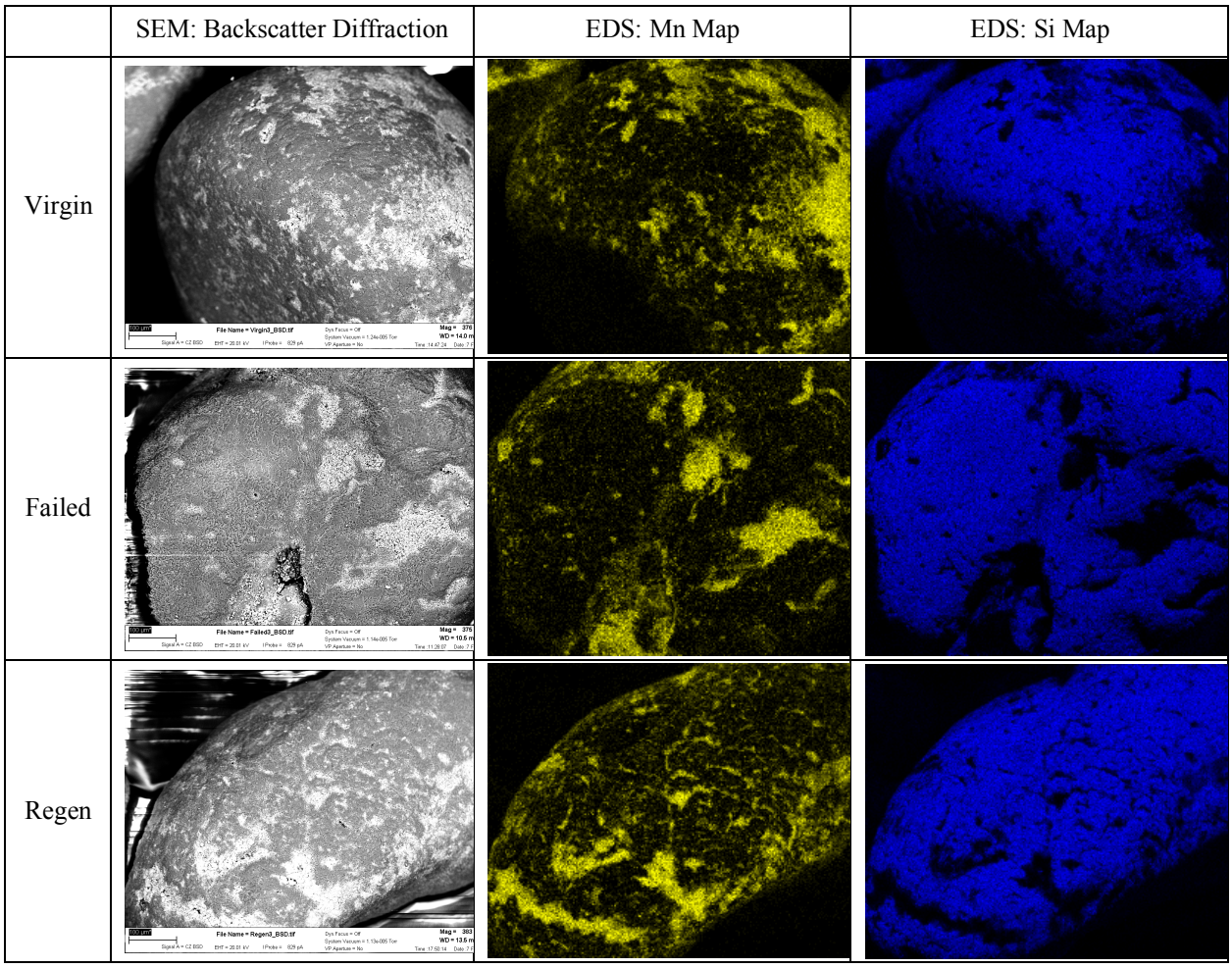

Figure 3.6 Backscatter diffraction scanning electron microscope image (left) and energy dispersive X-ray spectroscopy element maps (center, right) of representative virgin (top), failed (middle), and regenerated (bottom) manganese oxide-coated sand. All images app approximately 380X magnified. In the SEM images, Mn-oxide appears bright. In the element maps, Mn appears yellow and Si appears blue.

Table 3.1 Surface coverage of Mn on manganese oxide-coated sand as determined by EDS analysis of individual grains at approximately 1000x magnification.

Media Surface	Atomic Percentage Mn
Virgin	6.43 ± 4.85
Failed	3.26 ± 0.79
Regenerated	3.78 ± 0.99

The first derivative of the XANES spectrum of the failed geomedia (Figure 3.7) showed a subtle, but systematic increase and decrease in amplitudes of the lower and higher energy shoulders in the main feature near 6547 and 6559 eV, respectively, relative to the virgin and regenerated samples. Based on the linear combination fits, the change in Mn(IV) content (ΔMn(IV)) from the virgin to the failed sample was -8.3 ± 2.2%, which was accompanied by a positive ΔMn(III) of +3.5 ± 2.5% (Table 3.2; full linear combination fit results Table 3.3). The ΔMn(II) between the virgin to failed geomedia was negligible (on average, the total solid phase Mn(II) for the virgin and failed geomedia was < 1%, Table 3.4). These results indicate a decrease in average Mn oxidation state in the failed material that was similar to that observed in the chemical titrations. The effectiveness of the HOCl regenerant in converting Mn(III) back to Mn(IV) was confirmed by the linear combination fits of the regenerated geomedia, which showed a composition nearly identical to that of the virgin geomedia, with ΔMn(IV) from the failed to regenerated geomedia of +7.0 ± 1.4% and ΔMn(III) of –2.6 ± 1.9%. Similar to the virgin material, the average Mn(II) content (and ΔMn(II)) for the regenerated geomedia determined by linear combination fits was < 1%, suggesting that the redox changes in the solid phase due to regeneration were dominantly due to cycling between Mn(III) and Mn(IV). The increase in Mn(III) abundance is consistent with the reduction of Mn(IV) to Mn(III) suggested by the low concentrations of soluble Mn observed in the column effluent between 20 and 580 pore volumes of column operation.

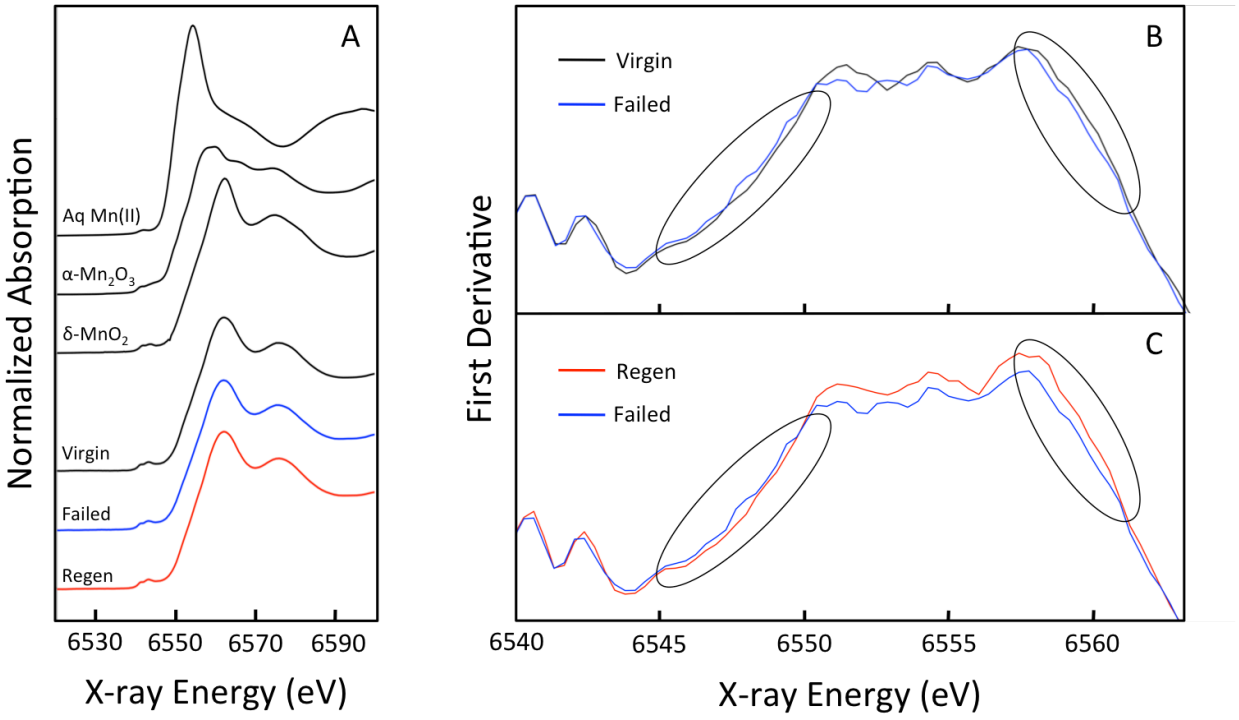

Figure 3.7 X-ray absorption near edge structure (XANES) spectra (A) and first derivative spectra (B and C) for the manganese oxide-coated sands and reference materials. The circles in B and C highlight regions that indicate changes in the average manganese oxidation state. The circle at the lower energy shoulder in the main feature shows a subtle increase in the amplitude of the failed sample, whereas the circle at the higher energy shoulder emphasizes a decrease in the intensity of the failed sample relative to the virgin and regen samples. These trends indicate a lower average manganese oxidation state in the failed sample compared to the virgin and regenerated samples.

Table 3.2 Changes in Mn(II), Mn(III), and Mn(IV) content derived by linear combination fits.

Samples	ΔMn(II)	ΔMn(III)	ΔMn(IV)
Virgin to Failed Geomedia	-0.1 ± 0.1%	+3.5 ± 2.5%	-8.3 ± 2.2%
Failed to Regenerated Geomedia	-0.7 ± 0.8%	-2.6 ± 1.9%	+7.0 ± 1.4%

Table 3.3 Summary of XANES linear combination fit results.

References*	Sample	% Mn(II)	% Mn(III)	%Mn(IV)	R-Factor
Mn^{2+}, α-Mn_2O_3, δ-MnO_2	Virgin	0	6	89	0.011
	Failed	0	10	80	0.0008
	Regen	0	6	88	0.0014
Mn^{2+}, α-Mn_2O_3, MnO_2	Virgin	1	14	78	0.0002
	Failed	1	19	69	0.0002
	Regen	0	15	77	0.0003
Mn^{2+}, γ-MnOOH, δ-MnO_2	Virgin	0	0	95	0.0009
	Failed	0	0	90	0.0007
	Regen	0	0	95	0.0003
Mn^{2+}, γ-MnOOH, MnO_2	Virgin	2	16	75	0.0002
	Failed	2	22	65	0.0003
	Regen	0	19	72	0.0013

*Combinations of the following references were used: aqueous Mn(II) (Mn^{2+}), manganite (γ-MnOOH), bixbyite (α-Mn_2O_3), ramsdellite (MnO_2) and δ-MnO_2.

Table 3.4 Ion-exchangeable Mn on the virgin, failed and regenerated geomedia.

Media	μmol Mn^{2+}/g Mn-oxide	Percentage of total Mn
Virgin	25.8 ± 5.0	0.22 ± 0.05%
Failed	181 ± 25	1.55 ± 0.16%
Regenerated	27.2 ± 6.0	0.24 ± 0.08%

XRD patterns of the virgin and regenerated geomedia coatings were similar, showing only broad peaks with low intensity at 12º, 28.8º and 37.5º 2θ, which is indicative of nanocrystalline cryptomelane. The coating of the failed geomedia exhibited intense peaks at 2θ = 28.8º (*d* = 3.12 Å) and 37.5º (*d* = 2.40 Å) that were considerably narrower than those observed in the virgin geomedia. In addition, the failed material exhibited small, well-defined peaks (e.g., at 2θ near 42º and 48º) that were not apparent in the virgin geomedia. These differences in the XRD patterns of the failed geomedia relative to the virgin and regenerated material are consistent with

an increase in the crystallinity of the manganese oxide after it reacts with bisphenol A. The peak positions in the XRD patterns were consistent with monoclinic manganese oxide in the C 1 2/m 1(12) space group (i.e., cryptomelane) (Figure 3.8) (Post et al., 1982).

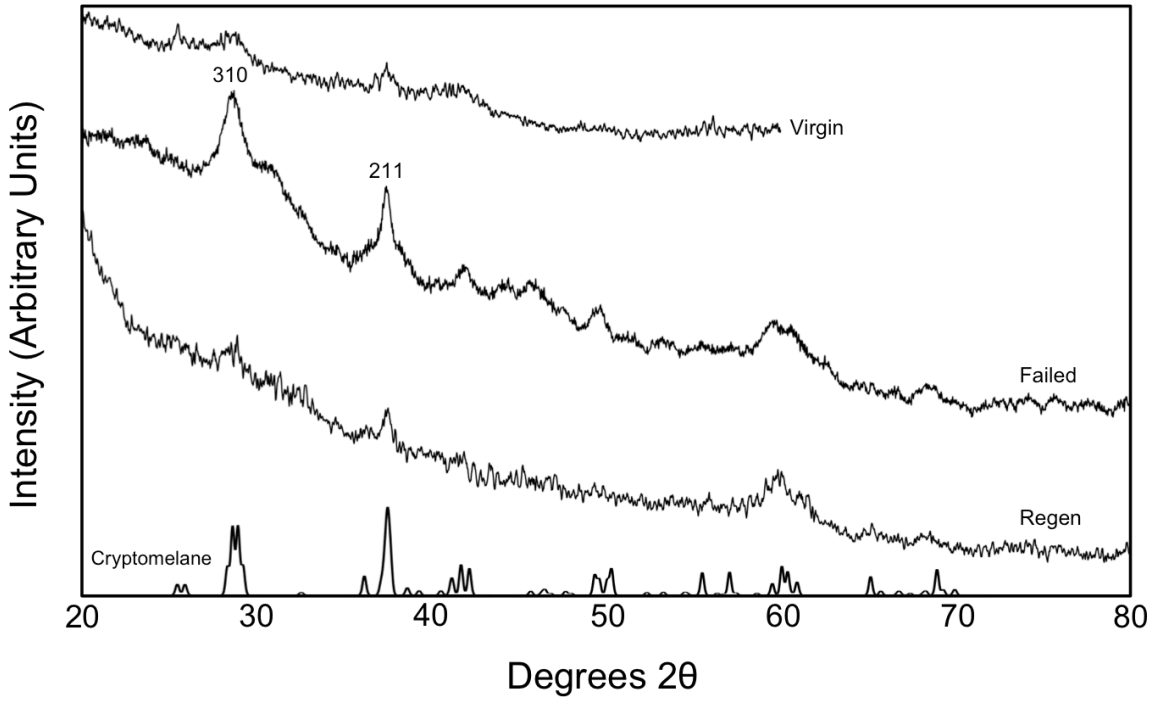

Figure 3.8 X-ray diffraction patterns for coating of virgin (top), failed (middle) and regenerated (bottom) manganese oxide-coated sand. The powder XRD pattern of cryptomelane (adapted from Post et al., 1982) is shown for comparison.

The Mn K-edge EXAFS spectra (Figure 3.9) of all geomedia exhibited the staircase pattern from 4 to 6 $Å^{-1}$ characteristic of Mn(IV)-oxides. Additional features in the EXAFS spectra suggested a local coordination environment similar to cryptomelane (Kim et al., 2011), particularly the humpbacked asymmetry of the oscillation at 6.8 $Å^{-1}$ (arrow in Figure 3.9), which is indicative of tunnel-structured MnO_6 octahedra (Manceau and Combes, 1988). The more pronounced shoulder of this feature in the failed geomedia suggests greater development of this structure (Manceau and Combes, 1988). Subtle differences in the EXAFS spectra between the virgin, failed and regenerated geomedia were evident in the region from 7-8.5 $Å^{-1}$ (* symbol in Figure 3.9). This region in the EXAFS spectrum of the failed geomedia exhibited a clearer double beat from 7-8.5 $Å^{-1}$, which is another characteristic feature of tunnel-type Mn(IV) oxides, such as cryptomelane, todorokite, and psilomelane (Manceau et al., 2007a). The Fourier-transformed EXAFS spectra of all samples showed first- and second-shell peaks characteristic of the edge-sharing MnO_6 octahedra expected for Mn(IV) oxides (Figure 3.9). However, an additional peak at larger radial distance, R, also appeared in all samples, which is characteristic of the corner-sharing MnO_6 octahedra that make up the tunnel structure of cryptomelane (Manceau and Combes, 1988; van Genuchten and Peña, 2017). Key differences between the

virgin, failed and regenerated geomedia appeared in the relative peak amplitudes of the Fourier transformed EXAFS spectra. The amplitude of the edge-sharing Mn-Mn peak relative to the Mn-O peak was largest in the failed geomedia, suggesting a more ordered Mn coordination environment in this sample. This result further suggests that the failed material was the most crystalline sample. This manganese oxide-coated sand, which was prepared using a modified cryptomelane synthesis method, may have demonstrated a longer reactive lifetime than birnessite-coated sands due to differences in reactivity between mineral forms of the manganese oxide, or a higher average Mn oxidation state (Grebel et al., 2016). Birnessite has a layered structure and is frequently employed in experiments with organic compounds (Lin et al., 2009; Zhang and Huang, 2003). In the cryptomelane structure, edge-sharing MnO_6 octahedra exhibit a tunnel-like, rather than sheet-like motif (Robinson et al., 2013). The difference in the arrangement of edge-sharing MnO_6 octahedra between these mineral polymorphs, exposing different crystal faces to solution, may help to explain the observed difference in their reactivity (Remucal and Ginder-Vogel, 2014).

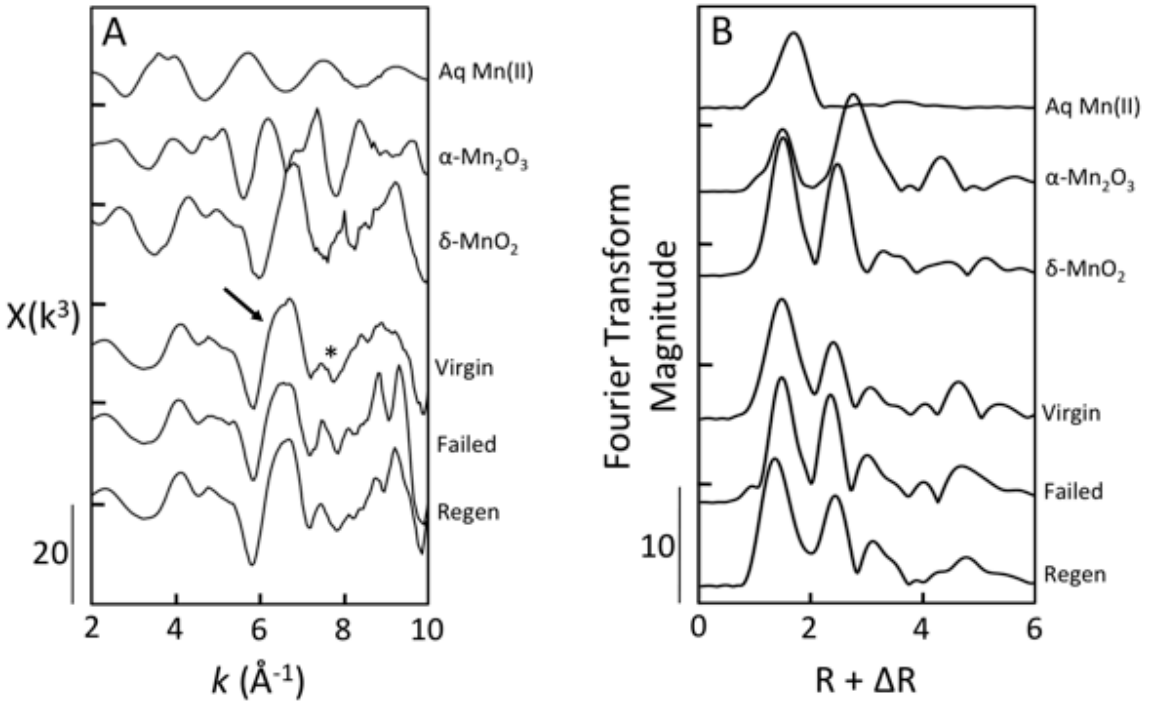

Figure 3.9 Mn K-edge EXAFS spectra (A) and Fourier transformed EXAFS spectra (B) of the virgin, failed and regenerated (regen) manganese oxide-coated sand and standards of aqueous Mn(II), α-Mn_2O_3 and δ-MnO_2.

3.3.5 Geomedia Passivation Mechanism

Results from the geomedia characterization provided evidence for the passivation mechanism during bisphenol A oxidation wherein Mn(II) is initially released, followed by an increase in surface-associated Mn(III) and mineral crystallinity. The XRD and EXAFS spectra indicated that both the virgin and failed geomedia had nanocrystalline, cryptomelane-like

coordination environments, while the failed geomedia coating was more crystalline. Additionally, chemical and XANES-derived oxidation state measurements demonstrate that Mn(III) was more abundant in the failed geomedia. However, very little Mn(II) was observed in any of the manganese oxide-coated sand.

In certain coordination environments, particularly at edge sites, Mn(III/IV) groups can be highly reactive (Liu et al., 2009b; Manceau et al., 1997; Nico and Zasoski, 2001; Simanova and Peña, 2015). The initial removal of greater than 98% of bisphenol A in the columns (i.e., before 150 pore volumes), coupled with the release of considerable amounts of Mn(II) may have been due to the reduction of these highly reactive sites.

The relatively fast geomedia passivation between 150 and 580 pore volumes was consistent with the reduction of Mn(IV) to less-reactive structural Mn(III) sites (Liu et al., 2009a). The increased crystallinity and simultaneous decrease in oxidation state are significant because less crystalline manganese oxides typically have higher concentrations of reactive sites and are more reactive than their crystalline counterparts (Hou et al., 2014; van Genuchten and Peña, 2017; Villalobos et al., 2014). This crystallization may be particularly important to cryptomelane. A mineral consisting of a network of tunnels may have a lower surface area accessible to dissolved organic species in the bulk solution upon crystallization, causing a more pronounced decrease in reactivity with crystal growth than might occur with phyllomanganates, if the organic molecule is too large to access tunnel sites. From 580 to 975 pore volumes, the sustained removal of 30-40% of influent bisphenol A demonstrates that the Mn(III)-rich cryptomelane retained some reactivity. The reductive dissolution of the Mn(III) was consistent with the increase of Mn(II) in the column effluent at later stages of the experiment and the negligible change in average Mn oxidation state as bisphenol A was oxidized and reduced Mn was released from the surface.

Mn^{2+} produced by the reaction can passivate manganese oxide-coated sand by blocking reactive sites (Gao et al., 2011; Klausen et al., 1997). However, given the small amount of Mn(II) detected in the geomedia, we conclude that Mn^{2+} contributed little to the observed passivation.

Several researchers have reported that manganese oxides adsorb bisphenol A as a precursor to oxidation, and that reversible sorption is unimportant compared to oxidation (Balgooyen et al., 2017; Grebel et al., 2016; Im et al., 2015). After passing Milli-Q water through the failed columns for 10 pore volumes, the concentration of bisphenol A coming out of the columns was 0.9 μM, which was approximately equal to the concentration observed in control columns filled with acid-washed sand under identical conditions. The small mass of bisphenol A (9.9 μg, 0.14% of the total influent) released during the rinse step was likely associated with the short sections of polyethylene fittings and Tygon tubing in the columns and peristaltic pumps. The major transformation products of bisphenol A, including 4-hydroxycumyl alcohol**,** do not reversibly sorb to manganese oxides in appreciable amounts under the conditions employed in these experiments (Im and Löffler, 2016; Lin et al., 2009). Therefore, it is unlikely that adsorbed bisphenol A or its transformation products contributed significantly to the passivation of the geomedia.

Microbial activity may have influenced the trend of geomedia performance. Although columns and tubing were rinsed with 1% HCl before testing, the possibility of inducing phase

change or chemical transformation reactions made chemical or thermal sterilization of manganese oxide-coated sand or bisphenol A stocks infeasible. Bisphenol A may have been biotransformed or absorbed by biofilms after several weeks of longevity testing, resulting in higher apparent reactivity and slower passivation of the geomedia (Kang and Kondo, 2002). Because of the high value of C/C_0 in the failed columns (>0.8), the maximum impact of microbial activity is necessarily limited to a small portion of bisphenol A removal. Further, the trend observed in C/C_0 supports breakthrough from an abiotic removal mechanism.

3.3.6 Regeneration Mechanism

The virgin and regenerated geomedia had comparable reactivity and longevity, and similar XRD and XAS spectra that suggest that both geomedia types were coated with poorly-ordered cryptomelane phases. This finding implies that the local coordination environment of the manganese oxide was largely preserved after regeneration (i.e., cryptomelane remained the dominant phase), but the disorder increased as the average Mn oxidation state rose.

Treatment with HOCl can oxidize surface-associated Mn(III), including those in crystal lattice orientations that may have played a role in decreasing surface reactivity (Elzinga, 2016). The rapid re-oxidation of the passivated manganese and the efficient scavenging of HOCl suggest that the oxidation of Mn(III) occurred quickly during regeneration. It may be possible that the oxidation of Mn(III) to Mn(IV) resulted in the loss of Jahn-Teller distortion, producing strain in the mineral, resulting in some bonds breaking and smaller crystal size. This process may have generated a mineral phase that, in addition to being more oxidized, was less ordered and more reactive with organic compounds. Unfortunately, the oxidation of Mn(III)-rich oxides has not been studied as extensively as Mn^{2+} oxidation (Nico and Zasoski, 2000; van Genuchten and Peña, 2017; Webb et al., 2005). Determination of the mechanisms of surface-associated Mn(III) oxidation could provide more insight into the nature of the manganese oxide generated in the reaction and the local structure of reactive sites.

3.4 Estimation of lifetime of manganese oxide-coated sand in simulated stormwater

Given its superior performance and relative ease of production, the manganese oxide-coated sand used in this study shows considerable promise for field applications. For example, a typical-sized stormwater infiltration system that treats 2×10^6 L of stormwater per year may cover 50 m^2 of ground surface with a 0.5 m-deep layer of manganese oxide-coated sand (Hatt et al., 2009). Assuming stormwater containing 50 μg/L of natural and anthropogenic oxidizable organic compounds, such a system could be expected to operate for decades before loss of reactivity occurs due to the mechanism observed in this study. Without regeneration, the system could operate approximately 45 years before a 20% loss of reactivity, 80 years before a 50% loss of reactivity, and 175 years before an 80% loss of reactivity (see calculations; below). Although approximately 25% of the Mn coating density of the geomedia was lost during one cycle of treatment and regeneration, the observation that manganese oxide reactivity did not change over the two treatment-regeneration cycles tested and the rates of Mn coating loss suggest that this geomedia would be effective for multiple treatment-regeneration cycles under field conditions. If

the Mn coating density decreases substantially after several treatment-regeneration cycles, more frequent geomedia regeneration may be required. It is possible that other processes, including clogging by suspended solids and microbial growth, could cause more rapid failure in field applications of this technology than were observed in this laboratory study (Alidina et al., 2014b). Researchers studying field-scale systems have employed settling prior to infiltration and bioturbation by plant roots as effective counter-measures to clogging (Grebel et al., 2013; Le Coustumer et al., 2012). The successful application of biogenic manganese oxides as a polishing step for municipal wastewater effluent suggests that while biological activity can slow reactions, it will not necessarily adversely affect the reactivity of manganese oxides (Forrez et al., 2010).

The lifetime of a typical stormwater treatment system employing manganese oxide-coated sand as a reactive geomedia for organic contaminants could be determined by:

$$\text{lifetime [years]} = \frac{\text{oxidative loading capacity [moles]}}{\text{oxidizable organic load } \left[\frac{\text{moles}}{\text{yr}}\right]} \quad \text{(Eq. 3.5)}$$

Where oxidative loading capacity can be determined by:

$$\text{oxidative loading cap.[moles]} = \text{bed mass[g]} * \text{reactive capacity } \left[\frac{\text{moles}}{\text{g}}\right] \quad \text{(Eq.3.6)}$$

- Assuming an infiltration bed 50 m^2 in area containing a 0.5 m-depth zone of manganese oxide-coated sand with a bulk density of 870 kg/m^3 yields a bed mass of 22×10^6 g manganese oxide-coated sand.
- The reactive capacity of the geomedia is defined as moles of oxidizable organic compounds to which the geomedia is exposed before a threshold for breakthrough (e.g. C/C_0=0.8) is observed. The reactive capacity was estimated from results of column breakthrough experiments.
- Per Eq. 3.6, multiplying bed mass by the reactive capacities measured in this study of:
    - 0.42 μmoles/g manganese oxide-coated sand (before C/C_0=0.2), yields 9.17 moles oxidative loading capacity.
    - 0.73 μmoles/g manganese oxide-coated sand (before C/C_0=0.5), yields 16.2 moles oxidative loading capacity.
    - 1.57 μmoles/g manganese oxide-coated sand (before C/C_0=0.8), yields 34.6 moles oxidative loading capacity.

Oxidizable organic load can be determined by:

$$ox.org.load\ \left[\frac{moles}{yr}\right] = stormwater\ load\ \left[\frac{L}{yr}\right] * oxidizable\ org.conc.[M] \quad \text{(Eq. 3.7)}$$

- Assuming stormwater catchment of 4000 m^2 receiving 0.5 m of rainfall/yr and a runoff coefficient of 1 yields 2×10^6 L stormwater/yr (Hatt et al., 2009).
- Assuming 50 μg/L oxidizable organic compounds (natural and anthropogenic) with average atomic mass of 500 g/mol and equal reactivity to BPA with manganese oxide yields. 0.1 μM oxidizable organic moieties.

- Multiplying stormwater load and oxidizable organics concentration per Eq. 3.7 yields a load of 0.2 moles oxidizable organic moieties/yr.

Dividing oxidative loading capacity by oxidizable organic load per Eq. 3.5 yields an estimated lifetime of:

- $\frac{9.17\ moles}{0.2\ moles/yr}$ = 45.9 years before C/C_0=0.2.
- $\frac{16.2\ moles}{0.2\ moles/yr}$ = 81.2 years before C/C_0=0.5.
- $\frac{34.6\ moles}{0.2\ moles/yr}$ = 173 years before C/C_0=0.8.

3.5 Environmental Implications

Manganese oxide geomedia are only capable of oxidizing certain organic stormwater contaminants (Grebel et al., 2016). Therefore, other geomedia, such as biochar, would be needed if runoff contained contaminants that do not react with the manganese oxide (Ulrich et al., 2017). Prior research suggests that oxidation of the bisphenol A by manganese oxide-coated sand produces 4-hydoxycumyl alcohol (Grebel et al., 2016), which is more estrogenic than its parent compound (Nakamura et al., 2011). 4-hydroxycumyl alcohol is susceptible to further biotransformation under oxic environments such as those encountered in stormwater infiltration systems (Im et al., 2015). Oxidation by manganese oxides does not always result in the mineralization-and therefore complete detoxification-of contaminants. However, the products of partial oxidation are frequently more susceptible to biotransformation or removal upon encountering other geomedia (e.g., biochar) that could be deployed alongside manganese oxide-coated sand (Grebel et al., 2013; Im and Löffler, 2016). Organic compounds with electron-withdrawing moieties are slow to react with manganese oxide-coated sand (Grebel et al., 2016). Nonetheless, the oxidation of organic contaminants by manganese oxides frequently diminishes the endocrine disrupting potential of the product water (Forrez et al., 2009; Li et al., 2008).

The introduction of hypochlorite to the subsurface during the regeneration process could result in the production of chlorine disinfection byproducts (Chowdhury et al., 2009). Because the reduced Mn reacted with HOCl very efficiently, proper dosing during regeneration would limit the formation of disinfection byproducts. Furthermore, if the chlorine solution used for regeneration consists of potable water, many of the disinfection byproduct precursors would likely have been removed (US Environmental Protection Agency, 2010). To minimize the potential for introducing these disinfection byproducts into the groundwater during regeneration, stormwater infiltration systems could be hydraulically isolated, allowing for the effluent from the regeneration process to be collected and disposed of rather than undergoing infiltration (Edwards et al., 2016). Regeneration of a 50 m^2 treatment system would require approximately 228 m^3 of a 25 mg HOCl-Cl_2/L solution (see calculations; below). This corresponds to approximately 200 L of a 3% solution of NaOCl (i.e., household bleach) which could be handled by a field crew without the need for extraordinary precautions.

The mass of HOCl required for regeneration is:

$$22 \times 10^6 \text{g geomedia} * \frac{1.69 \times 10^{-3} \text{g Mn}}{\text{g geomedia}} * \frac{1 \text{ mol Mn}}{54.9 \text{ g Mn}} * \frac{0.24 \text{ e}^- \text{equiv}}{1 \text{ mol Mn}} *$$

$$\frac{1 \text{ mol HOCl}}{2 \text{ e}^- \text{equiv}} * \frac{70.9 \text{ g HOCl}-\text{Cl}_2}{1 \text{ mol HOCl}} = 5750 \text{ g HOCl-Cl}_2 \qquad \text{(Eq. 3.8)}$$

This mass corresponds to a volume of 3% NaOCl solution calculated by:

$$5.75 \text{ kg NaOCl} \div 3\% \text{ NaOCl } \frac{\text{weight}}{\text{volume}} = 191 \text{ L} \qquad \text{(Eq. 3.9)}$$

This study provides insights into how subtle changes in manganese oxide oxidation state and mineralogy can have large implications for reactivity. Although the cryptomelane coating in this study has a slightly higher average manganese oxidation state than is usually found in naturally occurring cryptomelane (Manceau et al., 2007b), these results suggest that cryptomelane may be an important manganese oxide species given its relevance in both natural and engineered environments (Post, 1999). Cryptomelane is less frequently studied than birnessite, and may differ in reactivity and weathering due to its distinct structure (Kim et al., 2011). This study begins to elucidate mineralogy-reactivity relationships and how manganese oxide structure transforms during redox reactions.

Although this study focused on stormwater infiltration applications, this geomedia may have other applications, including managed aquifer recharge with municipal wastewater effluent and agricultural runoff (Alidina et al., 2014a; Dillon et al., 2009). Manganese oxides may also have applications in advanced wastewater treatment (Forrez et al., 2010, 2009; Rudder et al., 2004). Manganese and iron oxide-coated sand are already frequently used to remove dissolved metals during drinking water treatment (Goren et al., 2012; Knocke et al., 1991a; McKenzie, 1980). The methods described here may lead to geomedia with a longer lifetime that is less expensive to utilize and regenerate.

CHAPTER 4. The Use of Manganese Oxide-Coated Sand for the Adsorption of Metal Contaminants in Stormwater

To be submitted to *Environmental Science: Water Research and Technology.* Included here with permission from Duan, Y.; Sedlak, D. L.

4.1 Introduction

Managed aquifer recharge enables water-stressed cities to augment their local water supplies (Dillon et al., 2009; Drewes, 2009). Increasingly, stormwater is being used for aquifer recharge (Edwards et al., 2016; Page et al., 2014). Although it is a plentiful and under-exploited resource, urban stormwater is often contaminated with chemical contaminants (Andres et al., 2018; Regnery et al., 2013). In areas with substantial amounts of industrial activity, certain metals (e.g., Cd, Pb) can pose potential threats to human health and other metals (e.g., Cu, Zn) can pose threats to aquatic ecosystems (Los Angeles County Flood Control District and City of Los Angeles Department of Public Works Bureau of Sanitation, 2006; Pitt et al., 2015). These metals frequently originate from automobiles, construction materials and atmospheric deposition (Davis et al., 2001; Liu et al., 2005; Pagotto et al., 2001). In many cases their concentrations in urban stormwater exceed surface water and drinking water regulations (Table 1.2). As centralized managed aquifer recharge systems become more important to efforts to replenish drinking water supplies, and as regulations for stormwater discharge become more stringent, it will be necessary to treat metals in urban runoff (Page et al., 2010; Regnery et al., 2013).

During managed aquifer recharge, water is typically infiltrated through sand, gravel and natural soils, provided that they are sufficiently permeable (Daigger, 2009; Hatt et al., 2008). To improve water quality during the infiltration process, various materials, referred to as engineered geomedia, can be added to—or used instead of—the native soil. Manganese oxide-coated sand is an example of an engineered geomedia that oxidizes organic contaminants in stormwater (Chapter 3). Manganese oxide-coated sand has a higher hydraulic conductivity and lower propensity for transport away from treatment systems than pure manganese oxide minerals (Liu et al., 2005). Because manganese oxides regularly occur as coatings and nodules on sediments, manganese oxide-coated sands may also be accurate representations of the behavior of manganese oxides in natural systems (Dong et al., 2003; Tani et al., 2003). Manganese oxides exhibit high affinities for metal cations, therefore, this geomedia may also be useful in the treatment of toxic metals during stormwater recharge (Adams et al., 2009; Murray, 1975; O'Reilly and Hochella, 2003; Wan et al., 2015).

Manganese oxides can remove metals from water through several mechanisms. Electrostatic interactions are important to metal adsorption in some situations because structural vacancies and isomorphic substitution give manganese oxides pH_{pzc} values ranging from 1.5 to 6.0, and therefore a negative charge at environmentally relevant pH values (McKenzie, 1981; Stone and Morgan, 1984). In addition to electrostatic attraction, metal cations adsorb to manganese oxides via surface complexation (Boonfueng et al., 2009; Peña et al., 2010; Villalobos et al., 2005). Soft metals (e.g., Pb) tend to form strong surface complexes with the manganese oxide (McKenzie, 1980; Misono et al., 1967; Wan et al., 2015). The high adsorption capacity of Pb on manganese oxides may be due to its penetration into the interlayer and tunnels of manganese oxides and the complexation of Pb in both double-corner-sharing and triple-corner-sharing complexes (O'Reilly and Hochella, 2003; Villalobos et al., 2005). Other metals, such as Zn, can also form triple-corner-sharing complexes over Mn vacancies, though the interactions of other metals with the surface are weaker than those observed in Pb adsorption (Boonfueng et al., 2009; Li et al., 2004; Peña et al., 2010).

The conditions encountered in stormwater may influence the affinity of metals for manganese oxides. Solution pH and dissolved constituents, such as NOM, affect the speciation

of metals in stormwater, and other cations (e.g., Ca^{2+}) inhibit the adsorption of metals by competing for surface sites (Bradl, 2004; Lion et al., 1982; Tessier et al., 1996). For this reason, it is important to evaluate the treatment capacity of manganese oxide-coated geomedia in a matrix which contains the solutes that are typically found in stormwater.

The treatment capacity of the manganese oxide-coated sand may diminish as adsorption sites saturate (Adams et al., 2009; Wan et al., 2015). After the adsorptive capacity of the geomedia is exhausted, it may be possible to recover metal contaminants and restore the adsorptive capacity of the geomedia with a chemical treatment that removes metals from the geomedia without simultaneously stripping away the adsorbing sites. Periodic recovery of adsorbed metals would also limit the potential for release of metal contaminants if changing water chemistry favors desorption, which could occur during intermittent flow conditions (Drewes, 2009; Grebel et al., 2013; Ulrich et al., 2017) or through fluctuations in pH or ionic strength (e.g., from stormwater contaminated with deicing salts) (Amrhein et al., 1992; US Environmental Protection Agency, 1999).

The affinity of manganese oxide coated sand for Cu, Zn, Cd and Pb was tested in batch and column experiments in simulated stormwater to evaluate the potential for using this geomedia to remove metals in aquifer recharge and surface water treatment basins. The abilities of dilute acid and metal-complexing ligands to remove adsorbed metals were evaluated in order to develop a practical treatment for regenerating the adsorptive capacity of the geomedia.

4.2 Materials and Methods

4.2.1 Reagents and Simulated Stormwater

All chemicals used for simulated stormwater and in the synthesis of manganese oxide-coated sand were used as received from Fisher Chemical without further purification. Ultrapure water from a Milli-Q system (R = 18.2 MΩ) was used for all dilutions and for geomedia synthesis. All experiments were performed at room temperature (21 ± 2 °C).

Simulated stormwater, a mixture containing major anions and cations typically found in urban stormwater, was produced using the approach described in Chapter 2 (Grebel et al., 2016). The pH was adjusted to 5.0 ± 0.1 or 7.0 ± 0.1, with 1 N HCl and 1 N NaOH. To prevent the precipitation of Pb-phosphates, phosphate was not included in the simulated stormwater used in Pb adsorption experiments and ionic strength was maintained at 4.6 mM with NaCl. NOM was added to the simulated stormwater when noted. In batch tests, Suwannee River NOM (reverse osmosis isolation IHSS #2R101N) was added at a concentration of 8.0 mg-C/L and Sigma humic acid was added at 6.3 mg-C/L. In column tests, Sigma humic acid was added at 6.3 mg-C/L. Dissolved organic carbon was analyzed using a Shimadzu TOC-V_{CSH}.

Concentrated solutions of metal cations for use in experiments were made from dichloride salts obtained from Sigma Aldrich (> 98% purity) and stored in a pH 3 solution of trace metals-grade HCl. Regenerant solutions were made from trace metals-grade HCl, disodium ethylenediaminetetraacetic acid (EDTA) dihydrate, and crystalline anhydrous citric acid obtained from Fisher Chemical. Before use for experiments, all containers were washed in 2.5 N HNO_3 followed by multiple rinses with deionized water.

4.2.2 Manganese Oxide-Coated Sand

Manganese oxide-coated sand was synthesized using a modification of the cryptomelane synthesis method described by McKenzie (1971). Briefly, in a 1 L beaker, 100 g of acid-washed 20-30 mesh (595-841 μm) Ottawa sand obtained from Fisher Chemical was added to 250 mL of 2 N acetic acid containing 0.5 M $MnSO_4$. The sand was stirred vigorously as 200 mL of 0.43 M potassium permanganate solution was added drop-wise. The coated sand was settled overnight before air drying at 30 °C, after which it was sieved with 40 mesh and rinsed with Milli-Q water to remove loose manganese oxide and then re-dried. The sand had a coating density of 2.01 mg Mn/g geomedia. All geomedia was stored in amber glass bottles under N_2 at room temperature until use, which occurred within 45 days.

4.2.3 Batch Adsorption

Batch adsorption experiments were conducted in triplicate in polystyrene bottles containing 50 mL of simulated stormwater at pH 5.0 and 7.0 without NOM and at pH 7.0 with 8.0 mg-C/L Suwannee River NOM or 6.3 mg-C/L Sigma humic acid. Solutions of individual metal cations were added to produce initial metals concentrations ranging from 0.050 - 440 μM Cu, 0.20 - 460 μM Zn, 0.010 - 270 μM Cd or 0.010 - 1.0 μM Pb. Manganese oxide-coated sand (500 mg) was added to the containers and they were placed on a shaking table. Control batch experiments were conducted with uncoated, acid-washed sand to assess the loss of metals by mechanisms unrelated to the manganese oxide coatings. Negligible particulate manganese concentrations during batch experiments indicated that no geomedia coating was lost due to shaking.

Total and dissolved Cu, Zn, Cd, Pb and Mn were measured in unfiltered samples and in samples filtered with 0.22-μm polyethersulfone syringe filters. Samples (1 mL) were collected in plastic centrifuge tubes and immediately acidified by the addition of a solution of 1% HCl and 0.5% HNO_3 (4 mL).

Samples were collected before the addition of manganese oxide-coated sand and 24 hours after geomedia addition. Preliminary kinetic experiments indicated that equilibrium was reached within 24 hours. The quantity of metal adsorbed per unit mass of manganese oxide, q (mol Me/mg MnO_x), was calculated according to the relationship:

$$q = \frac{(C_i - C_e)V}{m} \qquad \text{(Eq. 4.1)}$$

where C_i is the initial metal concentration, C_e is the equilibrium metal concentration, V is the solution volume and m is the mass of manganese oxide.

Metals quantification was performed with an Agilent 7700 Series Inductively Coupled Plasma-Mass Spectrometer (ICP-MS). Each sample had a pre-run uptake of 45 seconds at 0.35 rotations per second (RPS) of the nebulizer pump followed by a pre-run stabilization of 30 seconds and acquisition at a pump rate determined by tuning (approximately 0.27 RPS). After acquisition, the probe was rinsed for 7 seconds in the sample and 30 seconds in each of two separate 1% HCl and 0.5% HNO_3 rinse ports at 0.35 RPS. Tuning and PA calibration were

carried out using Agilent standard tuning and PA solutions without further purification. Tune parameters are listed in Table 4.1. Samples were quantified using a 9-point calibration curve (R^2>0.98 for each analyte). Samples were analyzed in triplicate with 50 sweeps per replicate and a relative standard deviation quality control threshold for analysis of <5%. Two blank verification samples were analyzed after every 20 experimental samples. Quality controls (5% of samples) were run in duplicate with a threshold for analysis of <10% variation.

Table 4.1 Tuning parameters for ICP-MS Analysis.

Parameter	Value
Plasma	
RF Power	1550 W
RF Matching	1.80 V
Sample Depth	8 mm
Carrier Gas	0.56 L/min
Option Gas	0%
Nebulizer Pump	0.27 RPS
S/C Temp	5 °C
Gas Switch	Dilution Gas
Dilution Gas	0.45 L/min
Lenses	
Extract 1	0 V
Extract 2	-200.0 V
Omega Bias	-120 V
Omega Lens	10.0 V
Cell Entrance	-40 V
Cell Exit	-60 V
Deflect	0.0 V
Plate Bias	-60 V
Cell	
He Flow	4.3 mL/min
Oct P bias	-18.0 V
Oct P RF	180 V
Energy Discrimination	5.0 V

The aqueous activities of ions were calculated from concentrations at an ionic strength of 4.6 mM using the Davies Equation (Davies, 1938):

$$a_i = \gamma_i C_i \quad \text{(Eq. 4.2)}$$

$$\log \gamma_i = -0.5 Z_i^2 \left(\frac{\sqrt{I}}{1+\sqrt{I}} - 0.2I \right) \quad \text{(Eq. 4.3)}$$

where a_i is the activity of the ion, γ_i is the activity coefficient of the ion, C_i is the concentration of the ion, Z_i is the charge of the ion and I is the ionic strength of the solution ($I = 4.6 \times 10^{-3}$ M for simulated stormwater).

4.2.4 Geomedia Longevity Tests

To simulate infiltration systems, 16 mm inner-diameter glass columns with polyethylene fittings were packed with 10 g of manganese oxide-coated sand to a height of 36 mm. The porosity of a packed column was 0.33, the pore volume was 2.39 mL and hydraulic conditions were similar to those described in Chapter 2. Columns and tubing were washed prior to packing by flushing with 250 mL of a 1% HCl solution followed by 250 mL of Milli-Q water. Simulated stormwater solutions were autoclaved prior to use and columns were covered with aluminum foil. Columns were operated with saturated upwards flow using a peristaltic pump and Tygon and PTFE tubing. Simulated stormwater containing Cu, Zn, Cd or Pb was pumped through the columns at 0.4 mL/min, which is equivalent to an infiltration rate of 9.5 cm/h. This infiltration rate is typical for stormwater infiltration systems (Hatt et al., 2008). The average influent concentrations of dissolved metals were measured immediately upstream of the columns as follows: $Cu_0 = 2.5 \pm 0.7$ µM, $Zn_0 = 27 \pm 4$ µM, $Cd_0 = 3.9 \pm 0.5$ µM and $Pb_0 = 0.59 \pm 0.08$ µM. To obtain breakthrough from columns within the timeframe of the experiment, influent concentrations of metals ranged from 3 to 125 times higher than those typically observed in urban stormwater. Column feed solutions were stored in 2 L aluminum foil-wrapped glass containers that were continuously stirred with Teflon-coated magnetic stir bars. Samples were collected from the column effluent approximately every 240 pore volumes and a 1 mL aliquot was filtered with a 0.22 µm polyethersulfone syringe filter and immediately acidified with 4 mL of a solution of 1% HCl and 0.5% HNO_3 before measurement of dissolved Cu, Zn, Cd, Pb and Mn by ICP-MS. Flow into the columns was stopped after values of C/C_0 for the metal consistently exceeded 0.9, or after 2170 pore volumes. After the flow was stopped, pore water was drained and the geomedia was stored in columns with ends capped for no more than 24 hours prior to analysis or use in regeneration experiments.

Equilibrium speciation of metals in the column feed solutions was modelled using the Visual MINTEQ software (Gustafsson, 2014). The precipitation of solids was not allowed in the models, pH values were fixed at 7.00 and ionic strength was calculated by the model. Model temperature was fixed at 25 °C. The simulated stormwater was modelled with constituents as shown in Table 1.3. Total metal concentrations were fixed at $Cu(II)_{Tot} = 3.14$ µM, $Zn(II)_{Tot} = 30.6$ µM, $Cd(II)_{Tot} = 4.45$ µM and $Pb(II)_{Tot} = 0.724$ µM. The DOC-SHM model of NOM within Visual MINTEQ was used in to model NOM-containing simulated stormwater.

4.2.5 Geomedia Regeneration

Chemical regenerants were tested in batch to assess their ability to recover adsorbed metals by lowering pH (i.e., HCl), introducing metal-complexing ligands (i.e., EDTA) or both (i.e., citric acid). After completing column longevity tests, triplicate samples of 1 g of dry, homogenized manganese oxide-coated sand from each column experiment was added to a polystyrene container with 50 mL of regenerant solution and continuously shaken for 24.5 hours. Treatments with 100 mM and 1 mM HCl (i.e., pH 1 and pH 3) were tested. The EDTA and citric acid were each applied at a 1:1 and 2:1 stoichiometric ratio of ligand to adsorbed metal. Concentrations of ligands are shown in Table 4.2. Regenerant solutions were unbuffered. Equilibrium speciation of metals in the regenerant solutions was predicted using Visual MINTEQ with the parameters noted above and the concentrations of ligands shown in Table 4.2.

Table 4.2 Concentrations of ligands for regeneration.

Failed Geomedia	Concentration EDTA or Citric Acid (μM)	
	1:1 Ratio	2:1 Ratio
Cu Treatment	21.5	43.0
Zn Treatment	73.0	146
Cd Treatment	18.9	37.8
Pb Treatment	4.4	8.8

Samples of the regenerant solution (1 mL) were collected every 60-120 minutes and analyzed by ICP-MS to determine the amount of metal desorbed from the manganese oxide surface.

The pH 3 HCl solution was further evaluated as a regenerant by passing it through the failed columns at 0.4 mL/min for 150 pore volumes (50 hours). Samples of column effluent during regeneration were collected approximately every 20 pore volumes and acidified. Following the regeneration, flow into the columns was stopped, pore water was drained and the geomedia was stored in columns with ends capped for no more than 24 hours prior to analysis.

4.2.6 Geomedia Characterization

The Mn coating density and total adsorbed metal concentration on the geomedia were quantified after longevity and regeneration experiments. The geomedia from the upstream and downstream halves of the columns were individually collected, homogenized, and air dried at 30 °C. Triplicate 0.5 g samples were treated with 10 mL of 30 mM ascorbic acid overnight prior to filtration with a 0.22 μm polyethersulfone filter and quantification of dissolved metals by ICP-MS.

Scanning electron microscopy (SEM) was performed with a Zeiss EVO MA10 scanning electron microscope at 20 kV and a 1 nA current. Energy dispersive X-ray spectroscopy (EDS) was performed with an EDAX Genesis Imaging/Mapping analyzer.

The pH_{pzc} of the manganese oxide-coated sand was determined by sonicating 1 g of the geomedia in 5 mL Milli-Q water for 3 min to remove the manganese oxide coating. A 10 µL aliquot of the coating material suspension was mixed with dilute HCl to produce various pH conditions. The zeta potential was immediately measured using a Malvern Zetasizer Nano. The pH_{pzc} was determined using a linear fit of zeta potential vs. pH within 0.5 pH units of the pH_{pzc}.

4.3 Results and Discussion

4.3.1 Batch Adsorption

Batch experiments fit Freunlich isotherms for the adsorption of Cu, Zn, Cd and Pb onto manganese oxide-coated sand in NOM-free simulated stormwater at pH 5 (Figure 4.1) and pH 7 (Figure 4.2), and at pH 7 in the presence of NOM (Figure 4.3). Each metal was tested individually in separate experiments. At pH 7 in the absence of NOM, over 95% of Cu, Cd and Pb and 50% of Zn were removed from solutions with metal concentrations typical of stormwater (Table 4.3). Under the same conditions with 8.0 mg-C/L Suwannee River NOM present only about 50% of Cu was adsorbed, but over 90% of the Cd and Pb were adsorbed.

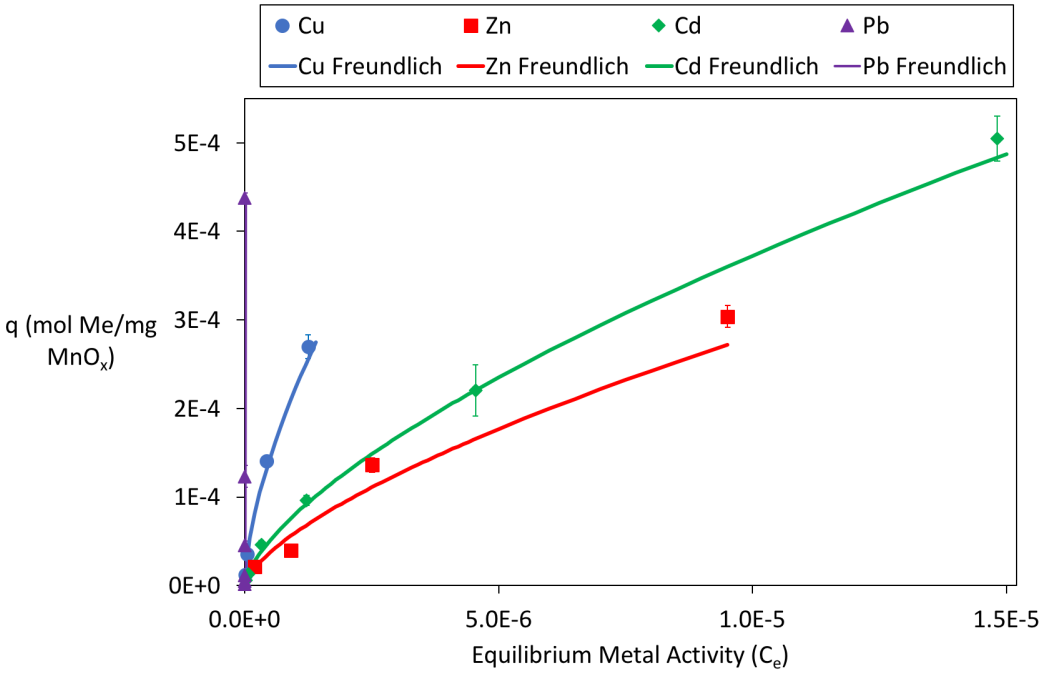

Figure 4.1 Batch adsorption isotherms and Freundlich model fits for Cu, Zn, Cd and Pb with 500 mg manganese oxide-coated sand in NOM-free simulated stormwater at pH 5. Error bars from triplicate experiments are smaller than symbols in some cases.

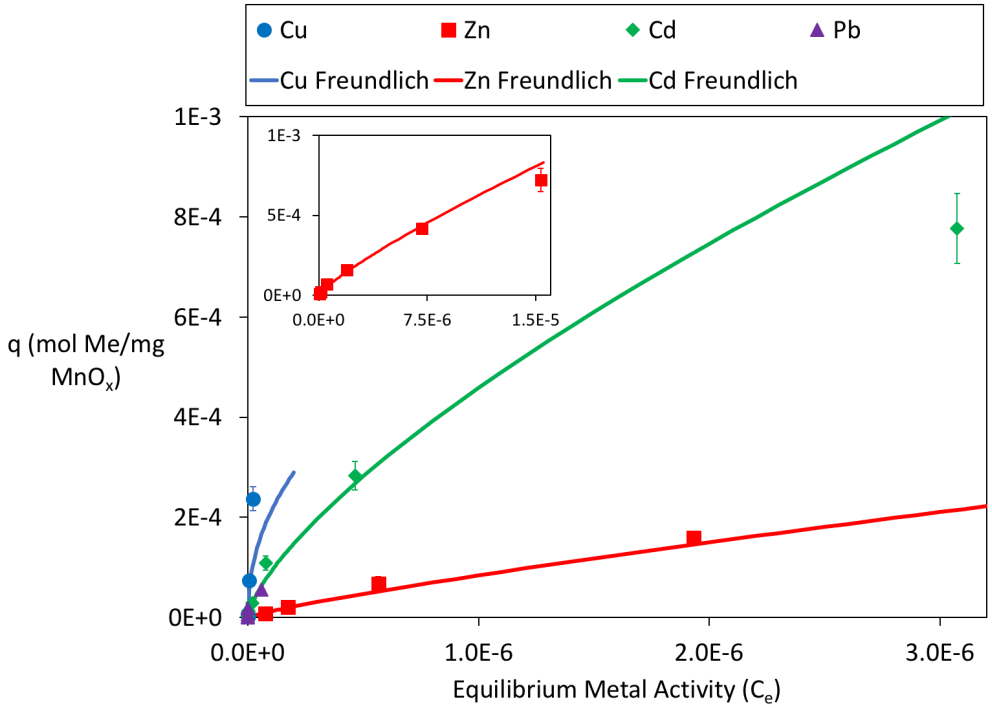

Figure 4.2 Batch adsorption isotherms and Freundlich model fits for Cu, Zn, Cd and Pb with 500 mg manganese oxide-coated sand in NOM-free simulated stormwater at pH 7. No isotherm model was developed to fit Pb due to low aqueous equilibrium concentrations. To illustrate the relative trends of metals, Zn data are truncated. The complete Zn isotherm is included in the inset. Error bars from triplicate experiments are smaller than symbols in some cases.

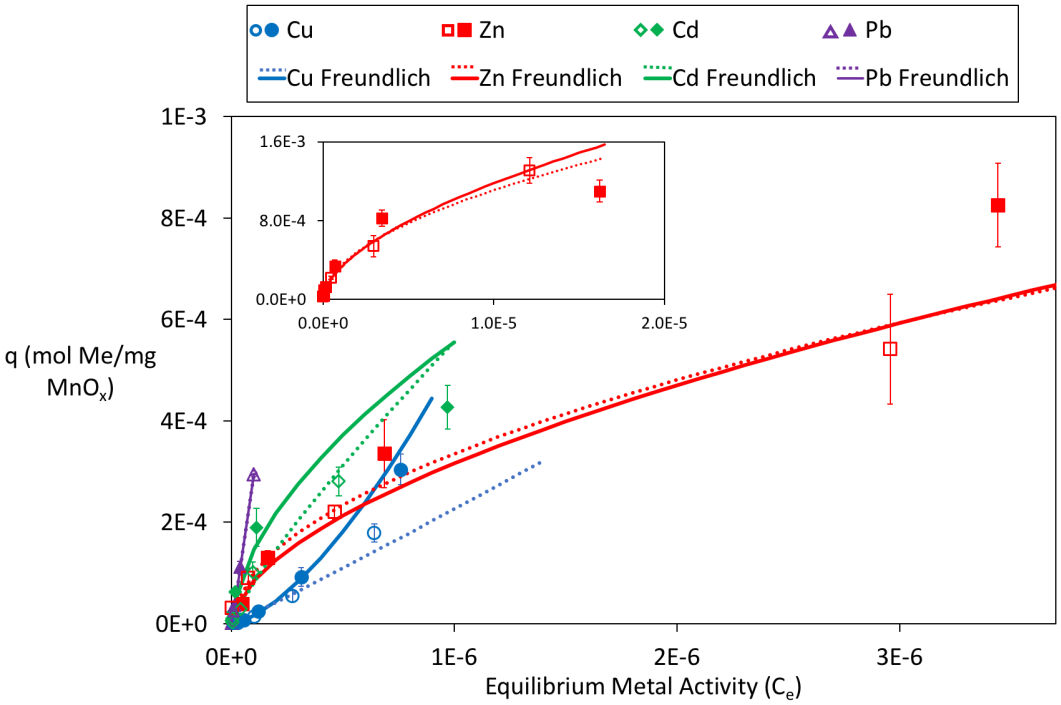

Figure 4.3 Batch adsorption isotherms and Freundlich model fits for Cu, Zn, Cd and Pb with 500 mg manganese oxide-coated sand in simulated stormwater with 8.0 mg-C/L Suwannee River (closed symbols, solid line) NOM and 6.4 mg-C/L Sigma humic acid (open symbols, dotted line). To illustrate the relative trends of metals, Zn data are truncated. The complete Zn isotherm is included in the inset. Error bars from triplicate experiments are smaller than symbols in some cases.

Table 4.3 Removal of metals at typical stormwater concentrations in batch experiments

		pH 7 Simulated Stormwater, No NOM			pH 7 Simulated Stormwater, 8.0 mg-C/L Suwannee River NOM		
Metal	Average Stormwater Conc.(nM)*	Initial Conc. (nM)	Final Conc. (nM)	Removal	Initial Conc. (nM)	Final Conc. (nM)	Removal
Cu	252	310 ± 3	0.3 ± 0.0	100%	312 ± 3	164 ± 2	48%
Zn	1790	1570 ± 20	760 ± 10	52%	2940 ± 30	920 ± 10	69%
Cd	13	40 ± 1	2 ± 0	95%	41 ± 1	1 ± 0	98%
Pb	38	76 ± 1	0.6 ± 0	99%	75 ± 1	7 ± 0	90%

*Pitt et al., 2015

In the absence of NOM, Pb was the most strongly adsorbed metal, followed by Cu, Cd and Zn, respectively. These relative affinities are consistent with previous research indicating that Cu and Pb are more strongly adsorbed by manganese oxides than Zn and Cd (Catts and Langmuir, 1986; Fu et al., 1991; Gadde and Laitinen, 1974; McKenzie, 1980; van Lienden et al., 2010; Wang and Stumm, 1987; Zasoski and Burau, 1988). In general, strongly hydrolysable metals exhibit a higher affinity for adsorbents than weakly hydrolysable metals (Morgan and

Stumm, 1964). This trend is due to the labile, polarizable electron configurations of large cations (e.g., Pb^{2+}) and transition metals high on the Irving-Williams order (e.g., Cu^{2+}) which results in poor solvation and specific interactions with surface sites (Sposito, 2008). The presence 0.75 mM Ca^{2+} in the simulated stormwater may have inhibited the adsorption of Zn more than of other metals. Ca and Zn have similar properties (e.g., $4s^2$ valence electron configuration) and compete for surface sites, resulting in diminished Zn adsorption (Catts and Langmuir, 1986). Ca may also strongly inhibit Cd adsorption, but has only a small effect on Cu or Pb adsorption, even at high Ca concentrations (Catts and Langmuir, 1986; Wan et al., 2015).

Langmuir and Freundlich isotherm models were applied to the adsorption data. Freundlich isotherm models were expressed by the following relationship:

$$q = K_F C_e^{\,1/n} \qquad \text{(Eq. 4.4)}$$

where q [mol Me/mg MnOx] is the concentration of the adsorbate on the adsorbent, C_e is the equilibrium activity of the adsorbate, and K_F and n are constants (Table 4.4). Freundlich models fit the results better than Langmuir models for all metals tested (data not shown). Freundlich models consistently fit the data well ($R^2 > 0.97$), except Cu and Pb at pH 5 and 7 in NOM-free stormwater. In this case, strong adsorption resulted in equilibrium concentrations of dissolved Cu and Pb below the method detection limit (i.e., 0.4 nM) for some conditions.

Table 4.4 Freundlich model constants estimated for metals with manganese oxide-coated sand in batch tests.

		$K_F \left[\frac{(\text{mol Me})^{(1-\frac{1}{n})} * L^{\frac{1}{n}}}{\text{mg } MnO_x}\right]$	n
pH 5 NOM-Free Simulated Stormwater	Cu	1.20	1.60
	Zn	0.66	1.48
	Cd	0.78	1.51
	Pb	1.20×10^5	0.95
pH 7 NOM-Free Simulated Stormwater	Cu	0.36	2.16
	Zn	8.6	1.20
	Cd	1.4	7.51
	Pb	N/A	N/A
pH 7 Simulated Stormwater, 8 mg-C/L Suwannee River NOM	Cu	7.5×10^5	0.66
	Zn	0.86	1.75
	Cd	1.7	1.72
	Pb	1.2×10^4	0.92
pH 7 Simulated Stormwater, 6.4 mg-C/L Sigma Humic Acid	Cu	420	0.97
	Zn	0.44	1.92
	Cd	56.0	1.20
	Pb	10×10^5	0.73

Previous studies also fit manganese oxide adsorption isotherms to the Freundlich model (Caliskan et al., 2011; Li et al., 2004; Zasoski and Burau, 1988). Other researchers fit adsorption isotherms to multi-component Langmuir models (Fu et al., 1991; Loganathan and Burau, 1973). Although fit to an isotherm model does not necessarily demonstrate the dominance of a particular adsorption mechanism, these models are consistent with mechanisms involving two or more distinct adsorption sites or variations in adsorption energy (e.g., differences between hydrolysis species) (Loganathan and Burau, 1973; Zasoski and Burau, 1988). Apparent equilibrium binding constants to the manganese oxide surface depend on fractional surface coverage (Catts and Langmuir, 1986) and manganese oxides exhibit heterogeneity in surface sites due to edges, kinks and vacancies. Given that the Freundlich model represents a multi-site Langmuir model with a specific site distribution wherein site abundance decreases geometrically with increasing affinity (Benjamin and Lawler, 2013; Halsey and Taylor, 1947), the fit to the Freundlich model in this study is consistent with the prevailing models of specific adsorption to manganese oxides (Catts and Langmuir, 1986; Gadde and Laitinen, 1974).

Unlike the Langmuir model, the Freundlich model cannot be used to calculate a theoretical q_{max} (i.e., the adsorbate saturation concentration on adsorbent). However, due to the relatively large ratios of adsorbent to solution volume tested and metal concentrations nearing supersaturation for the precipitation of metal oxide minerals, the maximum concentrations of metals on the manganese oxides in the batch experiments were an order of magnitude lower than saturation concentrations determined in other studies (Fu et al., 1991; Gadde and Laitinen, 1974).

Adsorption was stronger at pH 7 than at pH 5 for all metals, consistent with expected trends of cation adsorption (Fu et al., 1991; Gadde and Laitinen, 1974; Loganathan et al., 1977). Protons are released from the surface via the following reactions of metal cations (Me^{2+}) with uncharged surface reaction sites (>MnOH) (McKenzie, 1980):

$$>MnOH + Me^{2+} \rightarrow >MnO\text{-}Me^{+} + H^{+} \quad (4.1)$$

$$2>MnOH + Me^{2+} \rightarrow >(MnO\text{-})_2Me + 2H^{+} \quad (4.2)$$

$$>MnOH + Me^{2+} + H_2O \rightarrow >MnO\text{-}MeOH + 2H^{+} \quad (4.3)$$

where Reaction 4.1 is the formation of a surface complex displacing 1 proton from the surface and Reaction 4.2 is the formation of a bidentate surface complex, releasing 2 protons. Reaction 4.3 is a general two-step reaction that accurately describes both the adsorption of the unhydrolyzed metal followed by surface hydrolysis and hydrolysis in solution followed by adsorption of the hydrolysis species (James et al., 1975). Although the pH values in batch adsorption tests were above the adsorption edge for these metals on manganese oxides, the greater adsorption observed at higher pH is consistent with these models for surface complexation (Loganathan and Burau, 1973; McKenzie, 1981).

Other mechanisms could have contributed to the greater adsorption of metals at high pH values. A more electronegative surface charge at high pH may have been more attractive to cations (Fu et al., 1991; Loganathan et al., 1977). Further, higher pH conditions may have facilitated the adsorption of hydrolysis species, which have lower hydration energies than unhydrolyzed cations. These species typically become the dominant surface species above pH 6,

despite relatively low aqueous concentrations below pH 8 (Catts and Langmuir, 1986; James and Healy, 1972; Loganathan et al., 1977; Zasoski and Burau, 1988).

Metals removal was lower when NOM was present, although adsorption isotherms still fit a Freundlich model, consistent with the results previous studies (Figure 4.3) (Frimmel and Huber, 1996). Cu adsorption was the most diminished by the presence of NOM, followed by Pb. Zn and Cd adsorption were similar in the presence and absence of NOM. This result is consistent with the relative magnitudes of the stability constants for metal-NOM complexes $Cu^{2+} > Pb^{2+} >> Zn^{2+} \approx Cd^{2+}$ (Cabaniss, 2009; Christensen and Christensen, 1999; Saar and Weber, 1980; Stevenson, 1976; Takamatsu and Yoshida, 1978). NOM forms complexes with Cu, Zn, Cd and Pb cations, increasing their dissolved concentrations and decreasing their partitioning to the adsorbed phase (Christensen et al., 1996; Godtfredsen and Stone, 1994; Schmitt et al., 2003). A secondary cause of diminished adsorption may have been the reductive dissolution of the manganese oxide by NOM. This reaction could have produced Mn^{2+} which would compete with the metal contaminants for fewer adsorption sites (Godtfredsen and Stone, 1994).

Despite the fact that Sigma humic acid is considered to be a poor surrogate for dissolved organic matter in natural systems with respect to metal complexes, particularly in comparison to Suwannee River reverse osmosis isolate (Kim and Dempsey, 2013; Niederer et al., 2007), the two types of NOM had similar effects on metal adsorption (Figure 4.3, Table 4.4). On this basis, we concluded that Sigma humic acid is appropriate for column experiments. This substitute was important because 3 g of Suwannee River NOM (cost > $300/g) would have been required to conduct the column tests.

These experiments considered each metal contaminant in isolation. Previous research has established that these metals compete for adsorption sites on the manganese oxide surface when present as co-solutes. Pb out-competes all other metals on manganese oxides; its adsorption is unaffected by the presence other metals, while the presence of Pb lowers the manganese oxide adsorption capacity of Cu, Zn and Cd (Catts and Langmuir, 1986; Gadde and Laitinen, 1974). Likewise, the co-occurrence of Cu, Zn or Cd diminishes the adsorption of each metal present due to competition. (Gadde and Laitinen, 1974; Zasoski and Burau, 1988).

4.3.2 Column Longevity

Columns of manganese oxide-coated sand achieved high removal of all metals for at least the first 240 pore volumes of operation in the absence of NOM (circles and solid lines in Figure 4.4). Cu and Pb removal remained high throughout the entire experiment; however, Zn removal decreased rapidly, with complete breakthrough after 970 pore volumes. Complete breakthrough of Cd occurred after 1420 pore volumes.

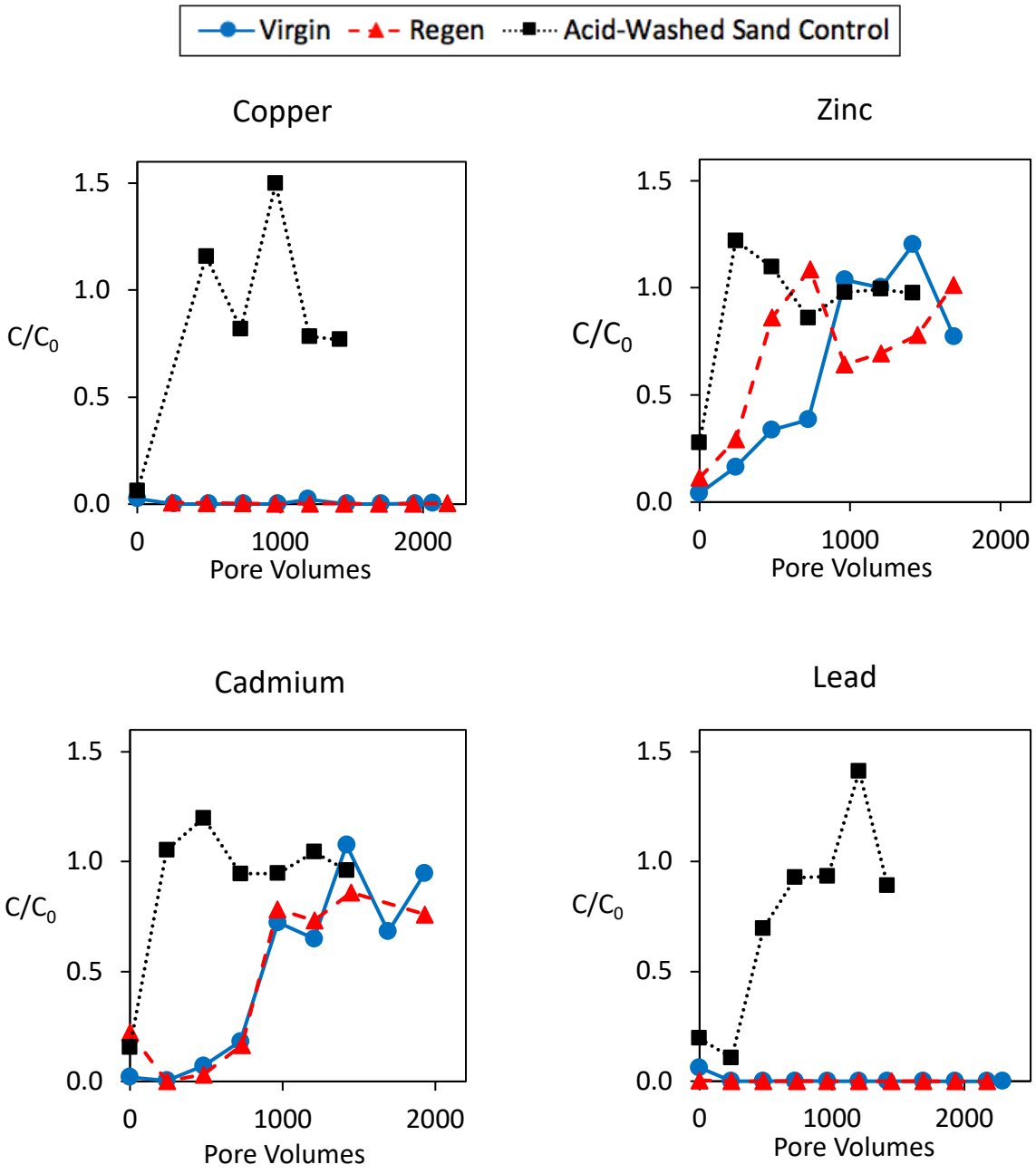

Figure 4.4 Relative concentration of metals in effluent from columns. Virgin geomedia (blue circles and solid lines), regenerated geomedia (red triangles and dashed lines) and control columns (black squares and dotted lines) of acid-washed sand were tested in pH 7 simulated stormwater without NOM. To facilitate comparison between virgin and regenerated geomedia, the X-axis designates pore volumes of experimentation beginning at 0 for both cases.

The manganese oxide was responsible for the removal of metals from solutions. Rapid breakthrough (i.e., $C/C_0 \approx 1$ after < 250 pore volumes) of Cu, Zn and Cd occurred in control columns of acid-washed sand. Breakthrough of Pb in control columns was slower than that of other metals (i.e., $C/C_0 \approx 1$ after < 750 pore volumes) but fast compared to the complete removal of Pb in geomedia-containing columns. SEM/EDS confirmed that metals were adsorbed to the manganese oxide coating on the geomedia. Element mapping demonstrated clear co-location of Mn and the adsorbed metal (e.g., Cd; Figure 4.5)

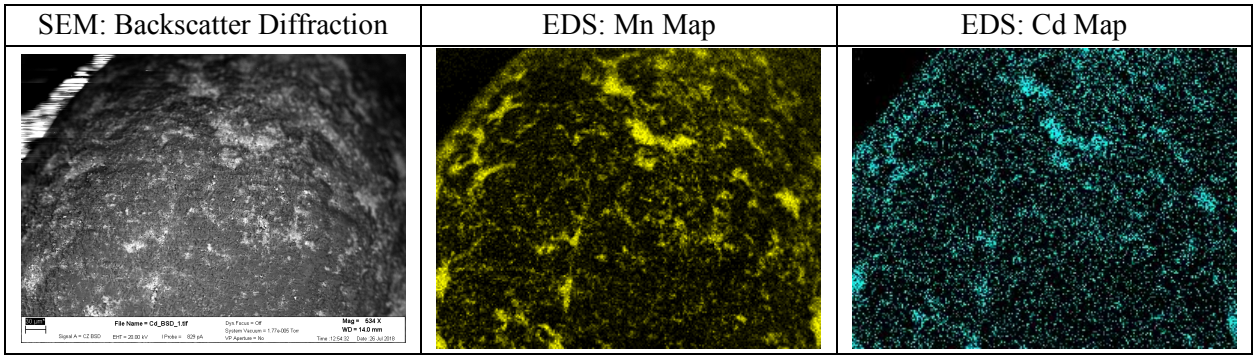

Figure 4.5 Backscatter diffraction scanning electron microscope image (left) and energy dispersive X-ray spectroscopy element maps (center, right) of representative geomedia used to treat of Cd-containing stormwater in columns. All images are approximately 534X magnified. In the SEM images, Mn-oxide appears bright. In the element maps, Mn appears yellow and Cd appears cyan.

Relative removal of metals from the columns followed the same trends observed in batch experiments. Zn broke through columns relatively quickly. Although the manganese oxide delayed breakthrough compared to control columns, removal of Zn was incomplete even before breakthrough occurred. Even after accounting for a Zn concentration in the simulated stormwater that was 15 times higher than typical Zn concentrations in stormwater (Table 1.2), this result suggests that treatment of Zn pollution with this technology would be the least effective of the metals tested. High levels of Cd removal were sustained for approximately 750 pore volumes of treatment. Although breakthrough did eventually occur, this result is promising for the long-term removal of Cd during stormwater infiltration, because Cd concentrations used in the column experiments were 300 times higher than typical Cd concentrations in stormwater (Table 1.2). Complete removal of Cu and Pb was sustained throughout column experiments in NOM-free simulated stormwater, which was consistent with high levels of metal adsorption in batch experiments.

The reported saturations in Table 4.5 are the maximum concentrations of metals on pure manganese oxide minerals as determined in batch experiments. Reported saturation capacities for these metals on manganese oxides vary considerably with the type of manganese oxide (Han et al., 2006; Su et al., 2009; Wan et al., 2015) and with solution pH (Gadde and Laitinen, 1974).

Table 4.5 Adsorbed metal concentration on upstream and downstream halves of geomedia following column tests in pH 7 NOM-free stormwater.

Column	mmol Me/g MnO_x: Upstream Geomedia	mmol Me/g MnO_x: Downstream Geomedia	Reported Saturation (mmol Me/g MnO_x)
Cu	1.9	0.06	1.54 (at pH 5.5)[*]
Zn	2.5	3.2	2.73 (at pH 6)[†]
Cd	0.82	0.74	1.93 (at pH 6)[†]
Pb	0.06	0.03	6.37 (at pH 6)[†]

[*]Fu et al., 1991; [†]Gadde and Laitinen, 1974

Cu- and Pb-treating columns, which did not exhibit breakthrough, had considerably higher concentrations of adsorbed metals on the upstream geomedia compared to the downstream geomedia. Due in part to its very high adsorption capacity on manganese oxide, the concentration of adsorbed Pb on the geomedia was two orders of magnitude below the reported saturation capacity after column tests. Based on literature values, Cu concentrations on the upstream portion of the geomedia were likely near saturation by the end of the column experiment, but the low Cu concentration on the downstream geomedia implies that significant capacity remained in the columns before breakthrough would occur. These results suggest that adsorptive equilibrium was reached quickly within the columns, as has been reported in other systems (Caliskan et al., 2011; Loganathan and Burau, 1973; Zou et al., 2006) and that the geomedia saturated pulse-wise within columns with small mass transfer limitations.

In columns for which complete breakthrough of metals occurred (i.e., Zn and Cd), the geomedia in the upstream and downstream sections of the columns adsorbed similar amounts of metal (Table 4.5). These metals concentrations were therefore the adsorption capacity of the manganese oxide-coated sand. The breakthrough of Cd suggests that the adsorption capacity of the geomedia was approximately 0.8 mmol Cd/g manganese oxide. This value is below previously reported values, possibly due to competition by Ca^{2+} in this system (Zasoski and Burau, 1988). The adsorption capacity for Zn was approximately 3 mmol Zn/g manganese oxide, which is consistent with previously measured adsorption capacities (Zasoski and Burau, 1988).

Similar to the results of batch tests, Cu and Pb removal in columns decreased markedly in the presence of organic matter relative to NOM-free simulated stormwater. Only partial removal of Cu and Pb was achieved when NOM was present (Figure 4.6). Adsorption likely declined because NOM complexation shifted equilibrium away from surface-associated Cu and Pb (Oden et al., 1993; Schmitt et al., 2003). The impact of NOM on geomedia performance was closely related to the abundance of metals complexed by NOM as predicted by Visual MINTEQ (Table 4.6). Over 96% of Cu and Pb were predicted to be complexed by NOM. Surface complexation models have established that the free metal ion and its first two hydrolysis species are important to the adsorption of metals on manganese oxides (Catts and Langmuir, 1986; Loganathan and Burau, 1973; Zasoski and Burau, 1988). The large decline in the abundance of these species in the presence of NOM may explain their reduced adsorption. Further, the consistent, low-concentration breakthrough of Pb in the presence of NOM (Figure 4.6) suggests that a small

number of strong ligands sites within NOM formed very stable Pb-NOM complexes (Filella, 2008; van de Weerd et al., 1999). If this complexation was practically irreversible within the conditions of column experiments, it may have limited the total amount of absorbable Pb in the system.

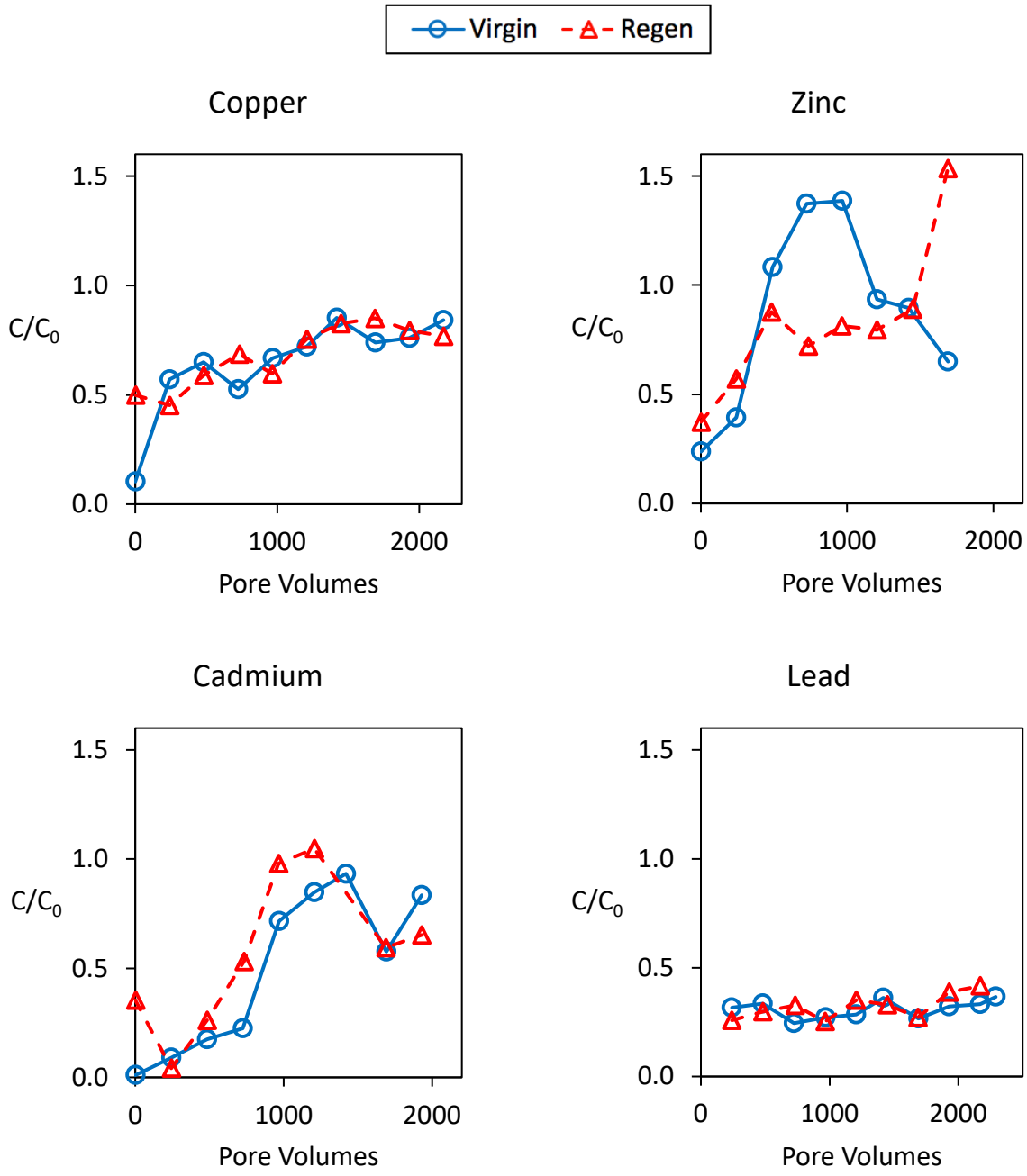

Figure 4.6 Relative concentration of metals in effluent from columns. Virgin geomedia (blue circles and solid lines) and regenerated geomedia (red triangles and dashed lines) were tested in pH 7 simulated stormwater containing 6.4 mg-C/L Sigma humic acid.

Table 4.6 Predicted proportions of total metals as free ions or hydrolysis species and as metal-NOM complexes in pH 7 simulated stormwater fed to columns.

	NOM-Free Stormwater	NOM-Containing Stormwater	
	$([Me^{2+}] + [Me(OH)^{+}] + [Me(OH)_2^0])/Me_T$	$([Me^{2+}] + [Me(OH)^{+}] + [Me(OH)_2^0])/Me_T$	$[Me\text{-}NOM]_T/ Me_T$
Cu	0.42	0.02	0.96
Zn	0.92	0.75	0.19
Cd	0.83	0.63	0.24
Pb	0.44	0.01	0.97

Zn and Cd exhibited small declines in performance in the presence of NOM relative to NOM-free simulated stormwater. This result is consistent with their relatively weaker complexation by NOM (Cabaniss, 2009; Saar and Weber, 1980). The equilibrium model predicted that less than 25% of Zn and Cd would be complexed by NOM in the simulated stormwater. These results suggest that complexation of the dissolved metal by NOM was responsible for most of the decline in column performance.

Other mechanisms may have contributed to diminished metals adsorption in the presence of NOM. The effect of NOM fouling adsorptive sites on the manganese oxides was likely small (Godtfredsen and Stone, 1994). The pH_{pzc} of the coating of the geomedia was approximately 3.3. Therefore, the negative surface charge of the manganese oxide in the pH 7 stormwater likely electrostatically repelled the negatively charged NOM and metal-NOM complexes (Gregor et al., 1955; Klučáková and Kolajová, 2014; Masini, 1993; Zhong et al., 2005). Reduction of manganese oxide by reactive groups in the NOM may have produced Mn^{2+}, which competes for a smaller number of adsorptive sites with other metals (Godtfredsen and Stone, 1994; Loganathan and Burau, 1973; McKenzie, 1970).

Some Mn was released during column experiments. When NOM was present, effluent Mn concentrations were approximately 0.6 μM (Figure 4.7). Over these experiments, approximately 1% of the manganese oxide coating was released from the columns. The release was likely caused by the reduction of the manganese oxide by phenolic groups in the NOM (Stone and Morgan, 1984; Sunda et al., 1983). In the absence of NOM, concentrations of Mn in the column effluent were less than 0.03 μM. Dissolved Mn can be an aesthetic concern in drinking water at concentrations as low as 1.4 μM (Sain and Dietrich, 2015); the US EPA secondary standard for maximum total dissolved Mn is 0.91 μM (US Environmental Protection Agency, 2004). The concentrations of Mn observed in this experiment suggest that Mn leaching is not expected to be a water quality concern, especially if the water is diluted in the aquifer or if dissolved Mn adsorbs onto surfaces in the aquifer.

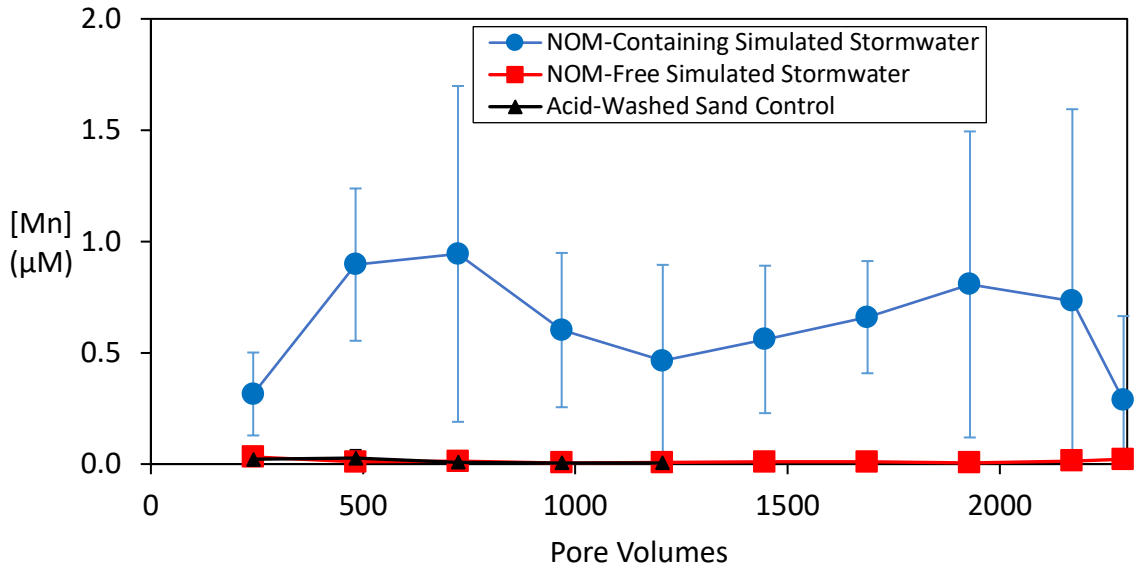

Figure 4.7 Average concentration of Mn in effluent from columns treating metals in NOM-containing (circles) and NOM-free (squares) simulated stormwater. Mn in effluent from acid-washed sand control column was negligible (triangles). Some error bars are smaller than the data symbols.

4.3.3 Geomedia Regeneration

Three different chemical treatments were evaluated in batch to determine the most effective regenerant of the manganese oxide-coated sand. HCl was applied at pH 1 and pH 3. Citric acid and EDTA were applied at 1:1 and 2:1 stoichiometric ratios relative to the total concentrations of adsorbed metals. The results of batch desorption experiments suggest that both lowering pH and adding ligands can cause the release of adsorbed metals, but that lowering pH is a more efficient regeneration technique (Figure 4.8).

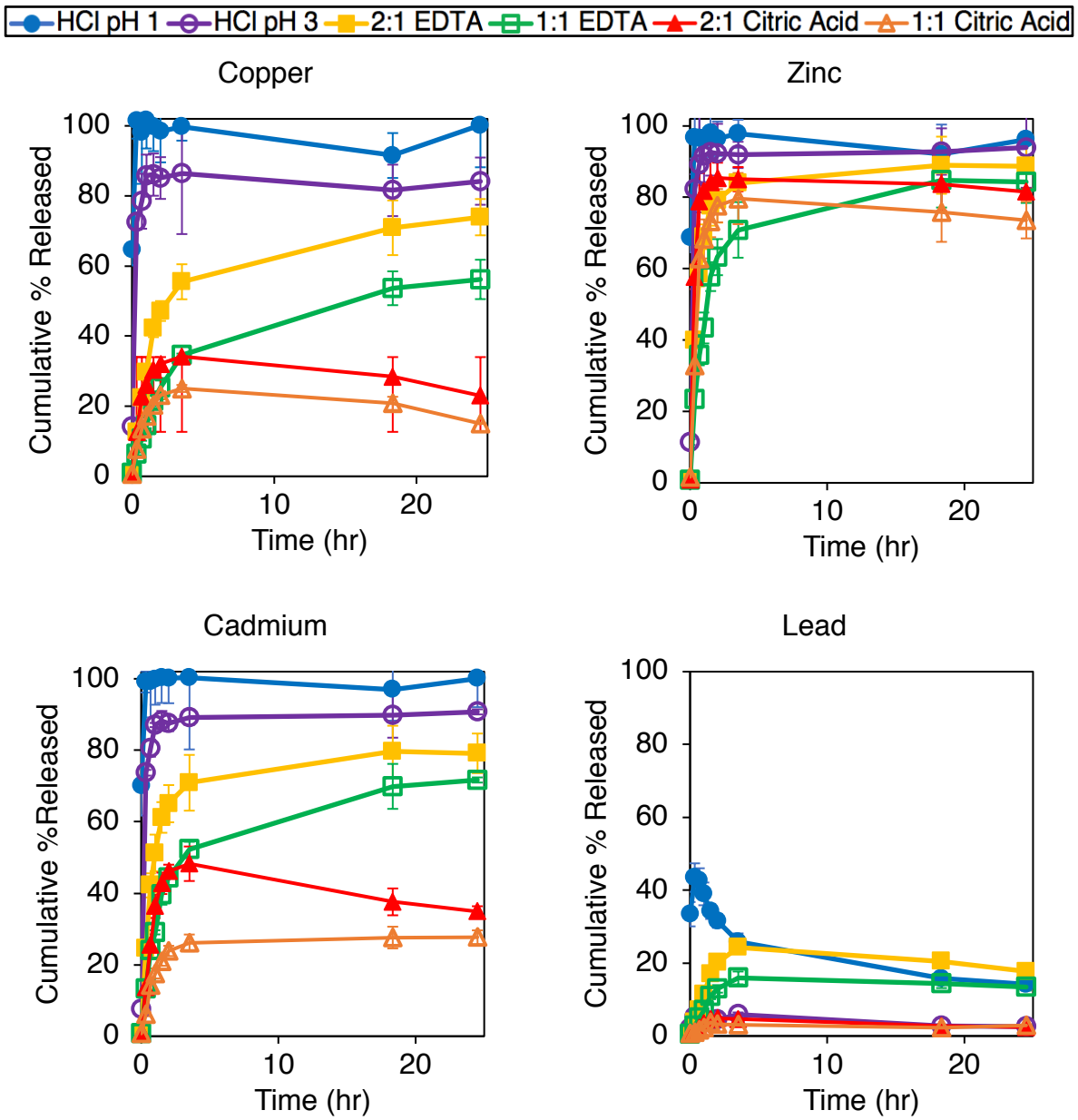

Figure 4.8 Percentage of the total adsorbed metals that were released to the aqueous phase during batch regeneration. 1 g of failed geomedia from column testing was shaken in 50 mL of regenerant solution containing either pH 1 or pH 3 HCl (circles), EDTA at a 2:1 or 1:1 stoichiometric ratio to the adsorbed metal (squares) or citric acid at a 2:1 or 1:1 stoichiometric ratio to the adsorbed metal (triangles). Error bars from triplicate experiments are smaller than symbols in some cases.

Batch regeneration tests indicated that hydrochloric acid was the most effective treatment. At pH 1 metal desorption occurred rapidly, with >96% of the Cu, Zn and Cd released after only 20 minutes. Desorption was also fast at pH 3, with >85% of adsorbed Cu, Zn and Cd released after 24.5 hours.

Treatment with EDTA also released significant quantities of Cu, Zn and Cd. 1:1 and 2:1 stoichiometric concentrations of EDTA resulted in the release of >50% and >70%, respectively, of adsorbed Cu, Zn and Cd during batch experiments. The EDTA shifted the equilibrium of metals in the system to the dissolved phase (Fendorf et al., 1999; Sun et al., 2001; Zachara et al., 1995). The equilibrium model predicted that during batch regeneration nearly 100% of dissolved metals were complexed by EDTA. The kinetics of release with EDTA treatment were slower than with HCl treatment; the dissolved Cu, Zn and Cd concentrations increased over the full 24-hour period. The initial pH of the EDTA solutions ranged from 5.1 to 5.6, and after regeneration pH values ranged from 6.0 to 6.4 (Table 4.7). These small changes in pH were anticipated, as the regenerant solutions were unbuffered. The increase of pH during experimentation was likely due to the protonation of manganese oxide surface groups (reactions 4.1, 4.2 and 4.3 in reverse).

Table 4.7 Initial and final pH of batch EDTA regenerant solutions

Treatment	Initial pH	Final pH
1:1 Cu	5.46	6.34
2:1 Cu	5.37	6.41
1:1 Zn	5.30	6.01
2:1 Zn	5.14	6.23
1:1 Cd	5.49	6.18
2:1 Cd	5.31	6.18
1:1 Pb	5.60	6.43
2:1 Pb	5.46	6.30

The citric acid was almost always the least effective regenerant. Treatment with citric acid resulted in the release of >70% of adsorbed Zn but little release of Cu, Cd or Pb. The greater release of Zn than other metals was anticipated; Zn adsorption on MnO_2 is known to be readily reversible (Li et al., 2004). Though citrate has been shown to compete with the manganese oxide surface for metals by shifting equilibrium towards the dissolved phase (Di Palma and Mecozzi, 2007; Godtfredsen and Stone, 1994), complexing by citric acid did not shift the equilibrium of the metals to the dissolved phase as much as EDTA did. The equilibrium model predicted that during batch regeneration over 90% of dissolved Cu was complexed by citrate, but only about 50% of dissolved Zn and less than 5% of dissolved Cd and Pb were complexed by citrate. The initial pH of the citric acid regenerant solutions ranged from 3.9 to 5.1. After regeneration, pH values ranged from 6.0 to 6.5 (Table 4.8). The low pH of the citric acid solution may have contributed to some of the release of adsorbed metals, but these pH values were still above the metals' adsorption edge (Wang and Stumm, 1987). Citrate also reacts slowly with manganese oxides and thus may have reduced some of the geomedia coating (Stone and Morgan, 1984).

Table 4.8 Initial and final pH of batch citric acid regenerant solutions

Treatment	Initial pH	Final pH
1:1 Cu	4.55	6.21
2:1 Cu	4.29	5.99
1:1 Zn	4.10	6.24
2:1 Zn	3.88	6.22
1:1 Cd	4.58	6.19
2:1 Cd	4.29	6.12
1:1 Pb	5.08	6.50
2:1 Pb	4.80	6.33

Pb was not recovered during any batch regeneration treatment, likely due strong specific adsorption. Previous research documented that very little Pb adsorbed by manganese oxide was recovered by treatment with 2.5% acetic acid (McKenzie, 1980), while desorption of Pb from manganese oxide-coated tea waste was documented after treatment with 0.5 M HCl (Wan et al., 2015). The electronic properties of Pb result in the formation of strong surface complexes with the manganese oxide (Wan et al., 2015; Wang and Stumm, 1987). Pb can enter into the interlayer and tunnels of manganese oxides, facilitating its strong adsorption (O'Reilly and Hochella, 2003). Researchers also have determined that it is unlikely that substitution reactions facilitate the formation of Pb-Mn minerals such as coronadite, even at high Pb surface concentrations (McKenzie, 1980). However, Pb can adsorb via strong, triple-corner-sharing complexes over internal vacancies in phyllomangate interlayers (Villalobos et al., 2005). The results of this study suggest that Pb adsorption on manganese oxide is geomedia is practically irreversible.

Treatments with HCl also released Mn from the coating of the geomedia. Approximately 6% of the manganese oxide coating was released during batch treatment with pH 1 HCl ($[Mn]_{diss}$ = 16 μM). Less than 2% of Mn was released at pH 3, which is consistent with the low solubility of manganese oxide ($K_{sp,birnessite} = 10^{-15.62}$) (Figure 4.9) (Gustafsson, 2014).

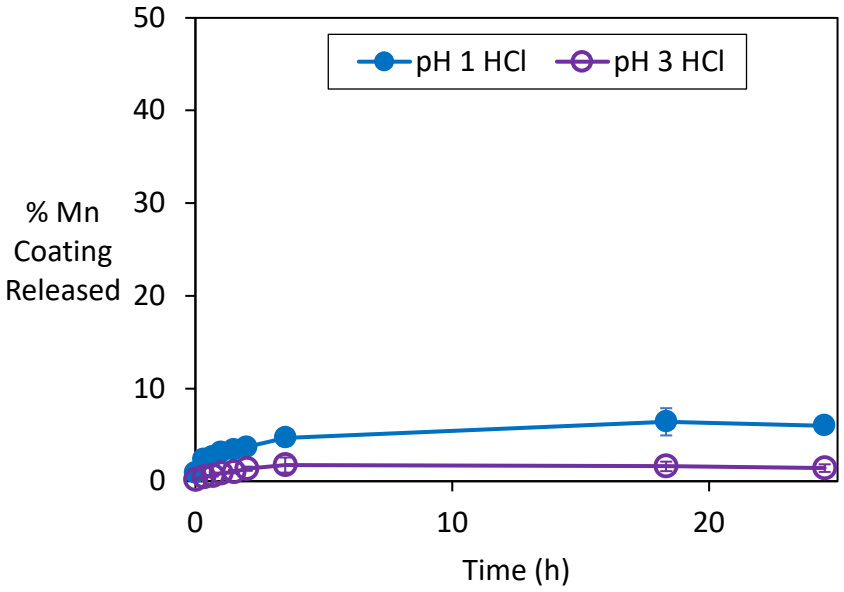

Figure 4.9 Cumulative Mn released during batch regeneration with HCl as a percentage of initial Mn coating on the geomedia. Error bars represent standard error from all batch regeneration experiments with HCl.

EDTA and citric acid treatments also resulted in the release of Mn. The 4.41 μM concentrations of the chelating compounds (used to regenerate the geomedia at a 1:1 ratio with adsorbed Pb) resulted in < 3% losses of the manganese oxide coating (Figure 4.10). However, the 146 μM doses of chelating compounds (used to regenerate geomedia at a 2:1 ratio with adsorbed Zn) resulted in large releases of manganese: 14% in the case of 146 μM EDTA and 26% in the case of 146 μM citric acid (Figure 4.11).

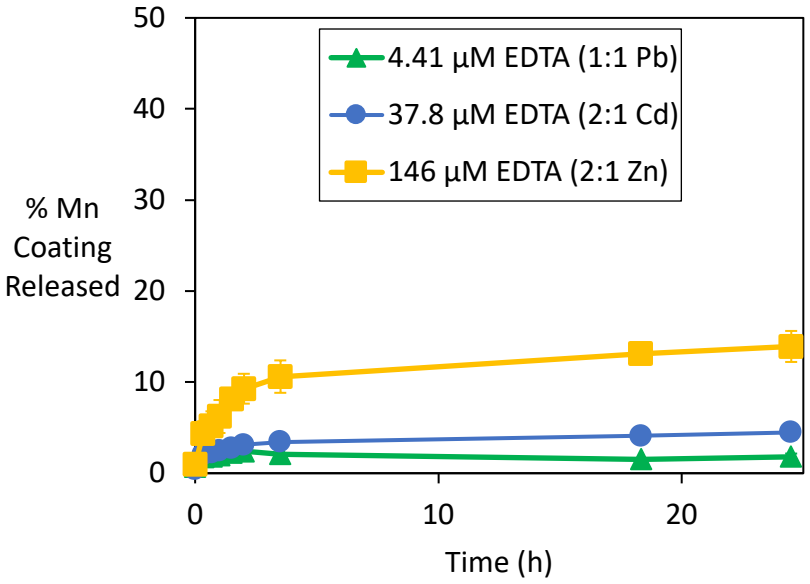

Figure 4.10 Cumulative Mn released during batch regeneration with EDTA as a percentage of initial Mn coating on the geomedia. Error bars represent standard error from triplicate regeneration experiments.

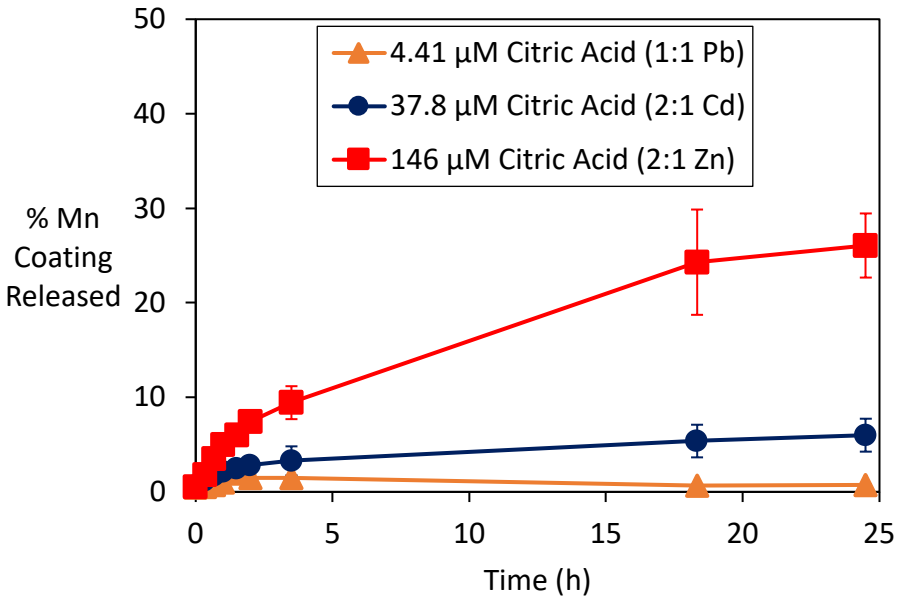

Figure 4.11 Cumulative Mn released during batch regeneration with citric acid as a percentage of initial Mn coating on the geomedia. Error bars represent standard error from triplicate regeneration experiments.

Because of its rapid and nearly complete desorption of Cu, Zn and Cd and its low impact on the manganese oxide coating, pH 3 HCl was selected for *in situ* column regeneration tests.

Failed columns of manganese oxide-coated geomedia (i.e., columns run under conditions described in Section 4.3.2) were regenerated by passing pH 3 HCl through them for 150 pore volumes. The release of Cu, Zn and Cd was rapid and complete. Within the first 50 pore volumes, over 97% of the adsorbed Cu, Zn and Cd were recovered from columns that treated NOM-free simulated stormwater (Figure 4.12). In columns that treated NOM-containing simulated stormwater over 96% of the adsorbed Cu, Zn and Cd were recovered after 150 pore volumes (Figure 4.13). Conversely, only about 0.2% of all adsorbed Pb was recovered from columns after 150 pore volumes. This result is likely due to strong specific and nearly irreversible adsorption of Pb on the manganese oxide surface (McKenzie, 1980).

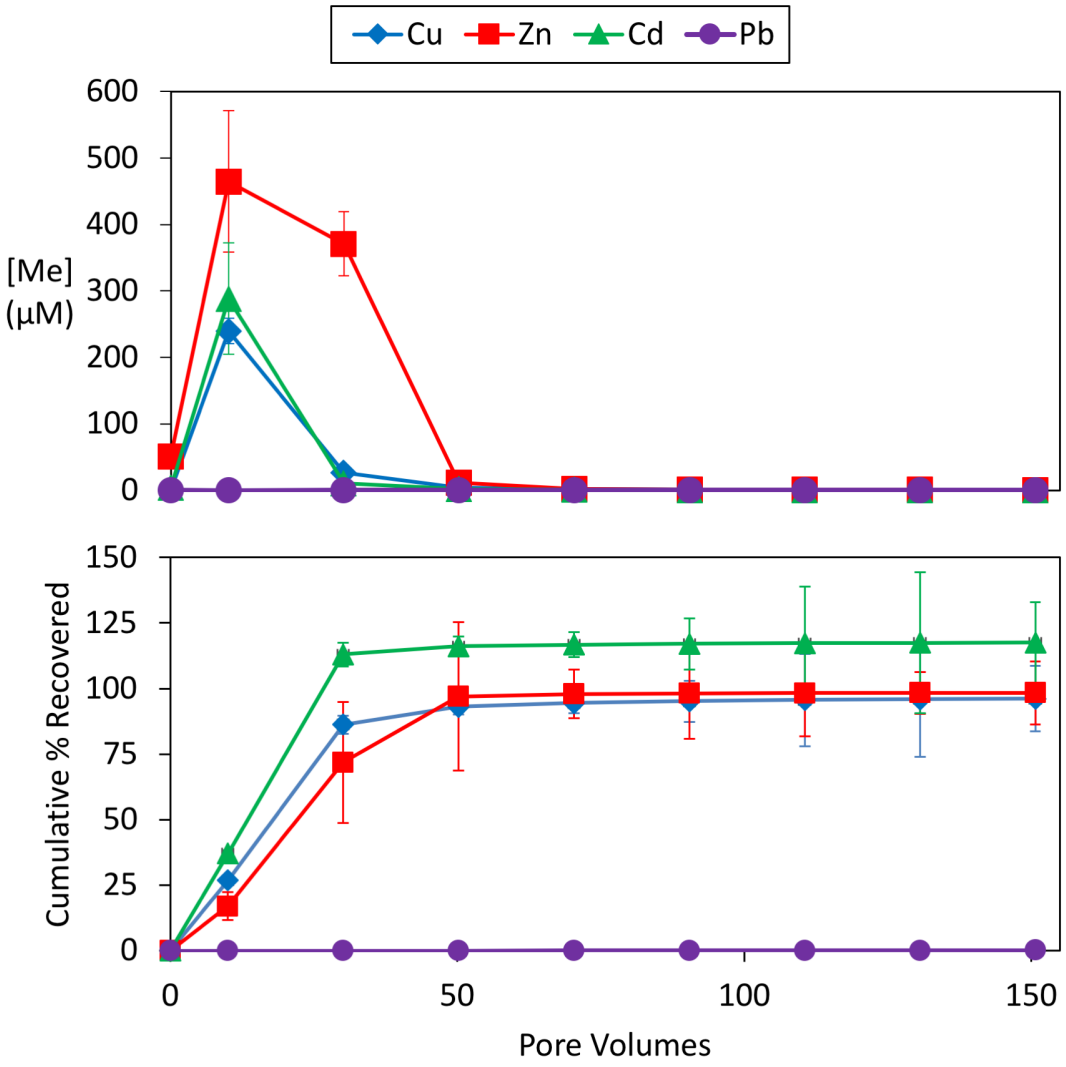

Figure 4.12 Concentrations of effluent Cu, Zn, Cd and Pb during regeneration with pH 3 HCl of columns that treated NOM-free stormwater (top) and cumulative percentage of adsorbed metal recovered during regeneration (bottom). X-axis designates pore volumes of regenerant treatment, immediately following column adsorption tests. Error bars represent standard error of multiple sample tests.

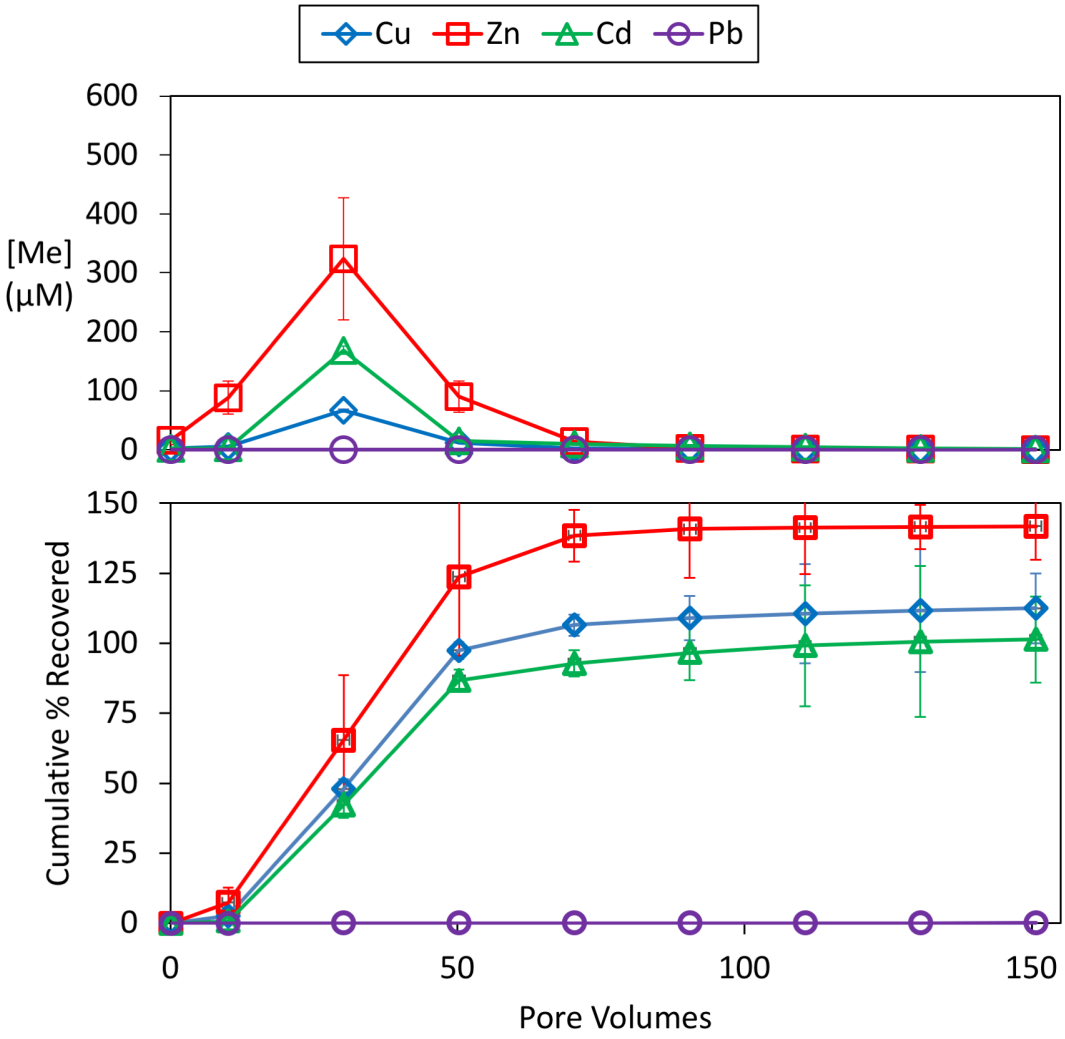

Figure 4.13 Concentrations of effluent Cu, Zn, Cd and Pb during regeneration with pH 3 HCl of columns that treated NOM-containing stormwater (top) and cumulative percentage of adsorbed metal recovered during regeneration (bottom). Zn recoveries greater than 100% are likely due to the use of a trapezoidal integral approximation that overestimated Zn recovered between 10 and 50 pore volumes. X-axis designates pore volumes of regenerant treatment, immediately following column adsorption tests. Error bars represent standard error of multiple sample tests.

These results imply that uncharacteristically low pH values in stormwater, such as those observed during "episodic acidification" events following snowmelt, heavy rain events, or polluted dry weather flows (King County, WA, 2016; US Environmental Protection Agency, 1999), could cause the inadvertent release of sequestered Cu, Zn or Cd. However, regeneration treatments could intentionally desorb and recover the metal contaminants to minimize the risk of desorption. If the infiltration system were built with the capacity to be hydraulically isolated, the effluent regenerant solution and desorbed metals could be collected and disposed of offsite.

Although Pb would be difficult to recover, low pH stormwater would be unlikely to cause the release of significant amounts of Pb.

Cu, Zn and Cd were desorbed approximately twice as slowly from columns that treated NOM-containing stormwater as those that treated NOM-free stormwater (Figure 4.13). Retarded desorption has been previously observed in column experiments with NOM and Cu, and may have been caused by the formation of ternary >MnO_x-Me-NOM complexes (Oden et al., 1993; Rozan et al., 1999). These complexes may move through the column more slowly due to charge reversal of the manganese oxide at pH 3 (pH_{pzc} = 3.3) resulting in electrostatic interactions (Gregor et al., 1955; Zhong et al., 2005).

The manganese oxide-coated sand used in this study initially had a manganese coating density of 1.17 ± 0.30 mg Mn/g geomedia. In NOM-free columns, Mn coating density was unchanged after regeneration (1.30 ± 0.23 mg Mn/g geomedia). This result is consistent with the low mass of Mn measured in the effluent of columns during regeneration (290 µg). In columns treating NOM-containing simulated stormwater, the Mn coating density decreased slightly to 1.02 ± 0.05 mg Mn/g geomedia after regeneration, a loss of 13% of coating density. This result is consistent with the 1200 µg of total Mn measured in the effluent of columns during regeneration (i.e., 0.12 mg Mn lost/g geomedia). The column that had been exposed to NOM released approximately four times more Mn than the NOM-free column and effluent Mn concentrations peaked 20 pore volumes later in the NOM-exposed columns. (Figure 4.14).

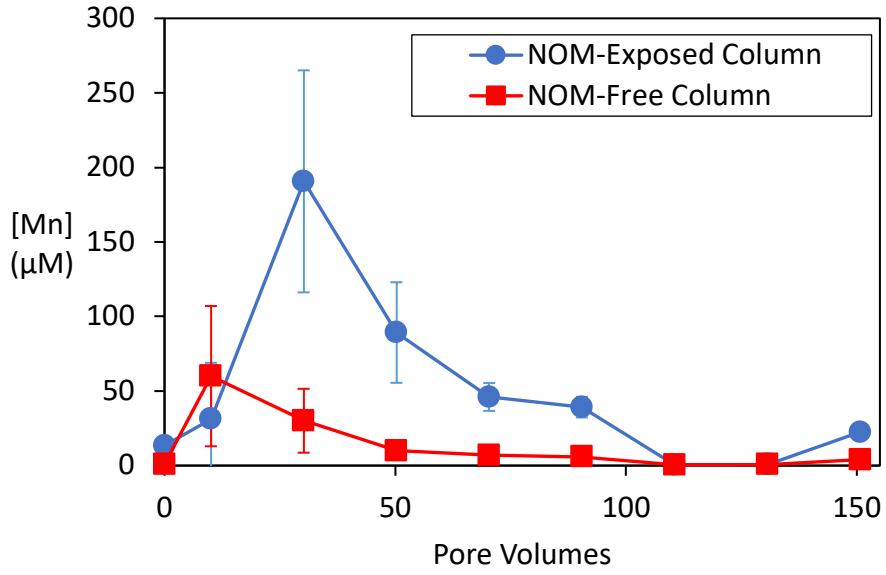

Figure 4.14 Concentrations of Mn in the column effluent during regeneration with pH 3 HCl. Results are shown for columns that treated metals in NOM-containing stormwater (circles) and NOM-free (squares) simulated stormwater. The x-axis designates pore volumes of regenerant treatment, immediately following column adsorption tests. Error bars represent standard error from all regeneration experiments

Longevity tests following regeneration demonstrated that, in all stormwater conditions and for all metals, the regenerated geomedia had a similar adsorptive capacity and longevity to that of the virgin geomedia (Figures 4.4 and 4.6). This result implies that the useful lifetime of systems employing this geomedia could be extended for at least one more cycle by regenerating them with a mild acid.

4.4 Geomedia Lifetime

Given its high adsorption capacity for trace metals in stormwater, relative ease of production and ability to oxidize certain organic contaminants in stormwater (Chapter 3), manganese oxide-coated sand geomedia could be an appropriate technology for managed aquifer recharge provided that the geomedia exhibits a suitable lifetime. The lifetime of a typical stormwater infiltration system employing this geomedia as an adsorptive for metals can be projected from the column experiments.

It was impossible to project of the lifetime of a full-size system treating Cu and Pb in the absence of NOM based on column experiments due to the complete removal of metals for their entire duration. Therefore projections were made based on previously published adsorption capacities of Cu and Pb by manganese oxides (Fu et al., 1991; Gadde and Laitinen, 1974; Pitt et al., 2015). The studies from which literature values were derived considered metal adsorbates individually in lightly buffered simple solutions (i.e., ≤ 0.01 M $NaNO_3$, pH titrated by HNO_3 and NaOH addition).

For example, a system with a 0.5 m-deep layer of manganese oxide-coated sand over a 50 m^2 area could treat 2×10^6 L of stormwater per year (Hatt et al., 2009). The lifetime of such a system could be estimated by:

$$\text{lifetime [years]} = \frac{\text{metal loading capacity [moles]}}{\text{metal load } \left[\frac{\text{moles}}{\text{yr}}\right]} \quad \text{(Eq. 4.5)}$$

Where metal loading capacity can be determined by:

$$\text{metal loading cap. [moles]} = \text{bed mass[g geomedia]} * \text{adsorptive capacity } \left[\frac{\text{moles Me}}{\text{g geomedia}}\right] \quad \text{(Eq. 4.6)}$$

Multiplying the volume of the system described by the geomedia bulk density of 870 kg/m^3 yields a bed mass of 22×10^6 g manganese oxide-coated sand. Per Eq. 4.6, multiplying this bed mass by the adsorptive capacities measured in this study (before C/C_0=1) yields the metal loading capacity (Table 4.9). For example, in NOM-containing stormwater, Cu breakthrough is projected to occur after 2500 pore volumes, when 1.48 µmoles Cu/g manganese oxide-coated sand have entered the column:

$$\frac{1.48\ \mu\text{moles Cu}}{\text{g geomedia}} * 22 \times 10^6\ \text{g geomedia} = 32.5\ \text{moles Cu loading capacity} \quad \text{(Eq. 4.7)}$$

Table 4.9 Parameters for projecting the lifetime of a full-sized infiltration system containing manganese oxide-coated sand before complete breakthrough of metals in a sand in stormwater with no NOM and with 8 mg-C/L NOM.

		Adsorp. cap. (μmol Me/g)	Metal loading cap. (mol Me)	Ave. metal conc. (μM)	Metal load (mol/yr)	Projected lifetime (yr)
Cu	NOM Absent	2.85*	62.7*	0.252	0.50	124*
	NOM Present†	1.48	32.5	0.252	0.50	65.0
Zn	NOM Absent	5.52	121	1.79	3.58	33.9
	NOM Present†	3.12	68.7	1.79	3.58	19.2
Cd	NOM Absent	1.32	29.1	0.013	0.03	1120
	NOM Present	1.01	22.3	0.013	0.03	858
Pb	NOM Absent	11.8*	259*	0.038	0.08	3410*
	NOM Present†	6.81	150	0.038	0.08	1970

†Only partial removal of the metal before complete breakthrough is anticipated; *lifetime projection based on previously published adsorption capacities because of complete metal removal for the duration of the column experiment.

System lifetime is also dependent on the load of metals entering the system. The metal load is determined by:

$$\text{metal load}\left[\frac{\text{moles}}{\text{yr}}\right] = \text{stormwater load}\left[\frac{\text{L}}{\text{yr}}\right] * \text{metal conc. [M]} \quad \text{(Eq. 4.8)}$$

A properly designed stormwater treatment system of the size described located in a region receiving 0.5 m of rainfall/yr would have a catchment area of approximately 4000 m^2 (Hatt et al., 2009). Assuming a runoff coefficient of 1 yields a stormwater load of 2×10^6 L/yr. Multiplying the stormwater load by the average metal concentration, per Eq. 4.8, yields the annual metal load (Table 4.9). For the example of Cu in NOM-containing stormwater:

$$\frac{2\times10^6\ \text{L}}{\text{yr}} * \frac{0.252\ \mu\text{moles}}{\text{L}}\ \text{Cu} = 0.5\ \text{moles Cu/yr} \quad \text{(Eq. 4.9)}$$

Dividing metal loading capacity by metal load per Eq. 4.5 yields a projected lifetime (Table 4.9). For the example of Cu:

$$\frac{32.5\ \text{moles}}{0.5\ \text{moles/yr}} = 65.0\ \text{years before breakthrough of Cu (with NOM present)} \quad \text{(Eq. 4.10)}$$

A summary of projected system lifetimes is shown in Figure 4.15. Assuming stormwater containing typical concentrations of NOM and metals, the system described could be expected to operate for decades before the complete loss of adsorption capacity for any metal tested. The lifetime projections were for systems containing virgin geomedia. System lifetimes could be significantly prolonged by periodic treatment with pH 3 HCl regenerant without removing substantial amounts of the manganese oxide coating from the geomedia. It is likely that a

treatment system would be regenerated before the complete breakthrough of a metal in order to maintain minimum level of metals removal and to ameliorate the risk of desorption.

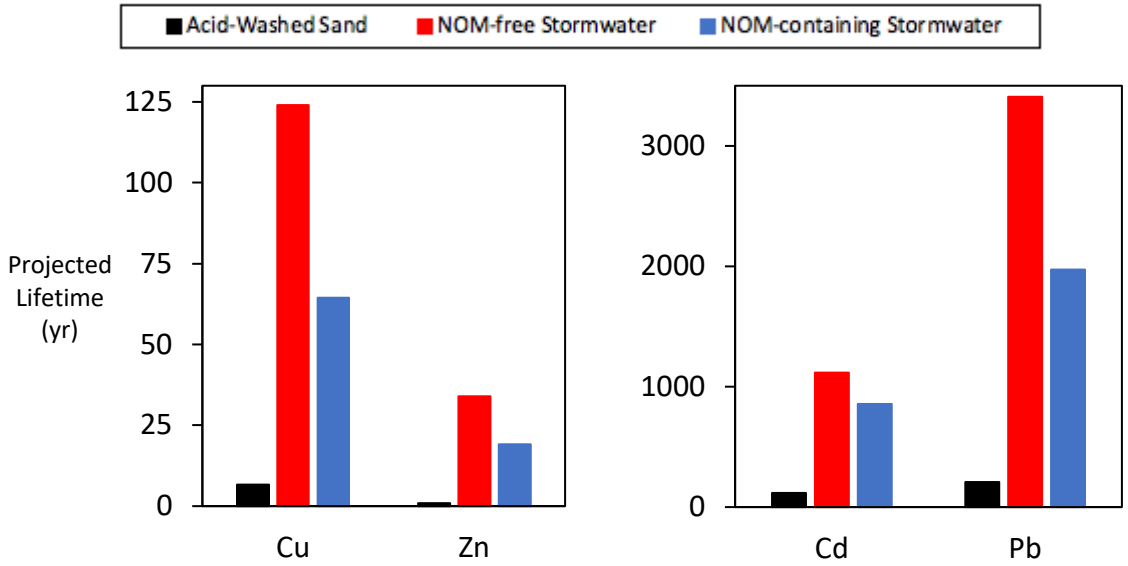

Figure 4.15 Projected lifetime before complete breakthrough of Cu and Zn (left) and Cd and Pb (right) in a full-sized infiltration system containing manganese oxide-coated sand.

The nearly indefinite lifetimes projected before breakthrough of Cd or Pb suggest that this technology could be applicable for systems intended to recharge drinking water supplies. Conversely, partial Zn and Cu removal were observed, even before complete breakthrough (Figure 4.6). Incomplete removal of Zn is common in stormwater treatment systems due to high Zn concentrations in stormwater and its low adsorption on many types of infiltration geomedia (Feng et al., 2012). Although partial removal of Zn and Cu may be unimportant for drinking water treatment systems, it may limit the applicability of this technology in infiltration systems designed for ecosystem protection.

Though the flow rate used in these experiments is typical of field systems, infiltration rates can vary and may affect geomedia performance (Feng et al., 2012; Hatt et al., 2008). Preliminary batch kinetic experiments indicated that adsorption occurred quickly and mass transfer is unlikely to be limiting within field applications. Projections of system lifetimes from these experiments are therefore useful, but should be confirmed at larger-scale hydraulic regimes.

Based on these results, it is unlikely that metals breakthrough will limit the lifetime of stormwater infiltration systems employing this geomedia. The projected lifetimes for the treatment of Cd and Pb are longer than the predicted lifetime for the oxidative removal of organic contaminants (Chapter 3), although Cu and Zn treatment would be sustained for less time. Cu and Zn are of greater concern for ecosystem health and Cd and Pb are more of a concern for human toxicity, while organic contaminants may be of concern in both systems.

Therefore, it is likely that the intended application of the stormwater infiltration system (i.e., for drinking water or ecosystem protection) will dictate the frequency of regeneration. Other failure mechanisms, including clogging by suspended sediments and biofilm growth, would most likely limit the lifetime of a stormwater treatment system before adsorption capacity is exhausted (Feng et al., 2012; Hatt et al., 2008). In field-scale studies, techniques such as settling before infiltration and bioturbation of infiltration media with plant roots have been effective in maintaining acceptable hydraulic conductivities (Grebel et al., 2013; Le Coustumer et al., 2012).

4.5 Environmental Implications

The ability to regenerate the manganese oxide-coated sand geomedia could make it more attractive for communities, but a mild acid wash could pose some environmental risks. The released metals could contaminate aquifers if not captured, and the acidic regenerant solution could cause the leaching of other adsorbed species in the aquifer, such as arsenic (Kocar et al., 2008). Although regeneration with pH 3 HCl resulted in high metal contaminant recovery with little leaching of the manganese oxide coating, citric acid could be used as a biodegradable alternative for regeneration. However, the introduction of this labile carbon source could facilitate unwanted biological activity in the infiltration system and induce reductive conditions and biofouling.

As previously noted, these experiments evaluated each metal in isolation; however, co-contamination by metals is probable in stormwater. Competition for adsorption sites on the manganese oxide surface could lead to faster breakthrough than predicted for some metals individually. Pb adsorption is unlikely to be diminished by the presence other metals (Catts and Langmuir, 1986). However, high concentrations of Pb could displace previously adsorbed Cu, Zn and Cd (Gadde and Laitinen, 1974). Co-contamination by Cu, Zn and Cd could lead to faster breakthrough of each of these metals (Gadde and Laitinen, 1974; Zasoski and Burau, 1988). Oxidizable organic carbon in the stormwater matrix may also diminish the number of adsorptive sites on the geomedia and increase the abundance of Mn^{2+}, which competes with adsorbed metals (Godtfredsen and Stone, 1994).

The types and concentrations of NOM used in this study are good representations of typical stormwater (California Department of Transportation, 2003; Grebel et al., 2016). However, dissolved organic matter concentrations as high as 73 mg-C/L have been observed in stormwater (California Department of Transportation, 2003; Pitt et al., 2015). The results of this study indicate that manganese oxide-coated sand may be less effective in systems with high organic carbon loads. A small amount of upstream carbonaceous geomedia (e.g., biochar) could remove organic matter from solution and enhance the geomedia performance without detrimental impacts to hydraulic conductivity (Ulrich et al., 2015). Sources of labile organic carbon (e.g., mulch) have been proposed to remove nitrate or organic contaminants during stormwater infiltration (Halaburka et al., 2017). These materials could be problematic upstream of manganese oxide-containing geomedia. In addition to creating reducing conditions that could dissolve manganese oxide, these materials would also increase the dissolved organic carbon, limiting metals removal.

An additional concern is that manganese oxides are known to oxidize Cr(III) to more mobile and toxic Cr(VI) (Fendorf and Zasoski, 1992). Though Cr(III) is extremely insoluble and typically occurs at low concentrations in stormwater, Cr(VI) is highly toxic and has a maximum contaminant level in California of 0.2 μM (Fendorf et al., 1999; Grebel et al., 2013; Mazzera, 2014). Therefore, stormwater infiltration systems employing manganese oxide geomedia should be monitored to ensure no Cr(VI) is produced.

CHAPTER 5. Conclusions

5.1 Summary

Increased water scarcity is a problem facing cities around the world. As urban populations grow and droughts become more severe, augmenting local water supplies will be a necessity for cities seeking to decrease their dependence on imported water and energy-intensive technologies like seawater desalination. Managed aquifer recharge conveys underutilized sources of water, including stormwater and tertiary-treated wastewater effluent, into the subsurface for later use; but, these sources of water also have the potential to contaminate aquifers. Centralized infiltration systems could be designed with infiltration media specifically engineered to remove contaminants that threaten drinking water quality. Engineered geomedia can provide passive, cost-effective treatment to water as it percolates into aquifer storage. New treatment technologies that can reliably and inexpensively protect water quality may be important to the widespread adoption of large-scale infiltration systems for managed aquifer recharge. Research on the longevity of engineered geomedia, mechanisms of contaminant removal and system maintenance and regeneration is critical to the adoption and dissemination of this treatment technology.

The research described in this dissertation evaluated the performance and regeneration of manganese oxide-coated sand as an engineered geomedia for treating both organic contaminants and metals in stormwater. In this chapter, further research to advance the use of geomedia is identified, including research on understanding the relationship between reactivity and manganese oxide mineralogy. This chapter also addresses the feasibility of using manganese oxide-coated sand as one of a series of treatment technologies in stormwater infiltration systems, including analysis of the practical challenges to field application and treatment system design. Finally, the environmental implications of this body of research are outlined and other, related research is identified.

5.2 The Effect of Chemical Regenerants on Manganese Oxide-Coated Sand Reactivity

The research described in Chapter 2 evaluated the effectiveness of several chemicals for regenerating the reactivity of passivated manganese oxide-coated sand with organic stormwater contaminants. Among oxidants, the hypohalites (i.e., HOCl, HOBr and a mixture of the two) and $KMnO_4$ both significantly raised the average oxidation state of the failed geomedia. However, only the hypohalites produced a manganese oxide phase with comparable reactivity to the virgin geomedia. At pH 6, $KMnO_4$ restored approximately 40% of the reactivity to the geomedia and at pH 10, H_2O_2 restored approximately 30% of reactivity. The hypohalite oxidants fully oxidized virtually all of the Mn on the geomedia to the +4.0 oxidation state, and stoichiometric excess of oxidant did not produce geomedia with significantly higher reactivity. Taken together, these observations are consistent with geomedia regeneration via the oxidation of Mn(II/III) to produce a highly oxidized, nanocrystalline manganese oxide phase.

Non-oxidizing chemicals did not restore the reactivity of the geomedia. The failure of methanol to restore geomedia reactivity suggests that fouling by organic oxidation products was not a cause of manganese oxide passivation. Treatment with HCl at pH 2 raised the average Mn oxidation state on the failed geomedia and restored its reactivity with bisphenol A to a rate approximately 30% of the virgin geomedia. This result suggests that some oxidation capacity could be regenerated by the release of Mn(II) and Mn(III), which are more soluble than Mn(IV)

and have been implicated in the passivation of manganese oxides (Balgooyen et al., 2017; Trouwborst, 2006). However, the effect of this type of regeneration was small compared to oxidative regeneration. This study suggested that treatments with hypohalites had the greatest potential for *in situ* regeneration of failed geomedia.

5.3 *In situ* Regeneration of Manganese Oxide-Coated Sand with HOCl

5.3.1 Cryptomelane-Coated Sand Longevity and Regeneration

In Chapter 3, research was presented on the use and regeneration of a novel cryptomelane-coated sand produced for use as a reactive geomedia under conditions encountered during managed aquifer recharge. This geomedia was tested in columns with pH 7 simulated stormwater containing 5 μM bisphenol A. The failed geomedia was regenerated with HOCl at pH 6 and the regenerated geomedia was again evaluated for longevity. Both the virgin and regenerated geomedia demonstrated exceptional reactive longevity with bisphenol A, with both types of geomedia removing over half of the influent bisphenol A for over 580 pore volumes. Scaled to a typical full-sized stormwater infiltration system, these data suggest that the geomedia could sustain reactivity with organic contaminants for approximately 80 years before failure due to the mechanism observed in this study, and that, upon regeneration, systems could sustain reactivity for at least one more cycle of comparable length.

The manganese oxide coatings of the virgin, failed and regenerated geomedia were characterized with chemical and spectroscopic techniques. Modest, yet significant decreases in the Mn coating density and average Mn oxidation state were observed when the geomedia failed. Regeneration of the failed geomedia was accomplished by passing a 0.31 mM HOCl solution through the column until enough oxidant entered the column to fully oxidize the reduced Mn to the +4.0 oxidation state. The average Mn oxidation state of the regenerated geomedia exceeded +3.90 and no HOCl was detected in the column effluent until after stoichiometric excess of the regenerant was applied, suggesting that the reduced Mn on the failed geomedia reacted quickly with the HOCl. The coatings of the virgin and regenerated geomedia exhibited X-ray diffraction and X-ray absorption spectroscopy spectra consistent with nanocrystalline cryptomelane, while the failed geomedia coating more closely resembled cryptomelane with greater long-range crystal order. The flow rate used in these experiments is typical for full-scale infiltration systems, infiltration rates can vary and may affect geomedia performance (Feng et al., 2012; Hatt et al., 2008). Batch kinetic experiments indicated that oxidation occurred quickly, so mass transfer is unlikely to be limiting within field applications. Therefore, projections of system lifetimes from these experiments are useful, but should be confirmed at larger-scale hydraulic regimes.

The decrease in the Mn coating density during both the treatment and regeneration phases suggests that the potential for repeated regeneration of this material may be limited. Although multiple failure and regeneration experiments were not conducted on the columns, about 25% of the manganese oxide coating of the geomedia was lost in one treatment-regeneration cycle. This loss of coating density did not decrease the geomedia performance in one subsequent treatment cycle, but at this rate of coating loss, the levels of reactivity observed would likely only be sustained for 2-3 cycles. However, given the decades-long lifetime of one treatment-regeneration cycle, it is probable that another failure mechanism (e.g., clogging, the development of

preferential flow paths) would limit the lifetime of a stormwater infiltration system before the complete loss of regenerable oxidation capacity by the manganese oxide-coated sand.

Another potential shortcoming of this technology is the use of hypochlorous acid in the regeneration process. Although proper dosing should limit the concentration of chlorine leaving the geomedia layers, it is possible that chlorine disinfection byproducts could be released to the aquifer during regeneration. To avoid this phenomenon, the infiltration system could be hydraulically isolated, allowing the effluent regenerant solution to be collected and disposed of offsite. Because regeneration will be necessary only on an infrequent basis (i.e., approximately once every 45 to 170 years) any impact from the use of chlorine will be small relative to the lifespan of the infiltration system.

Additionally, manganese oxide-coated sand is only reactive with certain classes of organic contaminants found in stormwater. This cryptomelane-coated sand demonstrated higher reactivity than some other manganese oxide-coated sands (Lin et al., 2013), and thus may be useful for the oxidation of more recalcitrant compounds, such as diuron; however, the geomedia will be most effective for oxidizing organic compounds with activated rings such as phenols and anilines. To overcome this limitation, other geomedia may be necessary for the removal of less reactive organic contaminants. For example, biochar could be deployed alongside the manganese oxide-coated sand (Ulrich et al., 2017).

5.3.2 Mineralogy-Reactivity Relationship

In manganese oxide minerals, MnO_6 octahedra can be arranged into corner- or edge-sharing structures, creating a diversity of phases. The physical and chemical properties of these different minerals vary considerably (Robinson et al., 2013). Because of their redox activity and adsorptive properties, manganese oxides are important in many biogeochemical cycles and engineered systems (Learman et al., 2011). Nonetheless, mineralogy-reactivity relationships for the various polymorphs of manganese oxide have not been well-studied (Nico and Zasoski, 2001; van Genuchten and Peña, 2017; Webb et al., 2005).

Differences in the reactivity of manganese oxide minerals due to variations in their surface area, average oxidation state, local coordination environment, pH_{pzc} or other factors influence their efficacy as engineered geomedia (Liu et al., 2009b; Remucal and Ginder-Vogel, 2014; Ukrainczyk and McBride, 1992). Nonetheless, more research is needed to determine how mineral structure, independent of oxidation state or surface area, influences manganese oxide reactivity. For example, the local coordination environment is known to be important to the reactivity of mineral surface sites, but the precise causes of the variation in reactivity are not well-understood (Nico and Zasoski, 2001).

Similarly, little research has been conducted on how amorphous manganese oxides and manganese oxide coatings differ in reactivity from pure minerals (Lin et al., 2013; Remucal and Ginder-Vogel, 2014; Wan et al., 2015). The research in Chapters 2 and 3 adds to the body of evidence which suggests that there is an inverse relationship between reactivity and long-range crystal order (Shin and Cheney, 2004). These results suggest that some nanocrystalline morphologies may be more reactive than the manganese oxides polymorphs frequently used in

research, such as birnessite (Laha and Luthy, 1990; Remucal and Ginder-Vogel, 2014; Stone, 1987). A higher concentration of reactive surface sites may be partly responsible for this effect. However, it is possible that a relatively small number of reactive sites in nanocrystalline structures more readily form surface complexes or more frequently exist in degenerate states which undergo rapid electron transfer, thus accelerating the rate-limiting steps of organic compound oxidation (Yamada and Tanaka, 1995; Zhang and Huang, 2005).

The mineralogy may also impact how the reactivity of the mineral changes over time. For instance, a highly oxidized manganese oxide with a tightly structured long-range order, such as pyrolusite, may have low reactivity due to its low surface area and small number of vacancies (Grebel et al., 2016). However, the reduction of Mn(IV) to Mn(III) within such a system could produce Jahn-Teller distortion and result in more vacancies, possibly causing less rapid passivation than would be predicted for birnessite. Similarly, the passivation of mechanism birnessite, postulated to be related to accumulation of Mn(II/III) in the interlayer, may not be relevant to tectomanganates such as cryptomelane (Balgooyen et al., 2017). Understanding these dynamics provides insight into the reactivity of natural manganese oxides, whose structures change with time (Webb et al., 2005).

5.4 Biogenic Manganese Oxides

In addition to the abiotic processes studied in this research, reduced manganese oxides could also be re-oxidized by microbes. Biological oxidation of Mn(II) is frequently catalyzed by a diverse and ubiquitous group of microbes (Tebo et al., 2005). Although the evolutionary advantages of oxidizing Mn(II) are still debated, possible explanations for this microbial activity include the utility of manganese oxides for scavenging trace metal nutrients, protection from environmental hazards or use as a respiratory electron acceptor under anoxic conditions (Tebo et al., 2005).

Biogenic manganese oxides react with contaminants (Forrez et al., 2010, 2009), and adsorb metals (Peña et al., 2010); however, it would be difficult to implement and control the biological re-oxidation of Mn in field applications (Learman et al., 2011). Studies conducted with biogenic manganese oxides that could strongly adsorb Ni^{2+} (Peña et al., 2011) showed no reactivity with bisphenol A (data not shown). Although biogenic manganese oxides are always precipitated as nanocrystalline phyllomanganates, in the environment they can quickly transform into secondary products with different structures (Bargar et al., 2009; Feng et al., 2010). These biogenic manganese oxides often lack the desirable properties of synthetic manganese oxides.

Nonetheless, in managed aquifer recharge systems, it is inevitable that Mn-oxidizing bacteria will produce some biogenic manganese oxides. Research is needed to assess the role of biogenic manganese oxides in infiltration systems. These species might prolong the lifetime of manganese oxide-coated sand in the field, or they could hasten geomedia fouling. Appropriate studies would require the use of larger-scale infiltration columns and authentic stormwater. Relevant analyses would include characterization and reactivity testing of the manganese oxides present after system aging (Bargar et al., 2009), as well as genomic and proteomic analyses of the microbial community present in the infiltration system to determine which microbial Mn(II)

oxidation pathways are present (e.g., multicopper oxidase enzymes) (Tebo et al., 2005; Webb, 2005).

5.5 Adsorption of Toxic Metal Cations with Manganese Oxide-Coated Sand Geomedia

The research presented in Chapter 4 describes the use of manganese oxide-coated geomedia as an adsorbent of four metal cations (i.e., Cu, Zn, Cd and Pb) in stormwater. In column tests with high concentrations of metal contaminants, the geomedia strongly adsorbed Cu and Pb in the absence of natural organic matter, removing virtually all of these metals for nearly 2200 pore volumes. Zn and Cd were partially removed, with performance declining over time (i.e., 970 pore volumes before breakthrough of Zn and 1420 pore volumes before breakthrough of Cd). In the presence of 6.3 mg-C/L NOM, the geomedia adsorbed much less Cu and Pb, while removal of Zn and Cd were only slightly diminished. Between 15 and 50% of influent Cu and 60 to 75% of influent Pb were removed from NOM-containing stormwater. NOM disrupted the adsorption of Cu and Pb most because of its strong complexation of these two metals. Steric hindrance and electrostatic repulsion of the metal-NOM complex from the negatively-charged geomedia surface reduced adsorption. Zn and Cd remained primarily uncomplexed by the NOM, and thus were removed to similar degrees in NOM-containing and NOM-free stormwater.

Chemical treatments were evaluated to determine their potential for recovering adsorbed metals and regenerating the adsorptive capacity of the geomedia. Treating failed geomedia columns with 150 pore volumes of EDTA recovered over 70% of the Cu, Zn and Cd adsorbed on the geomedia, though significant amounts of the manganese oxide coating were also released. An acidic wash (i.e., pH 3 HCl for 150 pore volumes) recovered over 90% of adsorbed Cu, Zn and Cd, and restored the adsorptive capacity of the saturated geomedia with minimal loss of the manganese oxide coating.

Pb was not recovered during washing with EDTA or HCl. Previous research has documented the uptake of Pb by manganese oxide even at very low pH values (Gadde and Laitinen, 1974; McKenzie, 1980). McKenzie (1980) reported that 91% of all Pb adsorbed by manganese oxide could not be recovered in 2.5% acetic acid after 24 hours. The large ionic radius and electronic properties of Pb result in the formation of strong surface complexes with the manganese oxide surface (Wan et al., 2015; Wang and Stumm, 1987). Pb can also enter into the interlayer and tunnels of manganese oxides, facilitating its strong adsorption (O'Reilly and Hochella, 2003). Studies have determined that it is unlikely that Pb-Mn minerals form even at high saturations of Pb on the manganese oxide surface (McKenzie, 1980), but that Pb can adsorb via strong, triple-corner-sharing complexes over internal vacancies in phyllomangate interlayers (Villalobos et al., 2005). This unusually strong specific adsorption implies that recovery of Pb during regeneration is infeasible, but also that the unexpected release of Pb during system operation is unlikely. Due to the very high adsorption capacity of Pb on manganese oxide (i.e., up to 0.56 mol Pb/mol MnO_x) (Gadde and Laitinen, 1974), saturation of the geomedia during normal system lifetimes is also unlikely.

The results of this study imply that manganese oxide-coated sand could be an effective way to remove metals from urban stormwater for decades, and that performance could be sustained without costly excavation using a simple regeneration with a mild acid. An infiltration system could be hydraulically isolated from the aquifer during regeneration to allow for recovery

and offsite disposal of the released metals (Edwards et al., 2016). Overall, this research demonstrates the versatility of manganese oxide-coated sand as both an oxidative geomedia for organic contaminants and adsorptive geomedia for metallic contaminants. The broad-spectrum applicability of the material makes it well-suited to remove contaminants from influent waters with a wide range of compositions and water quality concerns.

5.6 Field Applications of Manganese Oxide-Coated Sand Geomedia

In managed aquifer recharge systems, other geomedia will likely be used in conjunction with manganese oxide geomedia (Figure 5.1). For example, granular activated carbon, biochar or montmorillonite clays functionalized with polycation composites could be deployed to sorb hydrophobic compounds or metals (Radian et al., 2015; van Lienden et al., 2010). Wood chips and bark could provide labile organic carbon and stimulate biological nitrate removal or biotransformation of organic contaminants (Halaburka et al., 2017). Iron oxides could remove anionic compounds and pathogens (Mohanty et al., 2013) and zero-valent iron may remove phosphorus and transform certain halogenated compounds in stormwater (Erickson et al., 2007; Zhang, 2003).

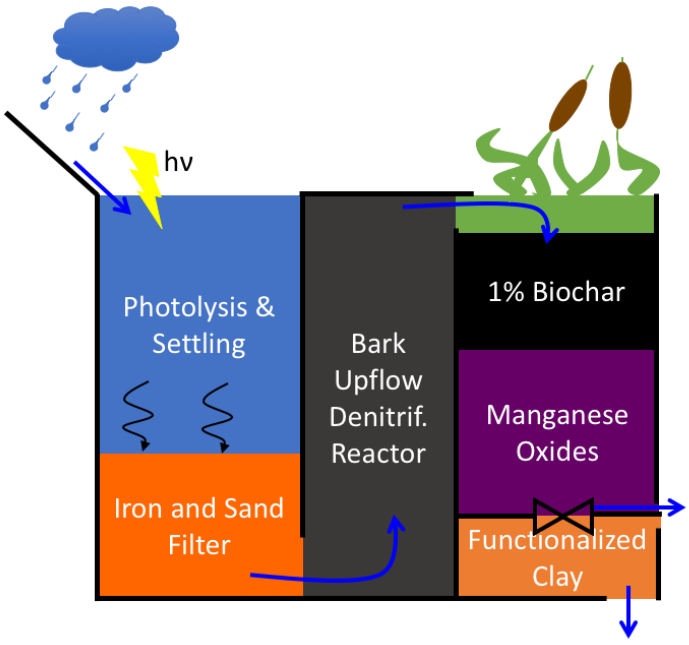

Figure 5.1 Possible unit process treatment train for stormwater infiltration including manganese oxide-coated sand.

Although there are benefits to using multiple types of geomedia for contaminant removal, the interactions of these geomedia in a system that includes manganese oxide are not well understood. For instance, biochar could improve the performance of manganese oxide geomedia by removing natural organic matter, but anoxic conditions induced by upstream processes (e.g., biological nitrate removal) could create conditions which reduce and dissolve manganese oxides.

Therefore, research is needed to understand how these geomedia will interact synergistically and antagonistically as they age in managed aquifer recharge systems, and how to best tailor treatment systems to target contaminants under different conditions.

The hydraulic and chemical properties of the system will evolve over time as sedimentation, sorption, precipitation and biofilm growth occur within the geomedia. Characterizing changes in geomedia properties and their effect on contaminant removal will be important to ensuring a sustained environmental benefit from these infiltration systems. Future research should focus on evaluating the practicality of manganese oxide-coated sand and a suite of other geomedia in real-world applications with authentic stormwater. Initial experiments to assess this issue were conducted in Sonoma, CA in 2017. There, columns of mixed geomedia in various configurations 1 m in length were tested through the infiltration of authentic stormwater from a nearby creek for a full year (Figure 5.2). These columns employed commercially marketed "manganese greensand" as a geomedia, which is widely available but not optimized for organic contaminant removal. The results of these tests will elucidate how variations in geomedia configuration, stormwater composition and temperature impact the performance and aging of geomedia in stormwater infiltration applications. Analysis of this field-scale study will inform the design of larger, pilot-scale applications of this technology.

Figure 5.2 One-meter columns of mixed geomedia in various configurations testing geomedia performance and aging in authentic stormwater at a Sonoma, CA field test site.

The manganese oxide-coated sand geomedia described in this research is relatively simple to produce and has demonstrated considerable promise for long-term removal of organic contaminants and toxic metals in stormwater and other source waters for managed aquifer recharge. These properties make it a very attractive tool for infiltration applications. However, the research described in this dissertation occurred only at the laboratory scale. Given the slow adoption rate of new technologies in the water sector (Parker, 2011), successful field-scale testing will be necessary for this technology to diffuse to a level of widespread adoption.

The research described in this dissertation primarily investigated managed aquifer recharge with stormwater. However, wastewater effluent has also been proposed as a water source for managed aquifer recharge (Dillon et al., 2009; Edwards et al., 2016). Particularly in Mediterranean climates with long dry periods, complementary amounts of stormwater and wastewater could be employed for optimal use of infiltration capacities (Bradshaw and Luthy, 2017). Additional research is necessary to determine the long-term performance of manganese oxide-coated sand in wastewater. Nonetheless, wastewater effluent tends to have concentrations of dissolved organic carbon comparable to that of stormwater (Amy and Drewes, 2007; Ma et al., 2001), and similar concerns related to toxic organic compounds and metals (Babel, 2003; Bolong et al., 2009; Ternes et al., 2004). Manganese oxides have been demonstrated to oxidize some trace organic compounds in wastewater effluent (Forrez et al., 2010, 2009). Therefore, manganese oxide-coated sand also has considerable promise as an engineered geomedia for removing contaminants during wastewater effluent recharge.

REFERENCES

Adams, J.P., Kirst, R., Kearns, L.E., Krekeler, M.P.S., 2009. Mn-oxides and sequestration of heavy metals in a suburban catchment basin of the Chesapeake Bay watershed. Environ. Geol. 58, 1269–1280. https://doi.org/10.1007/s00254-008-1628-y

Alidina, M., Li, D., Drewes, J.E., 2014a. Investigating the role for adaptation of the microbial community to transform trace organic chemicals during managed aquifer recharge. Water Res. 56, 172–180. https://doi.org/10.1016/j.watres.2014.02.046

Alidina, M., Li, D., Ouf, M., Drewes, J.E., 2014b. Role of primary substrate composition and concentration on attenuation of trace organic chemicals in managed aquifer recharge systems. J. Environ. Manage. 144, 58–66. https://doi.org/10.1016/j.jenvman.2014.04.032

Allard, S., Fouche, L., Dick, J., Heitz, A., von Gunten, U., 2013. Oxidation of Manganese(II) during Chlorination: Role of Bromide. Environ. Sci. Technol. 130716084332005. https://doi.org/10.1021/es401304r

Amrhein, C., Strong, J.E., Mosher, P.A., 1992. Effect of deicing salts on metal and organic matter mobilization in roadside soils. Environ. Sci. Technol. 26, 703–709. https://doi.org/10.1021/es00028a006

Amy, G., Drewes, J., 2007. Soil Aquifer Treatment (SAT) as a Natural and Sustainable Wastewater Reclamation/Reuse Technology: Fate of Wastewater Effluent Organic Matter (EfOM) and Trace Organic Compounds. Environ. Monit. Assess. 129, 19–26. https://doi.org/10.1007/s10661-006-9421-4

Andres, A.S., Ballestero, T.P., Musick, M.L., 2018. Stormwater Management: When Is Green Not So Green? Groundwater 56, 357–358. https://doi.org/10.1111/gwat.12653

Babel, S., 2003. Low-cost adsorbents for heavy metals uptake from contaminated water: a review. J. Hazard. Mater. 97, 219–243. https://doi.org/10.1016/S0304-3894(02)00263-7

Balgooyen, S., Alaimo, P.J., Remucal, C.K., Ginder-Vogel, M., 2017. Structural Transformation of MnO_2 during the Oxidation of Bisphenol A. Environ. Sci. Technol. 51, 6053–6062. https://doi.org/10.1021/acs.est.6b05904

Bargar, J.R., Fuller, C.C., Marcus, M.A., Brearley, A.J., Perez De la Rosa, M., Webb, S.M., Caldwell, W.A., 2009. Structural characterization of terrestrial microbial Mn oxides from Pinal Creek, AZ. Geochim. Cosmochim. Acta 73, 889–910. https://doi.org/10.1016/j.gca.2008.10.036

Barrett, K.A., McBride, M.B., 2005. Oxidative Degradation of Glyphosate and Aminomethylphosphonate by Manganese Oxide. Environ. Sci. Technol. 39, 9223–9228. https://doi.org/10.1021/es051342d

Belock, F., 2009. NC Chamber Public Policy Meeting.

Benjamin, M.M., Lawler, D.F., 2013. Water Quality Engineering: Physical / Chemical Treatment Processes. John Wiley & Sons.

Bichai, F., Ryan, H., Fitzgerald, C., Williams, K., Abdelmoteleb, A., Brotchie, R., Komatsu, R., 2015. Understanding the role of alternative water supply in an urban water security strategy: an analytical framework for decision-making. Urban Water J. 12, 175–189. https://doi.org/10.1080/1573062X.2014.895844

Blanchoud, H., Farrugia, F., Mouchel, J.M., 2004. Pesticide uses and transfers in urbanised catchments. Chemosphere 55, 905–913. https://doi.org/10.1016/j.chemosphere.2003.11.061

Bolong, N., Ismail, A.F., Salim, M.R., Matsuura, T., 2009. A review of the effects of emerging contaminants in wastewater and options for their removal. Desalination 239, 229–246. https://doi.org/10.1016/j.desal.2008.03.020

Boonfueng, T., Axe, L., Yee, N., Hahn, D., Ndiba, P.K., 2009. Zn sorption mechanisms onto sheathed Leptothrix discophora and the impact of the nanoparticulate biogenic Mn oxide coating. J. Colloid Interface Sci. 333, 439–447. https://doi.org/10.1016/j.jcis.2009.02.033

Bradl, H.B., 2004. Adsorption of heavy metal ions on soils and soils constituents. J. Colloid Interface Sci. 277, 1–18. https://doi.org/10.1016/j.jcis.2004.04.005

Bradshaw, J.L., Luthy, R.G., 2017. Modeling and Optimization of Recycled Water Systems to Augment Urban Groundwater Recharge through Underutilized Stormwater Spreading Basins. Environ. Sci. Technol. 51, 11809–11819. https://doi.org/10.1021/acs.est.7b02671

Bromfield, S., David, D., 1978. Properties of biologically formed manganese oxide in relation to soil manganese. Aust. J. Soil Res. 16, 79. https://doi.org/10.1071/SR9780079

Cabaniss, S.E., 2009. Forward Modeling of Metal Complexation by NOM: I. *A priori* Prediction of Conditional Constants and Speciation. Environ. Sci. Technol. 43, 2838–2844. https://doi.org/10.1021/es8015793

California Department of Transportation, 2003. Storm Water Monitoring & Data Management: 2002-2003 Annual Data Summary Report (No. CTSW-RT-03-069.51.42). Sacramento, CA.

California Department of Water Resources, 2018. Producing and Consuming Power [WWW Document]. URL https://www.water.ca.gov/What-We-Do/Power (accessed 5.25.18).

Caliskan, N., Kul, A.R., Alkan, S., Sogut, E.G., Alacabey, İ., 2011. Adsorption of Zinc(II) on diatomite and manganese-oxide-modified diatomite: A kinetic and equilibrium study. J. Hazard. Mater. 193, 27–36. https://doi.org/10.1016/j.jhazmat.2011.06.058

Cao, L.T.T., Kodera, H., Abe, K., Imachi, H., Aoi, Y., Kindaichi, T., Ozaki, N., Ohashi, A., 2015. Biological oxidation of Mn(II) coupled with nitrification for removal and recovery of minor metals by downflow hanging sponge reactor. Water Res. 68, 545–553. https://doi.org/10.1016/j.watres.2014.10.002

Careghini, A., Mastorgio, A.F., Saponaro, S., Sezenna, E., 2015. Bisphenol A, nonylphenols, benzophenones, and benzotriazoles in soils, groundwater, surface water, sediments, and food: a review. Environ. Sci. Pollut. Res. 22, 5711–5741. https://doi.org/10.1007/s11356-014-3974-5

Catts, J.G., Langmuir, D., 1986. Adsorption of Cu, Pb and Zn by delta-MnO2: applicability of the site binding-surface complexation model. Appl. Geochem. 1, 255–264.

Chowdhury, S., Champagne, P., McLellan, P.J., 2009. Models for predicting disinfection byproduct (DBP) formation in drinking waters: A chronological review. Sci. Total Environ. 2009, 4189–4206.

Christensen, J.B., Christensen, T.H., 1999. Complexation of Cd, Ni, and Zn by DOC in Polluted Groundwater: A Comparison of Approaches Using Resin Exchange, Aquifer Material Sorption, and Computer Speciation Models (WHAM and MINTEQA2). Environ. Sci. Technol. 33, 3857–3863. https://doi.org/10.1021/es981105t

Christensen, J.B., Jensen, D.L., Christensen, T.H., 1996. Effect of dissolved organic carbon on the mobility of cadmium, nickel and zinc in leachate polluted groundwater. Water Res. 30, 3037–3049. https://doi.org/10.1016/S0043-1354(96)00091-7

Clara, M., Strenn, B., Gans, O., Martinez, E., Kreuzinger, N., Kroiss, H., 2005. Removal of selected pharmaceuticals, fragrances and endocrine disrupting compounds in a membrane

bioreactor and conventional wastewater treatment plants. Water Res. 39, 4797–4807. https://doi.org/10.1016/j.watres.2005.09.015

Daigger, G.T., 2009. Evolving Urban Water and Residuals Management Paradigms: Water Reclamation and Reuse, Decentralization, and Resource Recovery. Water Environ. Res. 81, 809–823. https://doi.org/10.2175/106143009X425898

Davies, C.W., 1938. The extent of dissociation of salts in water. Part VIII. An equation for the mean ionic activity coefficient of an electrolyte in water, and a revision of the dissociation constants of some sulphates. J. Chem. Soc. Resumed 2093–2098. https://doi.org/10.1039/jr9380002093

Davis, A.P., Shokouhian, M., Ni, S., 2001. Loading estimates of lead, copper, cadmium, and zinc in urban runoff from specific sources 44, 997–1009.

Di Palma, L., Mecozzi, R., 2007. Heavy metals mobilization from harbour sediments using EDTA and citric acid as chelating agents. J. Hazard. Mater. 147, 768–775. https://doi.org/10.1016/j.jhazmat.2007.01.072

Dillon, P., Pavelic, P., Page, D., Beringen, H., Ward, J., 2009. Managed aquifer recharge: An introduction. Australia National Water Commission, Canberra, A.C.T.

Dong, D., Derry, L.A., Lion, L.W., 2003. Pb scavenging from a freshwater lake by Mn oxides in heterogeneous surface coating materials. Water Res. 37, 1662–1666. https://doi.org/10.1016/S0043-1354(02)00556-0

Drewes, J.E., 2009. Ground Water Replenishment with Recycled Water-Water Quality Improvements during Managed Aquifer Recharge. Ground Water 47, 502–505. https://doi.org/10.1111/j.1745-6584.2009.00587_5.x

Du, B., Lofton, J.M., Peter, K.T., Gipe, A.D., James, C.A., McIntyre, J.K., Scholz, N.L., Baker, J.E., Kolodziej, E.P., 2017. Development of suspect and non-target screening methods for detection of organic contaminants in highway runoff and fish tissue with high-resolution time-of-flight mass spectrometry. Environ. Sci. Process. Impacts 19, 1185–1196. https://doi.org/10.1039/C7EM00243B

Duckworth, O.W., Martin, S.T., 2003. Connections between surface complexation and geometric models of mineral dissolution investigated for rhodochrosite. Geochim. Cosmochim. Acta 67, 1787–1801. https://doi.org/10.1016/S0016-7037(02)01305-4

Edwards, E.C., Harter, T., Fogg, G.E., Washburn, B., Hamad, H., 2016. Assessing the effectiveness of drywells as tools for stormwater management and aquifer recharge and their groundwater contamination potential. J. Hydrol. 539, 539–553. https://doi.org/10.1016/j.jhydrol.2016.05.059

Ellis, J.B., 2000. Infiltration Systems: A Sustainable Source-Control Option for Urban Stormwater Quality Management? Water Environ. J. 14, 27–34.

Elzinga, E.J., 2016. ^{54}Mn Radiotracers Demonstrate Continuous Dissolution and Reprecipitation of Vernadite (δ-MnO_2) during Interaction with Aqueous Mn(II). Environ. Sci. Technol. 50, 8670–8677. https://doi.org/10.1021/acs.est.6b02874

Elzinga, E.J., Kustka, A.B., 2015. A Mn-54 Radiotracer Study of Mn Isotope Solid–Liquid Exchange during Reductive Transformation of Vernadite (δ-MnO_2) by Aqueous Mn(II). Environ. Sci. Technol. 49, 4310–4316. https://doi.org/10.1021/acs.est.5b00022

Erickson, A.J., Gulliver, J.S., Weiss, P.T., 2007. Enhanced Sand Filtration for Storm Water Phosphorus Removal. J. Environ. Eng. 133, 485–497.

Fendorf, S., Jardine, P.M., Patterson, R.R., Taylor, D.L., Brooks, S.C., 1999. Pyrolusite surface transformations measured in real-time during the reactive transport of Co(II)EDTA2–.

Geochim. Cosmochim. Acta 63, 3049–3057. https://doi.org/10.1016/S0016-7037(99)00232-X

Fendorf, S.E., Zasoski, R.J., 1992. Chromium(III) oxidation by .delta.-manganese oxide (MnO2). 1. Characterization. Environ. Sci. Technol. 26, 79–85. https://doi.org/10.1021/es00025a006

Feng, W., Hatt, B.E., McCarthy, D.T., Fletcher, T.D., Deletic, A., 2012. Biofilters for Stormwater Harvesting: Understanding the Treatment Performance of Key Metals That Pose a Risk for Water Use. Environ. Sci. Technol. 46, 5100–5108. https://doi.org/10.1021/es203396f

Feng, X.H., Zhu, M., Ginder-Vogel, M., Ni, C., Parikh, S.J., Sparks, D.L., 2010. Formation of nano-crystalline todorokite from biogenic Mn oxides. Geochim. Cosmochim. Acta 74, 3232–3245. https://doi.org/10.1016/j.gca.2010.03.005

Ficklin, D.L., Stewart, I.T., Maurer, E.P., 2013. Climate Change Impacts on Streamflow and Subbasin-Scale Hydrology in the Upper Colorado River Basin. PLoS ONE 8, e71297. https://doi.org/10.1371/journal.pone.0071297

Filella, M., 2008. NOM site binding heterogeneity in natural waters: Discrete approaches. J. Mol. Liq. 143, 42–51. https://doi.org/10.1016/j.molliq.2008.04.018

Forrez, I., Carballa, M., Noppe, H., De Brabander, H., Boon, N., Verstraete, W., 2009. Influence of manganese and ammonium oxidation on the removal of 17α-ethinylestradiol (EE2). Water Res. 43, 77–86. https://doi.org/10.1016/j.watres.2008.10.006

Forrez, I., Carballa, M., Verbeken, K., Vanhaecke, L., Ternes, T., Boon, N., Verstraete, W., 2010. Diclofenac oxidation by biogenic manganese oxides. Environ. Sci. Technol. 44, 3449–3454.

Frimmel, F.H., Huber, L., 1996. Influence of humic substances on the aquatic adsorption of heavy metals on defined mineral phases. Environ. Int. 22, 507–517.

Fu, G., Allen, H., Cowan, C., 1991. Adsorption of cadmium and copper by manganese oxide. Soil Sci. 152, 72–81.

Gadde, R.R., Laitinen, H.A., 1974. Heavy metal adsorption by hydrous iron and manganese oxides. Anal. Chem. 46, 2022–2026. https://doi.org/10.1021/ac60349a004

Gan, J., Bondarenko, S., Oki, L., Haver, D., Li, J.X., 2012. Occurrence of Fipronil and Its Biologically Active Derivatives in Urban Residential Runoff. Environ. Sci. Technol. 46, 1489–1495. https://doi.org/10.1021/es202904x

Gao, N., Hong, J., Yu, Z., Peng, P., Huang, W., 2011. Transformation of Bisphenol A in the Presence of Manganese Dioxide. Soil Sci. 176, 265–272. https://doi.org/10.1097/SS.0b013e31821d0b97

Genç-Fuhrman, H., Mikkelsen, P.S., Ledin, A., 2007. Simultaneous removal of As, Cd, Cr, Cu, Ni and Zn from stormwater: Experimental comparison of 11 different sorbents. Water Res. 41, 591–602. https://doi.org/10.1016/j.watres.2006.10.024

Gilliom, R.J. (Ed.), 2006. Pesticides in the nation's streams and ground water, 1992-2001: the quality of our nation's waters, Circular 1291. U.S. Geological Survey, Reston, VA.

Gleeson, T., Wada, Y., Bierkens, M.F.P., van Beek, L.P.H., 2012. Water balance of global aquifers revealed by groundwater footprint. Nature 488, 197–200. https://doi.org/10.1038/nature11295

Godtfredsen, K.L., Stone, A.T., 1994. Solubilization of Manganese Dioxide-Bound Copper by Naturally Occurring Organic Compounds. Environ. Sci. Technol. 28, 1450–1458. https://doi.org/10.1021/es00057a012

Gorelick, S.M., Zheng, C., 2015. Global change and the groundwater management challenge: Groundwater Management Challenge. Water Resour. Res. 51, 3031–3051. https://doi.org/10.1002/2014WR016825

Goren, O., Lazar, B., Burg, A., Gavrieli, I., 2012. Mobilization and retardation of reduced manganese in sandy aquifers: Column experiments, modeling and implications. Geochim. Cosmochim. Acta 96, 259–271. https://doi.org/10.1016/j.gca.2012.06.032

Grebel, J.E., Charbonnet, J.A., Sedlak, D.L., 2016. Oxidation of organic contaminants by manganese oxide geomedia for passive urban stormwater treatment systems. Water Res. 88, 481–491. https://doi.org/10.1016/j.watres.2015.10.019

Grebel, J.E., Mohanty, S.K., Torkelson, A.A., Boehm, A.B., Higgins, C.P., Maxwell, R.M., Nelson, K.L., Sedlak, D.L., 2013. Engineered Infiltration Systems for Urban Stormwater Reclamation. Environ. Eng. Sci. 30, 437–454. https://doi.org/10.1089/ees.2012.0312

Grebel, J.E., Pignatello, J.J., Mitch, W.A., 2010. Effect of Halide Ions and Carbonates on Organic Contaminant Degradation by Hydroxyl Radical-Based Advanced Oxidation Processes in Saline Waters. Environ. Sci. Technol. 44, 6822–6828. https://doi.org/10.1021/es1010225

Gregor, H.P., Luttinger, L.B., Loebl, E.M., 1955. Metal–Polyelectrolyte Complexes. I. The Polyacrylic Acid–Copper Complex. J. Phys. Chem. 59, 34–39. https://doi.org/10.1021/j150523a011

Gustafsson, J.P., 2014. Visual MINTEQ 3.1 user guide. KTH, Department of Land and Water Recources, Stockholm, Sweden.

Halaburka, B.J., LeFevre, G.H., Luthy, R.G., 2017. Evaluation of Mechanistic Models for Nitrate Removal in Woodchip Bioreactors. Environ. Sci. Technol. 51, 5156–5164. https://doi.org/10.1021/acs.est.7b01025

Halsey, G., Taylor, H.S., 1947. The Adsorption of Hydrogen on Tungsten Powders. J. Chem. Phys. 15, 624–630. https://doi.org/10.1063/1.1746618

Han, R., Zou, W., Zhang, Z., Shi, J., Yang, J., 2006. Removal of copper(II) and lead(II) from aqueous solution by manganese oxide coated sand. J. Hazard. Mater. 137, 384–395. https://doi.org/10.1016/j.jhazmat.2006.02.021

Hao, O.J., Davis, A.P., Chang, P.H., 1991. Kinetics of manganese (II) oxidation with chlorine. J. Environ. Eng. 117, 359–374.

Hatt, B.E., Fletcher, T.D., Deletic, A., 2009. Pollutant removal performance of field-scale stormwater biofiltration systems. Water Sci. Technol. 59, 1567. https://doi.org/10.2166/wst.2009.173

Hatt, B.E., Fletcher, T.D., Deletic, A., 2008. Hydraulic and Pollutant Removal Performance of Fine Media Stormwater Filtration Systems. Environ. Sci. Technol. 42, 2535–2541. https://doi.org/10.1021/es071264p

Hering, J.G., Waite, T.D., Luthy, R.G., Drewes, J.E., Sedlak, D.L., 2013. A Changing Framework for Urban Water Systems. Environ. Sci. Technol. 47, 10721–10726. https://doi.org/10.1021/es4007096

Hou, J., Li, Y., Mao, M., Ren, L., Zhao, X., 2014. Tremendous Effect of the Morphology of Birnessite-Type Manganese Oxide Nanostructures on Catalytic Activity. ACS Appl. Mater. Interfaces 6, 14981–14987. https://doi.org/10.1021/am5027743

Hunt, J.R., 2013. Partial Lecture Notes for Environmental Physical-Chemical Processes. University of California, Berkeley.

Im, J., Löffler, F.E., 2016. Fate of Bisphenol A in Terrestrial and Aquatic Environments. Environ. Sci. Technol. 50, 8403–8416. https://doi.org/10.1021/acs.est.6b00877

Im, J., Prevatte, C.W., Campagna, S.R., Löffler, F.E., 2015. Identification of 4-Hydroxycumyl Alcohol As the Major MnO_2-Mediated Bisphenol A Transformation Product and Evaluation of Its Environmental Fate. Environ. Sci. Technol. 49, 6214–6221. https://doi.org/10.1021/acs.est.5b00372

International Agency for Research on Cancer, World Health Organization, IARC Working Group on the Evaluation of Carcinogenic Risks to Humans (Eds.), 2013. Some chemicals present in industrial and consumer products, food and drinking-water, IARC monographs on the evaluation of carcinogenic risks to humans. IARC Press, Lyon.

Irving, H., Williams, R.J.P., 1953. The Stability of Transition-metal Complexes. J. Chem. Soc. 3192–3210.

Jacobsen, F., Holcman, J., Sehested, K., 1998. Oxidation of Manganese(II) by Ozone and Reduction of Manganese(III) by Hydrogen Peroxide in Acidic Solution. Int. J. Chem. Kinet. 30, 207–214.

James, R.O., Healy, T.W., 1972. Adsorption of hydrolyzable metal ions at the oxide—water interface. III. A thermodynamic model of adsorption. J. Colloid Interface Sci. 40, 65–81. https://doi.org/10.1016/0021-9797(72)90174-9

James, R.O., Stiglich, P.J., Healy, T.W., 1975. Analysis of models of adsorption of metal ions at oxide/water interfaces. Faraday Discuss. Chem. Soc. 59, 142. https://doi.org/10.1039/dc9755900142

Jasper, J.T., Nguyen, M.T., Jones, Z.L., Ismail, N.S., Sedlak, D.L., Sharp, J.O., Luthy, R.G., Horne, A.J., Nelson, K.L., 2013. Unit Process Wetlands for Removal of Trace Organic Contaminants and Pathogens from Municipal Wastewater Effluents. Environ. Eng. Sci. 30, 421–436. https://doi.org/10.1089/ees.2012.0239

Jiang, J., Wang, Z., Chen, Y., He, A., Li, J., Sheng, G.D., 2017. Metal inhibition on the reactivity of manganese dioxide toward organic contaminant oxidation in relation to metal adsorption and ionic potential. Chemosphere 170, 95–103. https://doi.org/10.1016/j.chemosphere.2016.12.015

Kallis, G., Kiparsky, M., Norgaard, R., 2009. Collaborative governance and adaptive management: Lessons from California's CALFED Water Program. Environ. Sci. Policy 12, 631–643. https://doi.org/10.1016/j.envsci.2009.07.002

Kang, J.-H., Kondo, F., 2002. Bisphenol A Degradation by Bacteria Isolated from River Water. Arch. Environ. Contam. Toxicol. 43, 265–269. https://doi.org/10.1007/s00244-002-1209-0

Kessick, M.A., Morgan, J.J., 1975. Mechanism of autoxidation of manganese in aqueous solution. Environ. Sci. Technol. 9, 157–159.

Kim, H.-C., Dempsey, B.A., 2013. Membrane fouling due to alginate, SMP, EfOM, humic acid, and NOM. J. Membr. Sci. 428, 190–197. https://doi.org/10.1016/j.memsci.2012.11.004

Kim, S.S., Bargar, J.R., Nealson, K.H., Flood, B.E., Kirschvink, J.L., Raub, T.D., Tebo, B.M., Villalobos, M., 2011. Searching for Biosignatures Using Electron Paramagnetic Resonance (EPR) Analysis of Manganese Oxides. Astrobiology 11, 775–786. https://doi.org/10.1089/ast.2011.0619

King County, WA, 2016. The science of stormwater [WWW Document]. URL https://www.kingcounty.gov/services/environment/water-and-land/stormwater/introduction/science.aspx (accessed 8.28.18).

Klausen, J., Haderlein, S.B., Schwarzenbach, R.P., 1997. Oxidation of substituted anilines by aqueous MnO2: Effect of co-solutes on initial and quasi-steady-state kinetics. Environ. Sci. Technol. 31, 2642–2649.

Klučáková, M., Kolajová, R., 2014. Dissociation ability of humic acids: Spectroscopic determination of pKa and comparison with multi-step mechanism. React. Funct. Polym. 78, 1–6. https://doi.org/10.1016/j.reactfunctpolym.2014.02.005

Knocke, W.R., Occiano, S.C., Hungate, R., 1991a. Removal of Soluble Manganese by Oxide-coated Filter Media: Sorption Rate and Removal Mechanism Issues. J. Am. Water Works Assoc. 83, 64–69.

Knocke, W.R., Van Benschoten, J.E., Kearney, M.J., Soborski, A.W., Reckhow, D.A., 1991b. Kinetics of Manganese and Iron Oxidation by Potassium Permanganate and Chlorine Dioxide. J. Am. Water Works Assoc. 83, 80–87.

Kocar, B.D., Polizzotto, M.L., Benner, S.G., Ying, S.C., Ung, M., Ouch, K., Samreth, S., Suy, B., Phan, K., Sampson, M., Fendorf, S., 2008. Integrated biogeochemical and hydrologic processes driving arsenic release from shallow sediments to groundwaters of the Mekong delta. Appl. Geochem. 23, 3059–3071. https://doi.org/10.1016/j.apgeochem.2008.06.026

Kozawa, A., Yeager, J.F., 1965. The Cathodic Reduction Mechanism of Electrolytic Manganese Dioxide in Alkaline Electrolyte. J. Electrochem. Soc. 112, 959. https://doi.org/10.1149/1.2423350

Laha, S., Luthy, R.G., 1990. Oxidation of aniline and other primary aromatic amines by manganese dioxide. Environ. Sci. Technol. 24, 363–373.

Larsen, T.A., Udert, K.M., Lienert, J., 2013. Source Separation and Decentralization for Wastewater Management. IWA Publishing.

Le Coustumer, S., Fletcher, T.D., Deletic, A., Barraud, S., Poelsma, P., 2012. The influence of design parameters on clogging of stormwater biofilters: A large-scale column study. Water Res. 46, 6743–6752. https://doi.org/10.1016/j.watres.2012.01.026

Learman, D.R., Wankel, S.D., Webb, S.M., Martinez, N., Madden, A.S., Hansel, C.M., 2011. Coupled biotic–abiotic Mn(II) oxidation pathway mediates the formation and structural evolution of biogenic Mn oxides. Geochim. Cosmochim. Acta 75, 6048–6063. https://doi.org/10.1016/j.gca.2011.07.026

Li, F., Liu, C., Liang, C., Li, X., Zhang, L., 2008. The oxidative degradation of 2-mercaptobenzothiazole at the interface of β-MnO2 and water. J. Hazard. Mater. 154, 1098–1105. https://doi.org/10.1016/j.jhazmat.2007.11.015

Li, X., Pan, G., Qin, Y., Hu, T., Wu, Z., Xie, Y., 2004. EXAFS studies on adsorption–desorption reversibility at manganese oxide–water interfaces. J. Colloid Interface Sci. 271, 35–40. https://doi.org/10.1016/j.jcis.2003.11.029

Lin, K., Liu, W., Gan, J., 2009. Oxidative Removal of Bisphenol A by Manganese Dioxide: Efficacy, Products, and Pathways. Environ. Sci. Technol. 43, 3860–3864. https://doi.org/10.1021/es900235f

Lin, K., Peng, Y., Huang, X., Ding, J., 2013. Transformation of bisphenol A by manganese oxide-coated sand. Environ. Sci. Pollut. Res. 20, 1461–1467. https://doi.org/10.1007/s11356-012-1049-z

Lion, L.W., Altmann, R.S., Leckie, J.O., 1982. Trace-metal adsorption characteristics of estuarine particulate matter: evaluation of contributions of iron/manganese oxide and organic surface coatings. Environ. Sci. Technol. 16, 660–666. https://doi.org/10.1021/es00104a007

Liu, C., von Gunten, U., Croué, J.-P., 2012. Enhanced Bromate Formation during Chlorination of Bromide-Containing Waters in the Presence of CuO: Catalytic Disproportionation of Hypobromous Acid. Environ. Sci. Technol. 46, 11054–11061. https://doi.org/10.1021/es3021793

Liu, C., Zhang, L., Li, F., Wang, Y., Gao, Y., Li, X., Cao, W., Feng, C., Dong, J., Sun, L., 2009a. Dependence of Sulfadiazine Oxidative Degradation on Physicochemical Properties of Manganese Dioxides. Ind. Eng. Chem. Res. 48, 10408–10413. https://doi.org/10.1021/ie900812j

Liu, C., Zhang, L.J., Feng, C.H., Wu, C.A., Li, F.B., Li, X.Z., 2009b. Relationship between oxidative degradation of 2-mercaptobenzothiazole and physicochemical properties of manganese (hydro)oxides. Environ. Chem. 6, 83. https://doi.org/10.1071/EN08053

Liu, D., Sansalone, J.J., Cartledge, F.K., 2005. Comparison of Sorptive Filter Media for Treatment of Metals in Runoff. J. Environ. Eng. 131, 1178–1186. https://doi.org/10.1061/(ASCE)0733-9372(2005)131:8(1178)

Liu, R., Xu, W., He, Z., Lan, H., Liu, H., Qu, J., Prasai, T., 2015. Adsorption of antimony(V) onto Mn(II)-enriched surfaces of manganese-oxide and FeMn binary oxide. Chemosphere 138, 616–624. https://doi.org/10.1016/j.chemosphere.2015.07.039

Liu, Y., Hejazi, M., Kyle, P., Kim, S.H., Davies, E., Miralles, D.G., Teuling, A.J., He, Y., Niyogi, D., 2016. Global and Regional Evaluation of Energy for Water. Environ. Sci. Technol. 50, 9736–9745. https://doi.org/10.1021/acs.est.6b01065

Loganathan, P., Burau, R.G., 1973. Sorption of heavy metal ions by a hydrous manganese oxide. Geochim. Cosmochim. Acta 37, 1277–1293. https://doi.org/10.1016/0016-7037(73)90061-6

Loganathan, P., Burau, R.G., Fuerstenau, D.W., 1977. Influence of pH on the Sorption of Co2+, Zn2+ and Ca2+ by a Hydrous Manganese Oxide1. Soil Sci. Soc. Am. J. 41, 57. https://doi.org/10.2136/sssaj1977.03615995004100010020x

Loraine, G.A., Pettigrove, M.E., 2006. Seasonal Variations in Concentrations of Pharmaceuticals and Personal Care Products in Drinking Water and Reclaimed Wastewater in Southern California. Environ. Sci. Technol. 40, 687–695. https://doi.org/10.1021/es051380x

Los Angeles and San Gabriel Rivers Watershed Council, 2010. Water Augmentation Study: Research Strategy and Implementation Report.

Los Angeles County Flood Control District, City of Los Angeles Department of Public Works Bureau of Sanitation, 2014. Sun Valley Watershed: Rory M. Shaw Wetlands Park Factsheet (Factsheet).

Los Angeles County Flood Control District, City of Los Angeles Department of Public Works Bureau of Sanitation, 2006. Concept Report: Strathern Pit Multiuse Project (Concept Report).

Los Angeles Department of Water and Power, 2013. Facts & Figures [WWW Document]. URL https://www.ladwp.com/ladwp/faces/ladwp/aboutus/a-water/a-w-factandfigures?_adf.ctrl-state=1b0vhrss47_4&_afrLoop=328191484034851 (accessed 7.19.18).

Ma, H., Allen, H.E., Yin, Y., 2001. Characterization of isolated fractions of dissolved organic matter from natural waters and a wastewater effluent. Water Res. 35, 985–996. https://doi.org/10.1016/S0043-1354(00)00350-X

Makepeace, D.K., Smith, D.W., Stanley, S.J., 1995. Urban stormwater quality: Summary of contaminant data. Crit. Rev. Environ. Sci. Technol. 25, 93–139. https://doi.org/10.1080/10643389509388476

Manceau, A., Combes, J.M., 1988. Structure of Mn and Fe oxides and oxyhydroxides: A topological approach by EXAFS. Phys. Chem. Miner. 15, 283–295. https://doi.org/10.1007/BF00307518

Manceau, A., Drits, V.A., Silvester, E., Bartoli, C., Lanson, B., 1997. Structural mechanism of Co2+ oxidation by the phyllomanganate buserite. Am. Mineral. 82, 1150–1175.

Manceau, A., Kersten, M., Marcus, M.A., Geoffroy, N., Granina, L., 2007a. Ba and Ni speciation in a nodule of binary Mn oxide phase composition from Lake Baikal. Geochim. Cosmochim. Acta 71, 1967–1981. https://doi.org/10.1016/j.gca.2007.02.007

Manceau, A., Lanson, M., Geoffroy, N., 2007b. Natural speciation of Ni, Zn, Ba, and As in ferromanganese coatings on quartz using X-ray fluorescence, absorption, and diffraction. Geochim. Cosmochim. Acta 71, 95–128. https://doi.org/10.1016/j.gca.2006.08.036

Manceau, A., Marcus, M.A., Grangeon, S., 2012. Determination of Mn valence states in mixed-valent manganates by XANES spectroscopy. Am. Mineral. 97, 816–827. https://doi.org/10.2138/am.2012.3903

Marafatto, F.F., Strader, M.L., Gonzalez-Holguera, J., Schwartzberg, A., Gilbert, B., Peña, J., 2015. Rate and mechanism of the photoreduction of birnessite (MnO_2) nanosheets. Proc. Natl. Acad. Sci. 112, 4600–4605. https://doi.org/10.1073/pnas.1421018112

Masini, J.C., 1993. Evaluation of neglecting electrostatic interactions on the determination and characterization of the ionizable sites in humic substances. Anal. Chim. Acta 283, 803–810. https://doi.org/10.1016/0003-2670(93)85295-U

Mayor's Office of Sustainability, 2018. 3rd Annual Report 2017-2018: City Sustainability Plan.

Mazzera, D., 2014. California Department of Public Health Memorandum: State Adoption of a Hexavalent Chromium MCL.

McCann, C.M., Gray, N.D., Tourney, J., Davenport, R.J., Wade, M., Finlay, N., Hudson-Edwards, K.A., Johnson, K.L., 2015. Remediation of a historically Pb contaminated soil using a model natural Mn oxide waste. Chemosphere 138, 211–217. https://doi.org/10.1016/j.chemosphere.2015.05.054

McKenzie, R., 1980. The adsorption of lead and other heavy metals on oxides of manganese and iron. Aust. J. Soil Res. 18, 61. https://doi.org/10.1071/SR9800061

McKenzie, R.M., 1981. The surface charge on manganese dioxides. Soil Res. 19, 41–50.

McKenzie, R.M., 1971. The synthesis of birnessite, cryptomelane, and some other oxides and hydroxides of manganese. Mineral. Mag. 38, 493–502.

McKenzie, R.M., 1970. The reaction of cobalt with manganese dioxide minerals. Soil Res. 8, 97–106.

Mekonnen, M.M., Hoekstra, A.Y., 2016. Four billion people facing severe water scarcity. Sci. Adv. 2, e1500323–e1500323. https://doi.org/10.1126/sciadv.1500323

Melichová, Z., Treindl, L., Valent, I., 2001. Kinetics and mechanism of the autocatalytic oxidation of Mn (II) by bromine. React. Kinet. Catal. Lett. 74, 79–86.

Minnesota Department of Health, 2014. Bisphenol A in Drinking Water (Scientific Investigations Report).

Misono, M., Ochiai, E., Saito, Y., Yoneda, Y., 1967. A new dual parameter scale for the strength of lewis acids and bases with the evaluation of their softness. J. Inorg. Nucl. Chem. 29, 2685–2691. https://doi.org/10.1016/0022-1902(67)80006-X

Moberg, L., Karlberg, B., 2000. An improved N, N′-diethyl-p-phenylenediamine (DPD) method for the determination of free chlorine based on multiple wavelength detection. Anal. Chim. Acta 407, 127–133.

Moglen, G.E., 2009. Discussion – '"Is Denser Greener? An Evaluation of Higher Density Development as an Urban Stormwater-Quality Best Management Practice"' by John S. Jacob and Ricardo Lopez. Journal of the American Water Resources Association (JAWRA). JAWRA J. Am. Water Resour. Assoc. 45, 1536–1538. https://doi.org/10.1111/j.1752-1688.2009.00381.x

Mohanty, S.K., Torkelson, A.A., Dodd, H., Nelson, K.L., Boehm, A.B., 2013. Engineering Solutions to Improve the Removal of Fecal Indicator Bacteria by Bioinfiltration Systems during Intermittent Flow of Stormwater. Environ. Sci. Technol. 47, 10791–10798. https://doi.org/10.1021/es305136b

Morgan, J.J., 2005. Kinetics of reaction between O2 and Mn(II) species in aqueous solutions. Geochim. Cosmochim. Acta 69, 35–48. https://doi.org/10.1016/j.gca.2004.06.013

Morgan, J.J., 1967. Chemical equilibria and kinetic properties of manganese in natural waters, in: Fausrt, S.D., Hunter, J.V. (Eds.), Principles and Applications of Water Chemistry. Wiley, pp. 561–623.

Morgan, J.J., 1964. Chemistry of aqueous manganese II and IV. Harvard, Cambridge.

Morgan, J.J., Stumm, W., 1964. Colloid-chemical properties of manganese dioxide. J. Colloid Sci. 19, 347–359.

Mullane, J.M., Flury, M., Iqbal, H., Freeze, P.M., Hinman, C., Cogger, C.G., Shi, Z., 2015. Intermittent rainstorms cause pulses of nitrogen, phosphorus, and copper in leachate from compost in bioretention systems. Sci. Total Environ. 537, 294–303. https://doi.org/10.1016/j.scitotenv.2015.07.157

Murray, J.W., 1975. The interaction of metal ions at the manganese dioxide-solution interface. Geochim. Cosmochim. Acta 39, 505–519. https://doi.org/10.1016/0016-7037(75)90103-9

Murray, J.W., Balistrieri, L., Paul, B., 1984. The oxidation state of manganese in marine sediments and ferromanganese nodules. Geochim. Cosmochim. Acta 48, 1237–1247.

Nakamura, S., Tezuka, Y., Ushiyama, A., Kawashima, C., Kitagawara, Y., Takahashi, K., Ohta, S., Mashino, T., 2011. Ipso substitution of bisphenol A catalyzed by microsomal cytochrome P450 and enhancement of estrogenic activity. Toxicol. Lett. 203, 92–95. https://doi.org/10.1016/j.toxlet.2011.03.010

National Research Council, 2012. Water Reuse: Potential for Expanding the Nation's Water Supply Through Reuse of Municipal Wastewater. National Academies Press, Washington, D.C. https://doi.org/10.17226/13303

National Research Council, 1972. Particulate Polycyclic Organic Matter. National Academies Press.

Nico, P.S., Zasoski, R.J., 2001. Mn(III) Center Availability as a Rate Controlling Factor in the Oxidation of Phenol and Sulfide on δ-MnO_2. Environ. Sci. Technol. 35, 3338–3343. https://doi.org/10.1021/es001848q

Nico, P.S., Zasoski, R.J., 2000. Importance of Mn(III) Availability on the Rate of Cr(III) Oxidation on δ-MnO_2. Environ. Sci. Technol. 34, 3363–3367. https://doi.org/10.1021/es991462j

Niederer, C., Schwarzenbach, R.P., Goss, K.-U., 2007. Elucidating Differences in the Sorption Properties of 10 Humic and Fulvic Acids for Polar and Nonpolar Organic Chemicals. Environ. Sci. Technol. 41, 6711–6717. https://doi.org/10.1021/es0709932

Oden, W.I., Amy, G.L., Conklin, M., 1993. Subsurface interactions of humic substances with copper(II) in saturated media. Environ. Sci. Technol. 27, 1045–1051. https://doi.org/10.1021/es00043a002

O'Reilly, S.., Hochella, M.F., 2003. Lead sorption efficiencies of natural and synthetic Mn and Fe-oxides. Geochim. Cosmochim. Acta 67, 4471–4487. https://doi.org/10.1016/S0016-7037(03)00413-7

Owen, D.M., 2015. Changing the Paradigm: Managing Water Throughout the Cycle for Total Water Solutions. J. - Am. Water Works Assoc. 107, 54–59. https://doi.org/10.5942/jawwa.2015.107.0092

Pagán, B.R., Ashfaq, M., Rastogi, D., Kendall, D.R., Kao, S.-C., Naz, B.S., Mei, R., Pal, J.S., 2016. Extreme hydrological changes in the southwestern US drive reductions in water supply to Southern California by mid century. Environ. Res. Lett. 11, 094026. https://doi.org/10.1088/1748-9326/11/9/094026

Page, D., Dillon, P., Vanderzalm, J., Toze, S., Sidhu, J., Barry, K., Levett, K., Kremer, S., Regel, R., 2010. Risk Assessment of Aquifer Storage Transfer and Recovery with Urban Stormwater for Producing Water of a Potable Quality. J. Environ. Qual. 39, 2029–2039. https://doi.org/10.2134/jeq2010.0078

Page, D., Miotliński, K., Gonzalez, D., Barry, K., Dillon, P., Gallen, C., 2014. Environmental monitoring of selected pesticides and organic chemicals in urban stormwater recycling systems using passive sampling techniques. J. Contam. Hydrol. 158, 65–77. https://doi.org/10.1016/j.jconhyd.2014.01.004

Pagotto, C., Rémy, N., Legret, M., Le Cloirec, P., 2001. Heavy Metal Pollution of Road Dust and Roadside Soil near a Major Rural Highway. Environ. Technol. 22, 307–319. https://doi.org/10.1080/09593332208618280

Parker, D.S., 2011. Introduction of New Process Technology into the Wastewater Treatment Sector. Water Environ. Res. 83, 483–497.

Peña, J., Bargar, J.R., Sposito, G., 2011. Role of Bacterial Biomass in the Sorption of Ni by Biomass-Birnessite Assemblages. Environ. Sci. Technol. 45, 7338–7344. https://doi.org/10.1021/es201446r

Peña, J., Kwon, K.D., Refson, K., Bargar, J.R., Sposito, G., 2010. Mechanisms of nickel sorption by a bacteriogenic birnessite. Geochim. Cosmochim. Acta 74, 3076–3089. https://doi.org/10.1016/j.gca.2010.02.035

Pitt, R., Field, R., Lalor, M., Brown, M., 1995. Urban stormwater toxic pollutants: assessment, sources, and treatability. Water Environ. Res. 67, 260–275. https://doi.org/10.2175/106143095X131466

Pitt, R., Maestre, A., Morquecho, R., 2015. National Stormwater Quality Database, Version 4.02.

Pitt, R., Talebi, L., Bean, R., Clark, S., 2012. Stormwater Non-Potable Beneficial Uses and Effects on Urban Infrastructure. Water Environment Research Foundation Alexandria, VA.

Post, J.E., 1999. Manganese oxide minerals: Crystal structures and economic and environmental significance. Proc. Natl. Acad. Sci. 96, 3447–3454.

Post, J.E., von Deele, R.B., Tentscher, P.R., 1982. Symmetry and Cation Displacements in Hollandites: Structure Refinements of Hollandite, Cryptomelane and Priderite. Acta Crystallogr. B38, 1056–1065.

Radian, A., Fichman, M., Mishael, Y., 2015. Modeling binding of organic pollutants to a clay–polycation adsorbent using quantitative structural–activity relationships (QSARs). Appl. Clay Sci. 116–117, 241–247. https://doi.org/10.1016/j.clay.2015.03.021

Regnery, J., Lee, J., Kitanidis, P., Illangasekare, T., Sharp, J.O., Drewes, J.E., 2013. Integration of Artificial Recharge and Recovery Systems for Impaired Water Sources in Urban Settings: Overcoming Current Limitations and Engineering Challenges. Environ. Eng. Sci. 30, 409–420. https://doi.org/10.1089/ees.2012.0186

Reisz, E., Leitzke, A., Jarocki, A., Irmscher, R., von Sonntag, C., 2008. Permanganate formation in the reactions of ozone with Mn(II): a mechanistic study. J. Water Supply Res. Technol. 57, 451. https://doi.org/10.2166/aqua.2008.091

Remucal, C.K., Ginder-Vogel, M., 2014. A critical review of the reactivity of manganese oxides with organic contaminants. Environ. Sci. Process. Impacts 16, 1247–1266. https://doi.org/10.1039/c3em00703k

Robinson, D.M., Go, Y.B., Mui, M., Gardner, G., Zhang, Z., Mastrogiovanni, D., Garfunkel, E., Li, J., Greenblatt, M., Dismukes, G.C., 2013. Photochemical Water Oxidation by Crystalline Polymorphs of Manganese Oxides: Structural Requirements for Catalysis. J. Am. Chem. Soc. 135, 3494–3501. https://doi.org/10.1021/ja310286h

Rozan, T.F., Benoit, G., Marsh, H., Chin, Y.-P., 1999. Intercomparison of DPASV and ISE for the Measurement of Cu Complexation Characteristics of NOM in Freshwater. Environ. Sci. Technol. 33, 1766–1770. https://doi.org/10.1021/es9810944

Rudder, J. d., Wiele, T.V. de, Dhooge, W., Comhaire, F., Verstraete, W., 2004. Advanced water treatment with manganese oxide for the removal of 17α-ethynylestradiol (EE2). Water Res. 38, 184–192. https://doi.org/10.1016/j.watres.2003.09.018

Saar, R.A., Weber, J.H., 1980. Lead(II)-fulvic acid complexes. Conditional stability constants, solubility, and implications for lead(II) mobility. Environ. Sci. Technol. 14, 877–880. https://doi.org/10.1021/es60167a001

Sain, A.E., Dietrich, A.M., 2015. Rethinking aesthetic guidelines for manganese and iron in drinking water. J. Water Supply Res. Technol. - Aqua 64, 775–782. https://doi.org/10.2166/aqua.2014.091

Sansalone, J.J., Buchberger, S.G., 1997. Partitioning and First Flush of Metals in Urban Roadway Storm Water. J. Environ. Eng. 123, 134–143. https://doi.org/10.1061/(ASCE)0733-9372(1997)123:2(134)

Schmitt, D., Saravia, F., Frimmel, F.H., Schuessler, W., 2003. NOM-facilitated transport of metal ions in aquifers: importance of complex-dissociation kinetics and colloid formation. Water Res. 37, 3541–3550. https://doi.org/10.1016/S0043-1354(01)00525-5

Schwarzenbach, R.P., Gschwend, P.M., Imboden, D.M., 2016. Environmental Organic Chemistry. John Wiley & Sons.

Sellers, R.M., 1980. Spectrophotometric determination of hydrogen peroxide using potassium titanium (IV) oxalate. Analyst 105, 950–954.

Sherman, L.S., Blum, J.D., Dvonch, J.T., Gratz, L.E., Landis, M.S., 2015. The use of Pb, Sr, and Hg isotopes in Great Lakes precipitation as a tool for pollution source attribution. Sci. Total Environ. 502, 362–374. https://doi.org/10.1016/j.scitotenv.2014.09.034

Shin, J.Y., Cheney, M.A., 2004. Abiotic transformation of atrazine in aqueous suspension of four synthetic manganese oxides. Colloids Surf. Physicochem. Eng. Asp. 242, 85–92. https://doi.org/10.1016/j.colsurfa.2004.04.061

Shorter, J., 1994. Compilation and critical evaluation of structure-reactivity parameters and equations: Part 1: Values of σm and σp based on the ionization of substituted benzoic acids in water at 25°C. Pure Appl. Chem. 66, 2451–2468.

Siegel, S.M., 2015. Let There Be Water: Israel's Solution for a Water-Starved World. Macmillan.

Simanova, A.A., Peña, J., 2015. Time-Resolved Investigation of Cobalt Oxidation by Mn(III)-Rich δ-MnO ₂ Using Quick X-ray Absorption Spectroscopy. Environ. Sci. Technol. 49, 10867–10876. https://doi.org/10.1021/acs.est.5b01088

Soller, J., Stephenson, J., Olivieri, K., Downing, J., Olivieri, A.W., 2005. Evaluation of seasonal scale first flush pollutant loading and implications for urban runoff management. J. Environ. Manage. 76, 309–318. https://doi.org/10.1016/j.jenvman.2004.12.007

Sposito, G., 2008. The Chemistry of Soils, 2nd ed. Oxford University Press, New York.

Stevenson, F.J., 1976. Stability constants of Cu2+, Pb2+, and Cd2+ complexes with humic acids. Soil Sci Soc Am J 40, 665–672.

Stokes, J., Horvath, A., 2006. Life Cycle Energy Assessment of Alternative Water Supply Systems (9 pp). Int. J. Life Cycle Assess. 11, 335–343. https://doi.org/10.1065/lca2005.06.214

Stone, A.T., 1987. Reductive dissolution of manganese (III/IV) oxides by substituted phenols. Environ. Sci. Technol. 21, 979–988.

Stone, A.T., Morgan, J.J., 1984. Reduction and dissolution of manganese (III) and manganese (IV) oxides by organics: 2. Survey of the reactivity of organics. Environ. Sci. Technol. 18, 617–624.

Su, Q., Pan, Bingcai, Pan, Bingjun, Zhang, Qingrui, Zhang, W., Lv, L., Wang, X., Wu, J., Zhang, Quanxing, 2009. Fabrication of polymer-supported nanosized hydrous manganese dioxide (HMO) for enhanced lead removal from waters. Sci. Total Environ. 407, 5471–5477. https://doi.org/10.1016/j.scitotenv.2009.06.045

Sun, B., Zhao, F.., Lombi, E., McGrath, S.., 2001. Leaching of heavy metals from contaminated soils using EDTA. Environ. Pollut. 113, 111–120. https://doi.org/10.1016/S0269-7491(00)00176-7

Sunda, W.G., Huntsman, S.A., Harvey, G.R., 1983. Photoreduction of manganese oxides in seawater ant its geochemical and biological implications. Nature 301, 234–236.

Takada, H., Onda, T., Ogura, N., 1990. Determination of polycyclic aromatic hydrocarbons in urban street dusts and their source materials by capillary gas chromatography. Environ. Sci. Technol. 24, 1179–1186. https://doi.org/10.1021/es00078a005

Takamatsu, T., Yoshida, T., 1978. Determination of stability constants of metal-humic acid complexes by potentiometric titration and ion-selective electrodes. Soil Sci. 125, 377–386.

Tani, Y., Miyata, N., Iwahori, K., Soma, M., Tokuda, S., Seyama, H., Theng, B.K.., 2003. Biogeochemistry of manganese oxide coatings on pebble surfaces in the Kikukawa River System, Shizuoka, Japan. Appl. Geochem. 18, 1541–1554. https://doi.org/10.1016/S0883-2927(03)00075-1

Tebo, B.M., Johnson, H.A., McCarthy, J.K., Templeton, A.S., 2005. Geomicrobiology of manganese(II) oxidation. Trends Microbiol. 13, 421–428. https://doi.org/10.1016/j.tim.2005.07.009

Ternes, T., Joss, A., Siegrist, H., 2004. Scrutinizing Pharmaceuticals and Personal Care Products in Wastewater Treatment. Environ. Sci. Technol. 393–398.

Tessier, A., Fortin, D., Belzile, N., DeVitre, R.R., Leppard, G.G., 1996. Metal sorption to diagenetic iron and manganese oxyhydroxides and associated organic matter: Narrowing the gap between field and laboratory measurements. Geochim. Cosmochim. Acta 60, 387–404.

Tipping, E., Heaton, M.J., 1983. The adsorption of aquatic humic substances by two oxides of manganese. Geochim. Cosmochim. Acta 47, 1393–1397. https://doi.org/10.1016/0016-7037(83)90297-1

Trouwborst, R.E., 2006. Soluble Mn(III) in Suboxic Zones. Science 313, 1955–1957. https://doi.org/10.1126/science.1132876

Ukrainczyk, L., McBride, M.B., 1992. Oxidation of Phenol in Acidic Aqueous Suspensions of Manganese Oxides. Clays Clay Miner. 40, 157–166. https://doi.org/10.1346/CCMN.1992.0400204

Ulrich, B.A., Im, E.A., Werner, D., Higgins, C.P., 2015. Biochar and Activated Carbon for Enhanced Trace Organic Contaminant Retention in Stormwater Infiltration Systems. Environ. Sci. Technol. 49, 6222–6230. https://doi.org/10.1021/acs.est.5b00376

Ulrich, B.A., Loehnert, M., Higgins, C.P., 2017. Improved contaminant removal in vegetated stormwater biofilters amended with biochar. Environ. Sci. Water Res. Technol. 3, 726–734. https://doi.org/10.1039/C7EW00070G

US Environmental Protection Agency, 2010. Comprehensive Disinfectants and Disinfection Byproducts Rules (Stage 1 and Stage 2): Quick Reference Guide (No. EPA 816-F-10-080). US EPA, Office of Water.

US Environmental Protection Agency, 2004. National Recommended Water Quality Criteria. Office of Science and Technology: Office of Water, Washington, DC.

US Environmental Protection Agency, 1999. Preliminary Data Summary of Urban Stormwater Best Management Practices.

Van Benschoten, J.E., Lin, W., Knocke, W.R., 1992. Kinetic modeling of manganese (II) oxidation by chlorine dioxide and potassium permanganate. Environ. Sci. Technol. 26, 1327–1333.

van de Weerd, H., van Riemsdijk, W.H., Leijnse, A., 1999. Modeling the Dynamic Adsorption/Desorption of a NOM Mixture: Effects of Physical and Chemical Heterogeneity. Environ. Sci. Technol. 33, 1675–1681. https://doi.org/10.1021/es980815w

van der Steen, P., Howe, C., 2009. Managing water in the city of the future; strategic planning and science. Rev. Environ. Sci. Biotechnol. 8, 115–120. https://doi.org/10.1007/s11157-009-9154-2

van Genuchten, C.M., Peña, J., 2017. Mn(II) Oxidation in Fenton and Fenton Type Systems: Identification of Reaction Efficiency and Reaction Products. Environ. Sci. Technol. 51, 2982–2991. https://doi.org/10.1021/acs.est.6b05584

van Lienden, C., Shan, L., Rao, S., Ranieri, E., Young, T.M., 2010. Metals Removal from Stormwater by Commercial and Non-Commercial Granular Activated Carbons. Water Environ. Res. 82, 351–356. https://doi.org/10.2175/106143009X12487095236874

Vandenberg, L.N., Hauser, R., Marcus, M., Olea, N., Welshons, W.V., 2007. Human exposure to bisphenol A (BPA). Reprod. Toxicol. 24, 139–177. https://doi.org/10.1016/j.reprotox.2007.07.010

Villalobos, M., Bargar, J., Sposito, G., 2005. Mechanisms of Pb(II) Sorption on a Biogenic Manganese Oxide. Environ. Sci. Technol. 39, 569–576. https://doi.org/10.1021/es049434a

Villalobos, M., Carrillo-Cárdenas, M., Gibson, R., López-Santiago, N.R., Morales, J.A., 2014. The influence of particle size and structure on the sorption and oxidation behaviour of birnessite: II. Adsorption and oxidation of four polycyclic aromatic hydrocarbons. Environ. Chem. 11, 279–288. https://doi.org/10.1071/EN13161

Von Langen, P.J., Johnson, K.S., Coale, K.H., Elrod, V., A., 1997. Oxidation kinetics of manganese (II) in seawater at nanomolar concentrations. Geochim. Cosmochim. Acta 61, 4945–4954.

Wan, S., Qu, N., He, F., Wang, M., Liu, G., He, H., 2015. Tea waste-supported hydrated manganese dioxide (HMO) for enhanced removal of typical toxic metal ions from water. RSC Adv 5, 88900–88907. https://doi.org/10.1039/C5RA16556C

Wang, Z.J., Stumm, W., 1987. Heavy metal complexation by surfaces and humic acids: a brief discourse on assessment by acidimetric titration. Neth. J. Agric. Sci. 35, 231–240.

Webb, S.M., 2005. SIXPack a Graphical User Interface for XAS Analysis Using IFEFFIT. Phys. Scr. 1011–1014. https://doi.org/10.1238/Physica.Topical.115a01011

Webb, S.M., Dick, G.J., Bargar, J.R., Tebo, B.M., 2005. Evidence for the presence of Mn (III) intermediates in the bacterial oxidation of Mn (II). Proc. Natl. Acad. Sci. U. S. A. 102, 5558–5563.

Weiser, M., 2017. Santa Monica Prepares to Eliminate Water Imports, Drought-Proof Supply [WWW Document]. Water Deep. URL https://www.newsdeeply.com/water/community/2017/12/13/santa-monica-prepares-to-eliminate-water-imports-drought-proof-supply (accessed 5.22.18).

Yamada, A., Tanaka, M., 1995. Jahn-Teller Structural Phase Transition around 280K in LiMn2O4. Mater. Res. Bull. 30, 715–721.

Yao, W., Millero, F.J., 1996. Adsorption of phosphate on manganese dioxide in seawater. Environ. Sci. Technol. 30, 536–541.

Zachara, J.M., Glassman, P.L., Smith, S.C., Taylor, D., 1995. Oxidation and adsorption of Co(II)EDTA2- complexes in subsurface materials with iron and manganese oxide grain coatings. Geochim. Cosmochim. Acta 59, 44494463.

Zasoski, R.J., Burau, R.G., 1988. Sorption and Sorptive Interaction of Cadmium and Zinc on Hydrous Manganese Oxide. Soil Sci. Soc. Am. J. 52, 81. https://doi.org/10.2136/sssaj1988.03615995005200010014x

Zhang, H., Chen, W.-R., Huang, C.-H., 2008. Kinetic modeling of oxidation of antibacterial agents by manganese oxide. Environ. Sci. Technol. 42, 5548–5554.

Zhang, H., Huang, C.-H., 2005. Reactivity and Transformation of Antibacterial *N* -Oxides in the Presence of Manganese Oxide. Environ. Sci. Technol. 39, 593–601. https://doi.org/10.1021/es048753z

Zhang, H., Huang, C.-H., 2003. Oxidative Transformation of Triclosan and Chlorophene by Manganese Oxides. Environ. Sci. Technol. 37, 2421–2430. https://doi.org/10.1021/es026190q

Zhang, K., Randelovic, A., Page, D., McCarthy, D.T., Deletic, A., 2014. The validation of stormwater biofilters for micropollutant removal using in situ challenge tests. Ecol. Eng. 67, 1–10. https://doi.org/10.1016/j.ecoleng.2014.03.004

Zhang, T., Zhang, X., Yan, X., Ng, J., Wang, Y., Sun, D.D., 2011. Removal of bisphenol A via a hybrid process combining oxidation on β-MnO2 nanowires with microfiltration. Colloids Surf. Physicochem. Eng. Asp. 392, 198–204. https://doi.org/10.1016/j.colsurfa.2011.09.056

Zhang, W., 2003. Nanoscale Iron Particles for Environmental Remediation: An Overview. J. Nanoparticle Res. 5, 323–332.

Zhong, Z., Postnikova, B.J., Hanes, R.E., Lynch, V.M., Anslyn, E.V., 2005. Large pKa Shifts of alpha-Carbon Acids Induced by Copper(II) Complexes. Chem. - Eur. J. 11, 2385–2394. https://doi.org/10.1002/chem.200400396

Zou, W., Han, R., Chen, Z., Jinghua, Z., Shi, J., 2006. Kinetic study of adsorption of Cu(II) and Pb(II) from aqueous solutions using manganese oxide coated zeolite in batch mode.

Colloids Surf. Physicochem. Eng. Asp. 279, 238–246. https://doi.org/10.1016/j.colsurfa.2006.01.008